DEPARTMENT OF THE AIR FORCE

AIR UNIVERSITY

AIR FORCE INSTITUTE OF TECHNOLOGY

Wright-Patterson Air Force Base, Ohio

AFIT/GA/ENY/91M-2

SENSITIVITY ANALYSIS FOR THE SELECTION OF LINEAR QUADRATIC REGULATOR WEIGHING PARAMETERS Q AND R FOR ACTIVE VIBRATION SUPPRESSION OF A CANTILEVERED BEAM

THESIS

Steven L. Story, Captain, USAF

AFIT/GA/ENY/91M-2

March 1991 MS Thesis

Sensitivity Analysis for the Selection of Linear Quadratic Regulator Weighing Parameters Q and R for Active Vibration Suppression of a Cantilevered Beam

Steven L. Story, Capt, USAF

School of Engineering
Air Force Institute of Technology (AU)
Wright-Patterson AFB, OH 45433-6583

Dr. V. V. Venkayya
WRDC/FIBR

There has been much interest during the past decade to develop and launch large space structures. The high cost of launching material into orbit will require that these structures be assembled in space using light weight elements which are vulnerable to dynamic excitations. Active control may be necessary to rapidly attenuate large amplitude vibrations. The active vibration control system is usually designed after the structure has been optimized. The integrated design of the control system and the structure may provide additional weight savings. This thesis presents a sensitivity analysis of the structure/control optimization problem. The structure used is an aluminum rectangular beam with proof mass actuators mounted on the free end and a structural dynamics shaker attached at the midpoint. A finite element model of the structure is developed using MSC/NASTRAN. LQR theory is used as the control law with velocity feedback. Constant and variable values of Q and R for the performance index are used. The variable values of Q and R are selected to minimize total system energy. Optimization methods examined are; first, the minimization of the performance index J and structural weight; second, Onada's formulation, which minimizes control weight and structural weight.

Active Vibration Suppression; Finite Element Modeling of Beam; Control/Structure Optimization; Vibration Suppression 158

UNCLASSIFIED UNCLASSIFIED UNCLASSIFIED UL

GENERAL INSTRUCTIONS FOR COMPLETING SF 298

The Report Documentation Page (RDP) is used in announcing and cataloging reports. It is important that this information be consistent with the rest of the report, particularly the cover and title page. Instructions for filling in each block of the form follow. It is important to **stay within the lines to meet optical scanning requirements.**

Block 1. Agency Use Only (Leave Blank)

Block 2. Report Date. Full publication date including day, month, and year, if available (e.g. 1 Jan 88). Must cite at least the year.

Block 3. Type of Report and Dates Covered. State whether report is interim, final, etc. If applicable, enter inclusive report dates (e.g. 10 Jun 87 - 30 Jun 88).

Block 4. Title and Subtitle. A title is taken from the part of the report that provides the most meaningful and complete information. When a report is prepared in more than one volume, repeat the primary title, add volume number, and include subtitle for the specific volume. On classified documents enter the title classification in parentheses.

Block 5. Funding Numbers. To include contract and grant numbers; may include program element number(s), project number(s), task number(s), and work unit number(s). Use the following labels:

C	- Contract	**PR**	- Project
G	- Grant	**TA**	- Task
PE	- Program Element	**WU**	- Work Unit Accession No.

Block 6. Author(s). Name(s) of person(s) responsible for writing the report, performing the research, or credited with the content of the report. If editor or compiler, this should follow the name(s).

Block 7. Performing Organization Name(s) and Address(es). Self-explanatory.

Block 8. Performing Organization Report Number. Enter the unique alphanumeric report number(s) assigned by the organization performing the report.

Block 9. Sponsoring/Monitoring Agency Names(s) and Address(es). Self-explanatory.

Block 10. Sponsoring/Monitoring Agency. Report Number. (If known)

Block 11. Supplementary Notes. Enter information not included elsewhere such as: Prepared in cooperation with...; Trans. of ..., To be published in .... When a report is revised, include a statement whether the new report supersedes or supplements the older report.

Block 12a. Distribution/Availablity Statement. Denote public availability or limitation. Cite any availability to the public. Enter additional limitations or special markings in all capitals (e.g. NOFORN, REL, ITAR)

DOD	- See DoDD 5230.24, "Distribution Statements on Technical Documents."
DOE	- See authorities
NASA	- See Handbook NHB 2200.2.
NTIS	- Leave blank.

Block 12b. Distribution Code.

DOD	- DOD - Leave blank
DOE	- DOE - Enter DOE distribution categories from the Standard Distribution for Unclassified Scientific and Technical Reports
NASA	- NASA - Leave blank
NTIS	- NTIS - Leave blank.

Block 13. Abstract. Include a brief (Maximum 200 words) factual summary of the most significant information contained in the report.

Block 14. Subject Terms. Keywords or phrases identifying major subjects in the report.

Block 15. Number of Pages. Enter the total number of pages.

Block 16. Price Code. Enter appropriate price code (NTIS only).

Blocks 17. - 19. Security Classifications. Self-explanatory. Enter U.S. Security Classification in accordance with U.S. Security Regulations (i.e., UNCLASSIFIED). If form contains classified information, stamp classification on the top and bottom of the page.

Block 20. Limitation of Abstract. This block must be completed to assign a limitation to the abstract. Enter either UL (unlimited) or SAR (same as report). An entry in this block is necessary if the abstract is to be limited. If blank, the abstract is assumed to be unlimited.

AFIT/GA/ENY/91M-2

SENSITIVITY ANALYSIS FOR THE SELECTION OF LINEAR QUADRATIC REGULATOR WEIGHING PARAMETERS Q AND R FOR ACTIVE VIBRATION SUPPRESSION OF A CANTILEVERED BEAM

THESIS

Presented to the Faculty of the School of Engineering
of the Air Force Institute of Technology
Air University
In Partial Fulfillment of the
Requirements for the Degree of
Master of Science in Astronautical Engineering

Steven L. Story, B.S.
Captain, USAF

March 1991

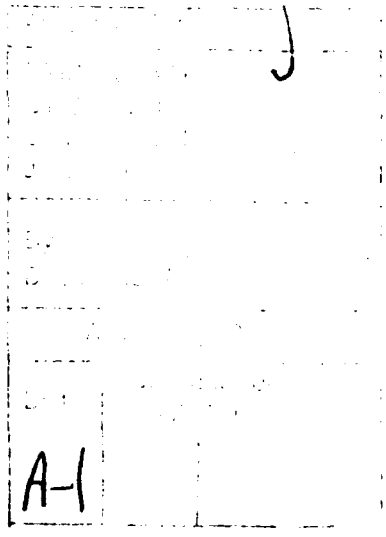

Approved for public release; distribution unlimited

Preface

This work uses a modified version of the Advanced Beam Experiment which was originally developed by the Vibrations Branch of the Flight Dynamics Lab at Wright-Patterson AFB. The modified version of the Advanced Beam Experiment was performed by Capt Jacques in the AFIT labs.

The goal of this work is to create a finite element model of the Advanced Beam Experiment using MSC/NASTRAN. The modal includes damping inherent in both the structure and the actuators. The finite element model is used to perform a sensitivity analysis on the selection of the weighing parameters Q and R used in Linear Quadratic Regulator theory. Sensitivity analysis is also performed on two optimization techniques. The first involves minimizing the performance index J and structural mass, while the second, Onada's formulation, involves minimizing control mass and structural mass. Chapters II and III cover the structure modeled. Chapter IV includes a brief review of finite elements and describes how the model was constructed. Chapter V is a review of LQR theory and describes the state-space formulation of the problem. For those interested in only the results of the sensitivity analysis, Chapter VI should provide all the necessary information.

This work would not have been possible without the help of many people. The previous work of Capt Jacques and Capt Cristler provided the details on which this work is based. Dr. Liebst spent many hours of his time working with me to clarify optimal control theory. Capt Gans, my thesis advisor, provided guidance while my committee, Lt Col Bagley and Dr. Spenny, gave valuable comments so that I could clarify the final work. Mom and Dad were always there to listen whenever I needed encouragement and support. And finally, I would like to thank my wife Joan. She always looked for ways to help and tried to understand what it was that I was doing. She sat through my defense and, when it was over, celebrated with me.

Steven L. Story

Table of Contents

List of Figures

List of Tables

Abstract

There has been much interest during the past decade to develop and launch large space structures. The high cost of launching material into orbit will require that these structures be assembled in space using light weight elements which are vulnerable to dynamic excitations. Active control may be necessary to rapidly attenuate large amplitude vibrations. The active vibration control system is usually designed after the structure has been optimized. The integrated design of the control system and the structure may provide additional weight savings. This thesis presents a sensitivity analysis of the structure/control optimization problem. The structure used is an aluminum rectangular beam with proof mass actuators mounted on the free end and a structural dynamics shaker attached at the midpoint. A finite element model of the structure is developed using MSC/NASTRAN. Linear Quadratic Regulator theory is used as the control law with velocity feedback. Constant and variable values of Q and R for the performance index are used. The variable values of Q and R are selected to minimize total system energy. Optimization methods examined are; first, the minimization of the performance index J and structural weight; second, Onada's formulation, which minimizes control weight and structural weight.

SENSITIVITY ANALYSIS FOR THE SELECTION OF LINEAR QUADRATIC REGULATOR WEIGHING PARAMETERS Q AND R FOR ACTIVE VIBRATION SUPPRESSION OF A CANTILEVERED BEAM

I. Introduction

During this decade, the deployment of large structures in space will become a reality. NASA is currently developing Space Station Freedom and the Department of Defense is interested in systems which, if deployed, will require large stable platforms in space. Because of the high cost of launching material into orbit and because of launch size restrictions, these built-up structures will be assembled in space using light weight truss-like elements. The truss-like elements will provide a framework to which mission-related functional components will be attached. Because of their low weight, however, these structures will be highly flexible which will make them vulnerable to dynamic excitations from a variety of sources.

Control Approaches To Vibration Damping

A structure's response to dynamic excitations is governed by its mass, damping, and stiffness characteristics. The large size of space structures coupled with their light weight results in many low frequency, lightly damped, closely spaced vibration modes. These vibration modes must be controlled in order to minimize their effect on the system. Passive damping, obtained by methods such as sophisticated shock absorbers and visco-elastic coatings, is a partial solution to the

problem, but it cannot control all of the vibration modes. Active control may be required to rapidly attenuate large amplitude vibration modes.

The early history of active control research for Large Space Structures (LSS) is well documented in Ref. 1. The authors of this paper suggest four challenges (1:515) which face researchers in the years ahead. These challenges are:

1. Design control systems sufficiently robust so that errors in structural modeling can be accommodated.

2. Establish reasonably accurate structural models.

3. Develop auxiliary control laws which adequately reduce plant excitations.

4. Establish the proper choice of control law, sensors, and actuators to maintain the shape of a large space structure.

To address these challenges, the authors divided the field of LSS research into structural dynamics and control theory.

The structural engineer's job is to develop a simplified mathematical abstraction (model) of a structure. Since all of the dynamic characteristics of a structure cannot be modeled, care must be taken to ensure that the most important dynamic characteristics are accurately represented in the model. A fundamental question, however, must be asked (2:4); "What is the purpose of the model?" Will an "exact" solution be required from a continuum model or will a lumped mass model be adequate? Once the model is developed, verification must be done to ensure that it accurately represents the structure.

Several methods of model verification are presented in Ref. 2. The most common method used is to compare the model dynamic characteristics to experimental results on the actual structure. The large size of space structures, however, makes it impossible to test the actual structure before it is deployed in space. Scale modeling of LSS will be necessary if actual ground tests are to be conducted. Past

experience (3:924) with finite element modeling in aircraft design suggests that finite element modeling would be a useful tool to dynamically model LSS. The system of linear differential equations resulting from finite element analysis is readily expressed in state-space form for use in designing the active control system.

The active control system for vibration damping of LSS generally consists of sensors, controllers, and actuators. Prior to 1980, there were very few LSS active control experiments (4:471). The first major U.S. Government program, Active Control of Space Structures (ACOSS), was started in 1978 and completed in 1984. In late 1989, the number of LSS experiments (4:472) "seem to be approaching flood level." This "flood level" is the focus of Ref. 4 which surveys the literature published on experimental LSS work accomplished during 1985-1989.

According to Ref. 4, the experience of many researchers suggests that the actuators play the dominant role in determining the success or failure of a LSS experiment. The type of actuators used in LSS experiments can be used to lump the experiments into one of two distinct categories. The first category of experiments are based on grounded actuators. Since it is impractical to ground an actual LSS actuator, the second category consists of those experiments using inertial actuators.

Previous Work on the Advanced Beam Experiment (ABE)

The original concept of the ABE developed by the Wright Research and Development Center Flight Dynamics Lab was to use four inertial proof mass actuators mounted in pairs to control bending in two orthogonal planes and torsion. Cristler (5) developed the actuator controller and then demonstrated active control using a Linear Quadratic Gaussian (LGQ) design and modal suppression techniques. Breitfeller (6) demonstrated active control by using a low authority controller based on root perturbation techniques and a high authority controller based on a

frequency-shaped cost function. Both of these experiments were partially successful.

Jacques (7) set out to resurrect the ABE in what is now known as the modified ABE. In the modified ABE, only two of the original four proof mass actuators were available. This limited the experiment to controlling only XY-plane bending and torsion. To provide better control over second and third mode bending, a structural dynamics shaker was added. This violated the original intent of the ABE which was to use only inertial actuators. It did, however, open the door for further research on the ABE.

Control/Structure Optimization

The ABE represents the traditional approach to controls research. The control engineer is given a structure and told to develop an optimal control system to achieve some dynamic response. This approach may not prove adequate with LSS because of the high cost of placing mass in orbit. Since the size of LSS requires that they be constructed in orbit, they do not have to be designed to withstand large launch forces. An immediate cost savings can be achieved by designing very light structures. Light structures, however, are susceptible to vibrations. Passive damping can attenuate some of the vibrations, but active vibration suppression will be necessary. To obtain maximum system performance for minimum cost, an integrated approach to structural/ control optimization is necessary. Refs. 3 and 8 survey some of the issues concerning the integrated optimization of structures and controls. Two of the important issues in integrated design according to (8:55-56) are, "cross-sensitivity information" and "the choice of objective function."

Problem Statement

There are three goals for the work presented in this thesis. The first goal is to develop an accurate finite element model of the ABE using MSC/NASTRAN. The model will include damping for both the structure and the actuators. The second goal is to examine the "cross-sensitivity" of the structure and the control system to the weighing parameters Q and R from Linear Quadratic Regulator (LQR) theory. Finally, two different objective functions used in the integrated structure/control optimization problem will be examined by using sensitivity analysis.

II. Structure

The Advanced Beam Experiment (ABE) configuration was originally developed by the Wright Research and Development Center Flight Dynamics Lab to model the large space structure characteristics of low frequency, lightly damped, and closely spaced vibration modes. The structure and its properties are presented in this chapter. The beam theoretical equations of motion for xy-plane bending and torsion are derived and numerical solutions given.

Structural Properties

The beam is a long, solid aluminum beam of rectangular cross-section. It is suspended in a vertical position with a circular disk attached to the free end. The circular disk provides a surface on which to mount the control actuators and has approximately the same mass as the beam. The disk provides the primary component of rotary inertia which lowers the first torsion mode frequency so that it is within the control bandwidth of the controllers. The beam is shown in Figure 2.1. The beam and disk physical and material properties are given in Table 2.1 and Table 2.2 respectively.

Equations of Motion

The equations of motion for the beam can be derived using Hamilton's principle. Hamilton's principle can be stated as (9:199)

$$\int_{t_1}^{t_2} \delta(T-V_e)\,dt + \int_{t_1}^{t_2} \delta W_{nc}\,dt = 0 \qquad (2.1)$$

where

T = total kinetic energy of the system.

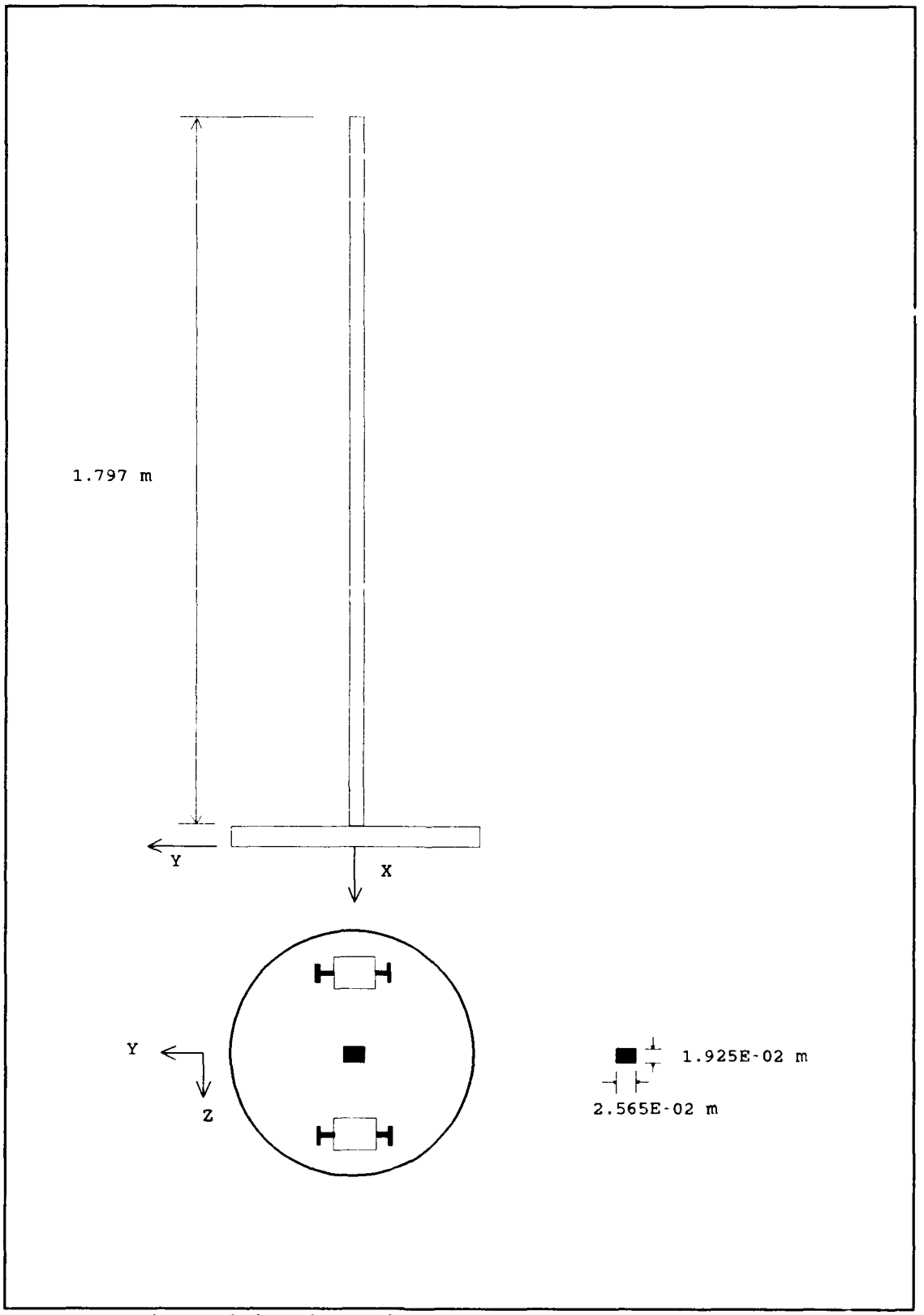

Figure 2.1 Advanced Beam Experiment Configuration

Table 2.1 Beam Properties (7:26)

Beam Property Description	Value	Units
Beam Length (L)	1.797	m
Y Cross-Section Width (a)	2.565×10^{-2}	m
Z Cross-Section Width (b)	1.925×10^{-2}	m
Cross-Section Area (A)	4.939×10^{-4}	m^2
Young's Modulus (E)	7.446×10^{10}	N/m^2
Shear Modulus (G)	2.827×10^{10}	N/m^2
Beam Density (ρ)	2.766×10^{3}	kg/m^3
Beam Mass (m)	2.455	kg
Y Moment of Inertia (I_y)*	1.526×10^{-8}	m^4
Z Moment of Inertia (I_z)*	2.709×10^{-8}	m^4
Torsional Moment of Inertia (J)*	3.292×10^{-8}	m^4
Polar Moment of Inertia (I_p)*	4.235×10^{-8}	m^4

* See Appendix A for sample calculations.

V_e = potential energy of the system, including the strain energy and the potential energy of the conservative external forces.

δW_{nc} = virtual work done by nonconservative forces, including damping forces and external forces not accounted for in V.

Table 2.2 Disk Properties (7:26)

Disk Property Description	Value	Units
Disk Diameter (d)	3.048×10^{-1}	m
Disk Thickness (t)	2.540×10^{-2}	m
Disk Mass (m_d)	4.986	kg
X Mass Moment of Inertia (I_{dxx})*	5.790×10^{-2}	kg-m^2
Y Mass Moment of Inertia (I_{dyy})*	2.895×10^{-2}	kg-m^2
Z Mass Moment of Inertia (I_{dzz})*	2.895×10^{-2}	kg-m^2

* See Appendix A for sample calculations.

$\delta( )$ = the symbol denoting the first variation, or virtual change, in the quantity in parentheses.

t_1, t_2 = times at which the configuration of the system in known.

Equations of Motion - XY-Plane Bending. For a beam in bending, shear deformation will occur as shown in Figure 2.2. In Figure 2.2, $\alpha(x,t)$ is the rotation of the cross section and $v(x,t)$ is the total transverse displacement of the beam neutral axis in the y direction. The shear angle β is defined as

$$\beta(x,t) = \alpha(x,t) - \frac{\partial v(x,t)}{\partial x} \qquad (2.2)$$

For a long, thin beam undergoing transverse vibration, however, the equations of motion can be approximated by using the Bernoulli Euler assumptions of elementary beam theory. These assumptions are (9:193):

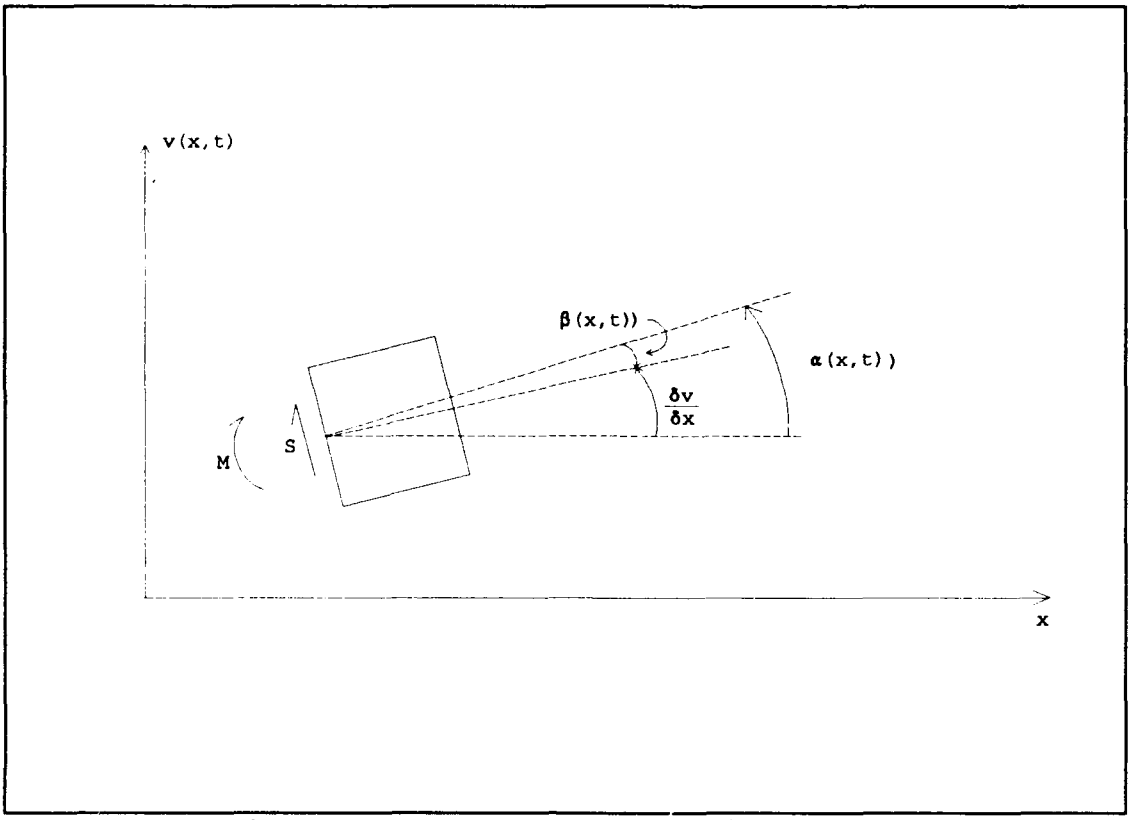

Figure 2.2 Beam Shear Deformation (9:203)

-There is an axis of the beam which undergoes no extension or contraction. The x-axis is located along this neutral axis.

-Cross sections perpendicular to the neutral axis in the undeformed beam remain plane and remain perpendicular to the deformed neutral axis, that is, transverse shear deformation is neglected.

-The material is linearly elastic and the beam is homogeneous at any cross section.

-σ_y and σ_z are negligible compared to σ_x.

-The xy-plane is the principal plane.

In addition to these assumptions, rotary inertia and gravity will be neglected in the theoretical calculations. Equation 2.2 becomes

$$\frac{\partial v(x,t)}{\partial x} = \alpha(x,t) \tag{2.3}$$

For displacement in the y-direction, the beam internal strain energy is

$$V_e = \frac{1}{2}\int_0^L E(x) I_z(x) \left(\frac{\partial \alpha(x,t)}{\partial x}\right)^2 dx \tag{2.4}$$

and the beam kinetic energy due to translation is

$$T = \frac{1}{2}\int_0^L \rho(x) A(x) \left(\frac{\partial v(x,t)}{\partial t}\right)^2 dx \tag{2.5}$$

where

- $E(x)$ is Young's Modulus.
- $I_z(x)$ is the moment of inertia about the z-axis.
- $\rho(x)$ is the density.
- $A(x)$ is the cross-sectional area.

For transverse loading, the virtual work is

$$\partial W_{nc} = \int_0^L p(x,t)\partial v(x,t) dx \tag{2.6}$$

Substituting equations 2.4, 2.5, and 2.6 into Hamilton's equation, integrating by parts, and applying geometric boundary conditions gives the equation of motion

$$\frac{\partial^2}{\partial x^2}\left[E(x) I_z(x) \frac{\partial^2 v(x,t)}{\partial x^2}\right] + \rho(x) A(x) \frac{\partial^2 v(x,t)}{\partial t^2} = p(x,t) \tag{2.7}$$

and the natural boundary conditions

$$E(x)I_z(x)\frac{\partial^2 v(x,t)}{\partial x^2}\Big|_{x=L}=M_z(t) \tag{2.8}$$

$$E(x)I_z(x)\frac{\partial^3 v(x,t)}{\partial x^3}\Big|_{x=L}=V_y(t) \tag{2.9}$$

For free vibration, equation 2.7 reduces to

$$\frac{\partial^2}{\partial x^2}\left[E(x)I_z(x)\frac{\partial^2 v(x,t)}{\partial x^2}\right]+\rho(x)A(x)\frac{\partial^2 v(x,t)}{\partial t^2}=0 \tag{2.10}$$

Assume a solution of the form

$$v(x,t)=V(x)\cos(\omega t-\alpha) \tag{2.11}$$

Substituting equation 2.11 into equation 2.10

$$\frac{d^2}{dx^2}\left[E(x)I_z(x)\frac{d^2V(x)}{dx^2}\right]-\rho(x)A(x)V(x)\omega^2=0 \tag{2.12}$$

For a uniform beam

$$\frac{\partial^4 V(x)}{\partial x^4}-\frac{\rho A\omega^2}{EI_z}V(x)=0 \tag{2.13}$$

Let

$$\beta_y^4=\frac{\rho A\omega^2}{EI_z} \tag{2.14}$$

then the eigenvalue problem

$$\frac{\partial^4 V(x)}{\partial x^4}-\beta_y^4 V(x)=0 \tag{2.15}$$

has a general solution of the form

$$V(x)=C_1\sin(\beta_y x)+C_2\cos(\beta_y x)+C_3\sinh(\beta_y x)+C_4\cosh(\beta_y x) \tag{2.16}$$

Equations of Motion - Torsion. Hamilton's principle can also be used to derive the equations of motion for torsion. The potential energy for torsion is given by (9:200-202)

$$V_e = \frac{1}{2}\int_0^L G(x)J(x)\left[\frac{\partial\theta(x,t)}{\partial x}\right]^2 dx \tag{2.17}$$

and the kinetic energy is

$$T = \frac{1}{2}\int_0^L \rho(x)I_p(x)\left[\frac{\partial\theta(x,t)}{\partial t}\right]^2 dx \tag{2.18}$$

where

- $G(x)$ is the shear modulus.
- $J(x)$ is a geometric property of the cross section.
- $I_p(x)$ is the polar moment of inertia.
- $\theta(x,t)$ is the rotation at x.

The virtual work of the external forces is

$$\partial W_{nc} = \int_0^L \tau(x,t)\partial\theta(x,t)dx + T_L(L,t)\partial\theta(L,t) \tag{2.19}$$

where

- $\tau(x,t)$ is a distributed moment.
- $T_L(t)$ is a concentrated end moment.

Substituting equations 2.17, 2.18, and 2.19 into Hamilton's equation, integrating by parts, and applying the geometric boundary conditions, the equation of motion is found to be

$$\rho(x)I_p(x)\frac{\partial^2\theta(x,t)}{\partial t^2} - \frac{\partial}{\partial x}\left[G(x)J(x)\frac{\partial\theta(x,t)}{\partial x}\right] = \tau(x,t) \tag{2.20}$$

and the natural boundary condition is

$$[G(x)J(x)\frac{\partial\theta(x,t)}{\partial x}]\Big|_{x=L}=M_x(L,t) \tag{2.21}$$

For free torsional vibration $\tau(x,t) = 0$, thus

$$\frac{\partial}{\partial x}[G(x)J(x)\frac{\partial\theta(x,t)}{\partial x}]=I_p(x)\frac{\partial^2\theta(x,t)}{\partial t^2} \tag{2.22}$$

For a uniform bar

$$\rho I_p\frac{\partial^2\theta(x,t)}{\partial t^2}-GJ\frac{\partial^2\theta(x,t)}{\partial x^2}=0 \tag{2.23}$$

Assume a solution of the form

$$\theta(x,t)=\Phi(x)\cos(\omega t-\alpha) \tag{2.24}$$

Substitute equation 2.24 into equation 2.23

$$GJ\frac{d^2\Phi(x)}{dx^2}+\omega^2\rho I_p\Phi(x)=0 \tag{2.25}$$

and let

$$\beta_x^2=\frac{\rho I_p}{GJ}\omega^2 \tag{2.26}$$

The torsional equation of motion can then be written as

$$\frac{d^2\Phi(x)}{dx^2}+\beta_x^2\Phi(x)=0 \tag{2.27}$$

The general solution is of the form

$$\Phi(x)=C_1\sin(\beta_x x)+C_2\cos(\beta_x x) \tag{2.28}$$

Numerical Solutions

The position dependent equations of motion for x-y plane bending and torsion are again

$$\frac{d^4V(x)}{dx^4} - \beta_y^4 V(x) = 0 \tag{2.29}$$

$$\frac{d^2\Phi(x)}{dx^2} + \beta_x^2 \Phi(x) = 0 \tag{2.30}$$

with general solutions

$$V(x) = A_1 \sin(\beta_y x) + A_2 \cos(\beta_y x) + A_3 \sinh(\beta_y x) + A_4 \cosh(\beta_y x) \tag{2.31}$$

$$\Phi(x) = C_1 \sin(\beta_x x) + C_2 \cos(\beta_x x) \tag{2.32}$$

The boundary conditions at the clamped end are

$$v(0,t) = 0 \tag{2.33}$$

$$\theta(0,t) = 0 \tag{2.34}$$

$$\frac{\partial V(0,t)}{\partial t} = 0 \tag{2.35}$$

At x = L, the boundary conditions are

$$V_y = m_d \frac{\partial^2 v(L,t)}{\partial t^2} \tag{2.36}$$

$$M_x = I_{dxx} \frac{\partial^2 \theta(L,t)}{\partial t^2} \tag{2.37}$$

$$M_z = I_{dzz} \frac{\partial^2}{\partial t^2} \left[\frac{\partial v(x,t)}{\partial x} \right] \tag{2.38}$$

where the shear force and moments are

After applying the above boundary conditions the equation of motion for x-y plane bending reduces to 2 equations and 3 unknowns while

$$V_y = EI_z \frac{\partial^3 v(x,t)}{\partial x^3} \tag{2.39}$$

$$M_x = -GJ \frac{\partial \theta(x,t)}{\partial x} \tag{2.40}$$

$$M_z = EI_z \frac{\partial^2 v(x,t)}{\partial x^2} \tag{2.41}$$

the equation of motion for torsion reduces to 1 equation and 2 unknowns. The x-y bending plane equation of motion can be represented in matrix form as

$$F(\beta_y L)[A_1 \ A_4]^T = [0] \tag{2.42}$$

with

$$\begin{aligned} A_1 &= -A_3 \\ A_4 &= -A_2 \end{aligned} \tag{2.43}$$

$F(\beta_y L)$ is defined as

$$F(\beta_y L) = \begin{bmatrix} F_{11} & F_{12} \\ F_{21} & F_{22} \end{bmatrix} \tag{2.44}$$

where

$$F_{11} = -(\beta_y L)^2 m_p(\sin(\beta_y L) - \sinh(\beta_y L)) + L\rho A(\beta_y L)(\cos(\beta_y L) + \cosh(\beta_y L)) \tag{2.45}$$

$$F_{12} = (\beta_y L)^2 m_p(\cos(\beta_y L) - \cosh(\beta_y L)) + L\rho A(\beta_y L)(\sin(\beta_y L) - \sinh(\beta_y L)) \tag{2.46}$$

$$F_{21} = (\beta_y L)^3 I_{zz}(\cos(\beta_y L) - \cosh(\beta_y L)) - L^3 \rho A(\sin(\beta_y L) + \sinh(\beta_y L)) \tag{2.47}$$

$$F_{22} = (\beta_y L)^3 I_{zz}(\sin(\beta_y L) + \sinh(\beta_y L)) + L^3 \rho A(\cos(\beta_y L) + \cosh(\beta_y L)) \tag{2.48}$$

For equation 2.42 to have a non-trivial solution, the determinant must be zero. The natural frequencies for bending are found by setting

$$\det F(\beta_y L) = 0 \tag{2.49}$$

solving for $\beta_y L$, then using

$$\omega_y = \left(\frac{\beta_y L}{L}\right)^2 \left[\frac{EI_z}{\rho A}\right]^{\frac{1}{2}} \tag{2.50}$$

to solve for the natural frequencies.

After applying the boundary conditions for torsion we find $C_2 = 0$. The equation of motion can be written as a transcendental function

$$\tan(\beta_x L) - \frac{\rho I_p L}{(\beta_x L) I_{xx}} = 0 \tag{2.51}$$

of $\beta_x L$.

The natural frequencies are found from

$$\omega_x = \frac{\beta_x L}{L}\left[\frac{GJ}{\rho I_p}\right]^{\frac{1}{2}} \tag{2.52}$$

Once $\beta_y L$ and $\beta_x L$ are found, the constants A_1, A_4, and C_1 can be found from equations 2.31 and 2.32.

Equations 2.49 and 2.51 were solved numerically. The natural frequencies of the beam without the end mass were also determined. Table 2.3 contains the numerical solutions to the theoretical equations of motion.

Table 2.3 Numerical Results

	Beam without End Mass	Beam with End Mass
XY Bending		
M-1	6.65	2.17
M-2	41.72	28.01
M-3	116.81	76.36
M-4	228.91	138.35
M-5	378.40	240.29
Torsion		
T-1	391.89	15.07
T-2	1176.00	784.25

III. Actuators, Sensors, Measurement Channel, and Configuration

The original Advanced Beam Experiment conducted by Cristler used two pairs of linear proof mass actuators mounted on a circular disk attached to the beam. The actuators, mounted in orthogonal axis, theoretically allowed for simultaneous control of the beam in both bending planes and torsion. The weight of the actuators, however, created second and third bending modes close to the free end of the beam. In addition, the actuators could not achieve full force output below 5 Hz. Since the first bending mode in both the x-y plane and the x-z plane was below 5 Hz, effective control was achieved with only the first torsion mode.

The modified ABE conducted by Jacques used only 1 pair of linear proof mass actuators to control first mode bending in the x-y plane and the first torsion mode. To control second and third mode bending, a structural dynamics shaker was added. In addition, improved accelerometers and integration circuits were used. This chapter covers the changes implemented in the modified ABE which was used as the model for this work.

Actuators

In the original ABE, AFWAL chose linear proof mass actuators based (7:2.1) on a design by TRW. The actuators are linear dC motors which use momentum exchange between the base plate and the moving mass to provide a control force. The actuators consist of a linear motor coil mounted on two support brackets connected to the base disk. The motor coil is driven by a power amplifier circuit which transforms a voltage command into a drive current. The drive current is limited to 2 amps by a current limiter to prevent burning out the motor coils. The motor coils drive the motor magnets which are contained in the 0.9258 kg

cylindrical proof mass. The proof mass travels on linear bearings which allow for ±1.067E-02 meters of travel. Below 5 Hz the maximum force output is limited by the distance the proof mass can travel. For low frequencies, the peak force can be predicted by

$$F_{out} = m_d \omega^2 d \tag{3.1}$$

where m_d is the mass of the proof mass and attached accelerometer, ω is the frequency in rad/sec of the signal driving the motor, and d is the peak displacement. Figure 3.1 is a graph of the theoretical force output for each actuator. Above 5 Hz the maximum force output of an actuator is limited to about 8.9 N by the motor coil capability of 2 amps. Jacques (7:18) measured the actual control force available from the actuators to control mode 1 bending. Table 3.1 gives Jacques' measured results versus predicted results. The total force available at

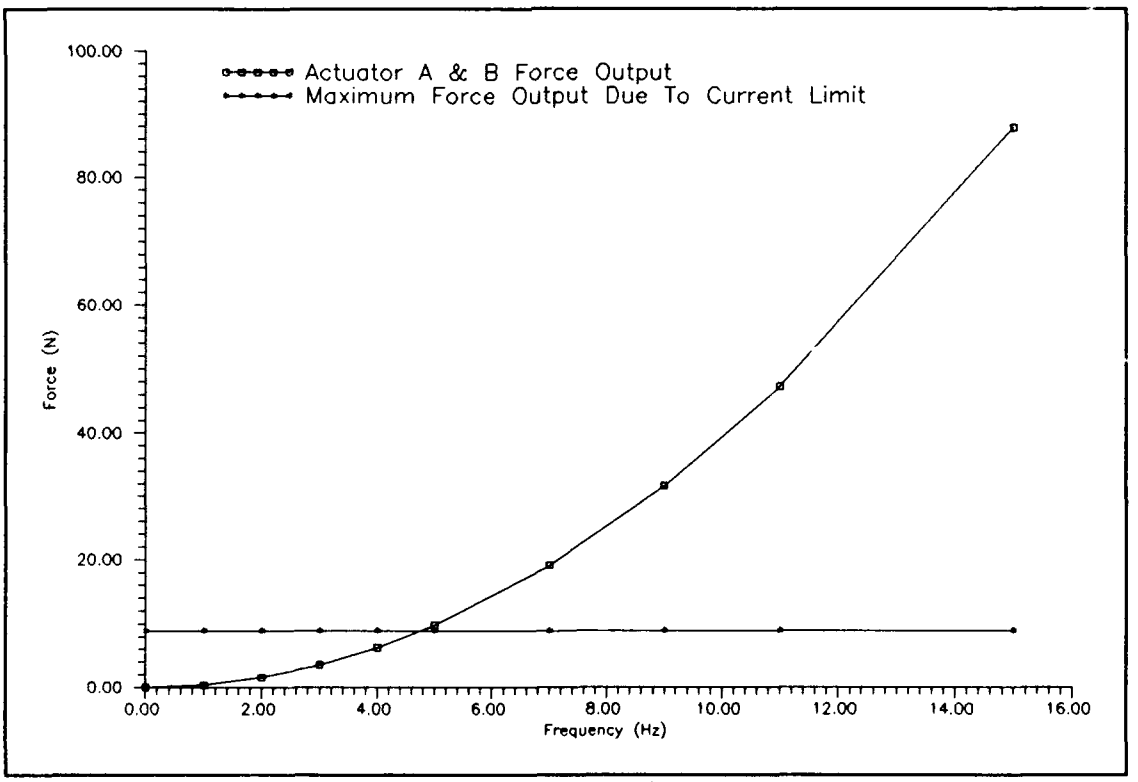

Figure 3.1 Actuator Theoretical Force Ouput

2 Hz is found to be ± 2.625 N which is the sum of maximum output for both actuators.

Table 3.1 Actuator Maximum Force Outputs at 2 Hz (7:18)

Actuator	$F_{predicted}$ (N)	$F_{measured}$ (N)	Efficiency (%)
A	1.606	1.326	82.5
B	1.606	1.299	80.9

The actuators are instrumented with Linear Variable Differential Transformers (LVDT) which provide feedback of the relative position between the proof mass and the motor base. The proof mass is instrumented with an Endevco piezoresistive accelerometer. Figure 3.2 is a schematic of the linear proof mass actuators from Christler (5:C.1 - C.4). Table 3.2 gives a description of each component, its mass, and its dimensions. Tables 3.3 and 3.4 list the center of gravity

Table 3.2 Actuator Mass Model Components (5:C.1)

Part	Figure Description	Mass (kg)	Dimensions (10^{-2}m)			
			Length	Width	Height	Diameter
1	Rectangular Plate	2.49E-2	2.79	0.76	4.32	-
2	Circular Cylinder	3.49E-2	11.43	-	-	0.64
3	Rectangular Plate	8.48E-2	2.79	0.76	4.32	-
4	Rectangular Plate	3.49E-2	2.79	0.76	5.40	-
5	Circular Cylinder	9.47E-2	13.97	-	-	1.91
6	Hollow Circular Cylinder	51.36E-2	5.72	Inside Diameter = 0.64 Outside Diameter = 5.40		

Top View

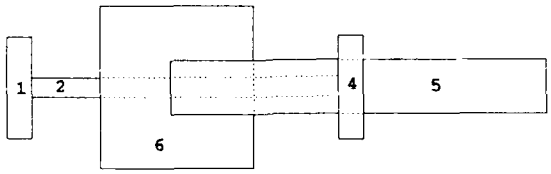

Side View

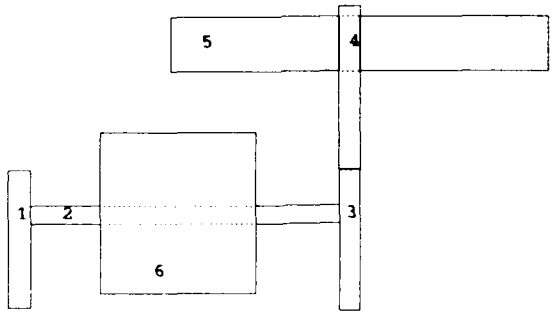

Figure 3.2 Proof Mass Actuator (5:C.2)

and mass moments of inertia for each component of actuators A and B. The specifications for the linear motors, the LVDT's, and the Endevco accelerometers are listed in Appendix B. The power amplifier circuit is also given.

Table 3.3 Actuator A Mass Model (5:C.3)

Part	Center of Gravity (10^{-2} m)			Mass Moment of Inertia (10^{-5} kg-m^2)		
	$\bar{x}$	$\bar{y}$	$\bar{z}$	I_x	I_y	I_z
1	177.55	-5.72	-10.16	0.17	0.55	0.40
2	176.78	0.00	-10.16	3.81	0.018	3.81
3	177.55	5.72	-10.16	0.59	1.87	1.36
4	172.70	5.72	-10.16	0.24	1.07	0.86
5	171.32	6.20	-10.16	15.62	0.43	15.62
6	176.78	0.00	-10.16	40.99	33.13	40.99

Table 3.4 Actuator B Mass Model (5:C.4)

Part	Center of Gravity (10^{-2} m)			Mass Moment of Inertia (10^{-5} kg-m^2)		
	$\bar{x}$	$\bar{y}$	$\bar{z}$	I_x	I_y	I_z
1	177.55	5.72	10.16	0.17	0.55	0.40
2	176.78	0.00	10.16	3.81	0.018	3.81
3	177.55	-5.72	10.16	0.59	1.87	1.36
4	172.70	-5.72	10.16	0.24	1.07	0.86
5	171.32	-6.20	10.16	15.62	0.43	15.62
6	176.78	0.00	10.16	40.99	33.13	40.99

Initial open loop testing of the actuators by Cristler found them to have several undesirable characteristics. These characteristics (5:8-9) are

1. The low frequency behavior was non-linear due to several factors. The bearing friction and associated hysteresis caused drift of the center position. Also, the limited stroke length would not allow for maximum force output below about 5 Hz. For very low frequencies (< 1 Hz), the bearing friction often overcame the commanded force output of the actuator.

2. The zero adjustment of the power amplifier circuit required continual adjustment, as the zero position would shift as a function of both frequency and amplitude.

3. The open loop frequency response has a roll off and associated phase shift in the vicinity of one of the fundamental bending mode frequencies.

4. Non-linear bracket dynamics appeared in the region of 120-150 Hz.

A closed loop feedback system was designed to overcome these open loop characteristics. The details of this design are completely described in Reference 7. The overall goals (7:2-4) of the design were:

1. Actuator frequency response should be "flat" over the structure control bandwidth. While the original ABE limited the control bandwidth to 0 to 50 Hz, the modified experiment uses an expanded control bandwidth of 0 to 100 Hz.

2. The actuator proof mass should maintain an inertial position when the actuator is not being commanded.

3. The proof mass should maintain its centering when commanded at different frequencies and amplitudes.

4. The actuator proof mass should remain within the ±0.5 inch actuator stroke limits.

The actuator compensator circuit used in the modified ABE was identical to the circuit used in the original experiment except for modifications in resistance values. These modifications (7:10) were necessary for the following reasons:

1. The characterization of the open loop actuator changed slightly. The low frequency pole shifted higher, the bearing friction deteriorated further, and the actuators were sensitive to environmental changes.
2. The modified ABE required a bandwidth of 0-100 Hz because the third mode bending frequency of 60-70 Hz was included.
3. Different feedback accelerometers were used, and the difference in the sensitivities had to be compensated for.

The details of these modifications are covered in detail in Reference 7. The final control configuration is shown in Figure 3.3.

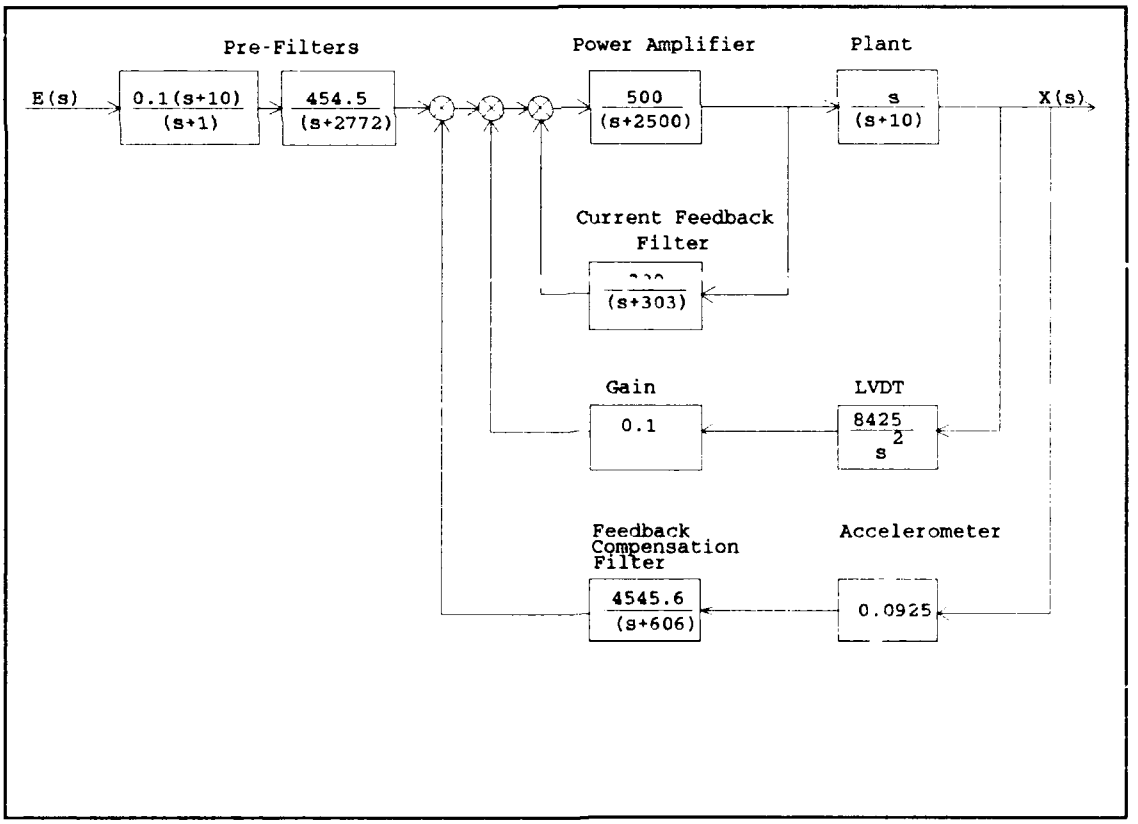

Figure 3.3 Actuator Compensation Block Diagram (7:12)

Structural Dynamics Shaker

The third actuator was added to control second and third mode bending. The actuator used was an Acoustic Power Systems (APS) Model 113-LA Structural Dynamics Shaker driven by an APS Model 114 dual mode power amplifier. This shaker was chosen because of its long stroke limit and excellent response in the control bandwidth. The exceptionally flat response allowed "open loop" operation, thereby eliminating the feedback problems encountered with the proof mass actuators. Since the structural dynamics shaker was physically mounted in the laboratory, the original intent of the ABE to use inertial controllers mounted to the beam was violated. In future experiments, Jacques suggested (7:22) that the structural dynamics shaker should be freely suspended. Since the goal here is to model the results of Jacques' work, the structural dynamics shaker will be modeled as a non-inertial controller. Details of the open loop testing are in Reference 7. Specification sheets for the shaker and the amplifier are in Appendix B.

Sensors/Measurement Channels

One of the goals of the modified ABE was to improve the sensors and integrator circuit. The original ABE used piezoelectric accelerometers which provided relatively poor low frequency responses and the original integration circuit was susceptible to drift caused by integrating dC offsets or very low frequency signals. The modified ABE used Endevco Model 2262 piezoresistive accelerometers which have a good low frequency response. The integrator circuit used in the modified ABE was designed by WRDC/FIBG to have negligible phase shift and a straight -20 dB/decade magnitude slope above 1 Hz. Specifications for the accelerometers and the integration circuit diagram are contained in Appendix B.

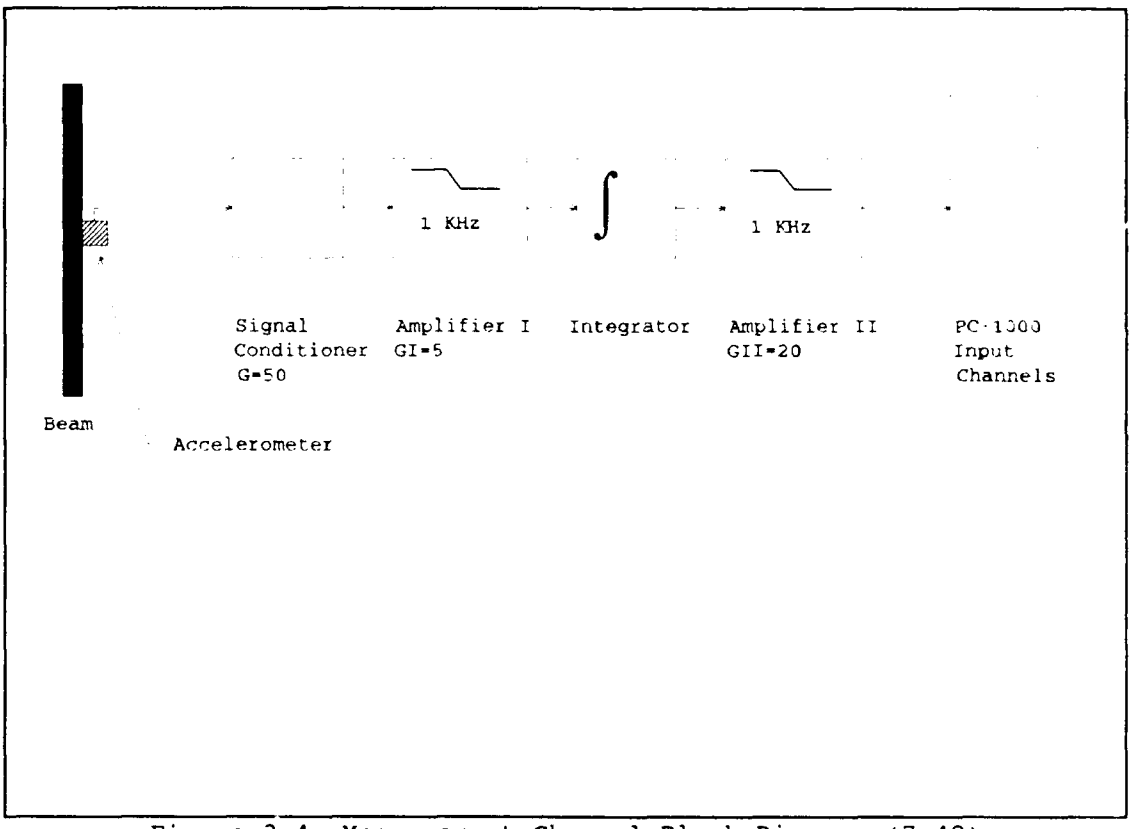

Figure 3.4 Measurement Channel Block Diagram (7:48)

A side effect of signal integration was attenuation of the signal. Amplification was necessary to boost the analog-to-digital input signal up to the minimum range. Two amplification stages were necessary. The first stage was placed before the integrator while the second stage was placed after the integrator. Gain had to be kept low in the first stage to avoid clipping the signals in the integrator. The remainder of the required gain was provided in the second stage. The low pass filter on both amplifiers was set to 1 KHz. While this thesis will use velocity feedback as shown in Figure 3.4 to examine the integration or structure/control optimization, the control law will be implemented using perfect sensors.

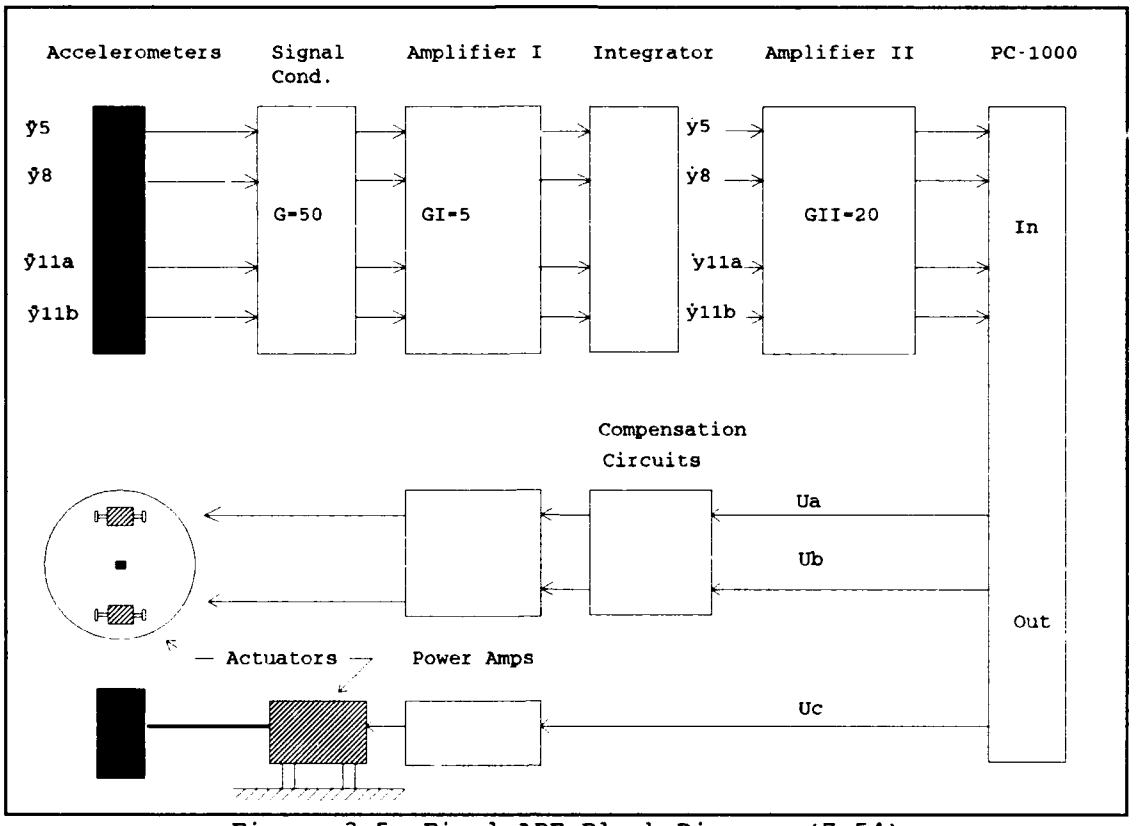

Figure 3.5 Final ABE Block Diagram (7:54)

Final Configuration

Figure 3.5 shows the modified ABE final hardware configuration. The hardware consisted of an inverted cantilevered beam with base plate, two linear proof mass actuators, two linear proof mass actuator compensation circuits, a structural dynamics shaker, four accelerometers, four signal conditioning/integrator circuits, a PC-1000 Array processor and its host computer. Figure 3.6 shows the system configuration for the beam with base plate, the actuators, and the structural dynamics shaker. There are 11 positions located 7 inches apart. The shaker is located at position 4 (28 inches from the fixed end) and provides good control over second and third mode bending. The proof mass actuators, shown in Figure 3.7, are mounted parallel to the

y-axis. When they are operated symmetrically they provide control over x-y plane bending modes and when they are operated asymmetrically the provide control of the torsion mode. The arrows indicate positive direction for measurement of force input.

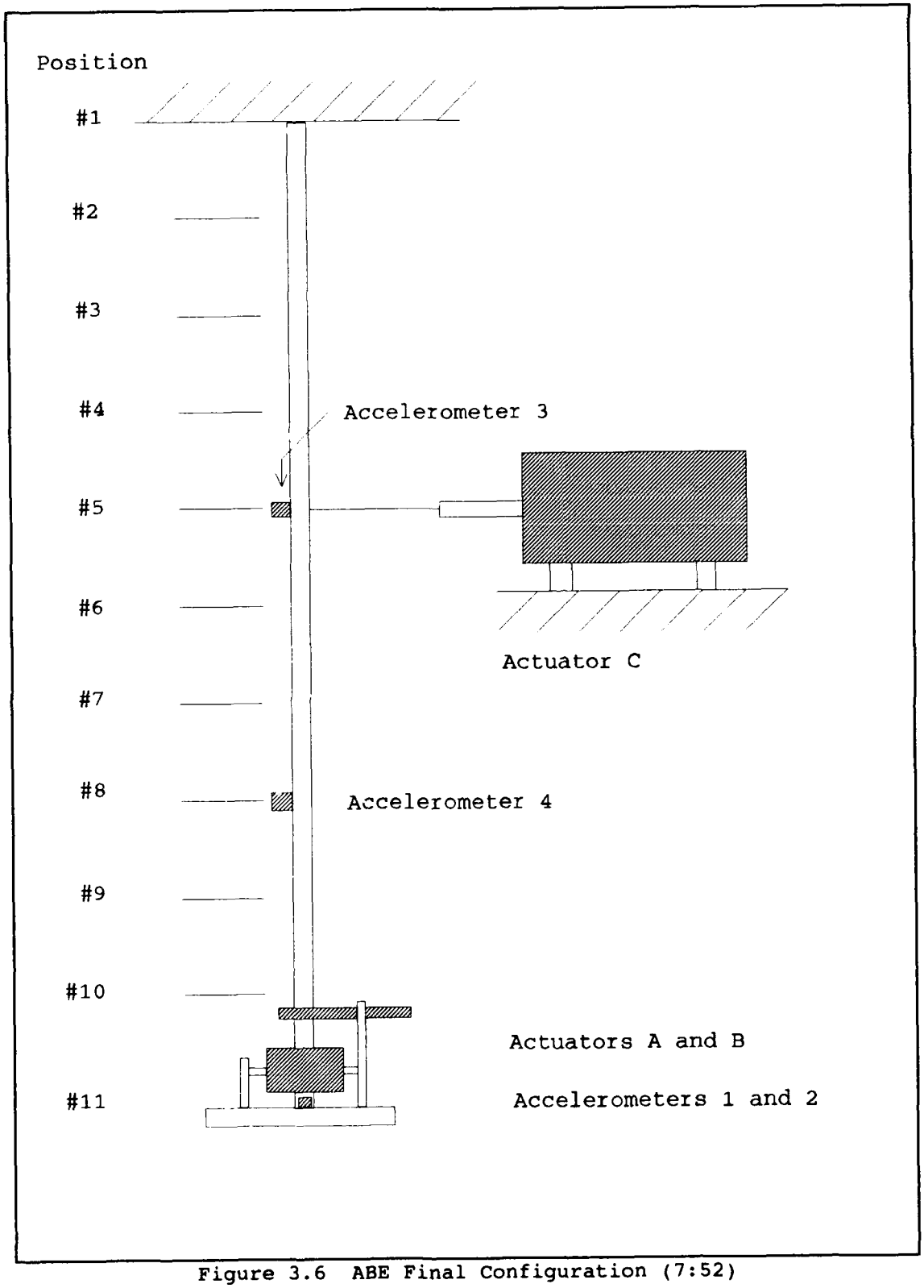

Figure 3.6 ABE Final Configuration (7:52)

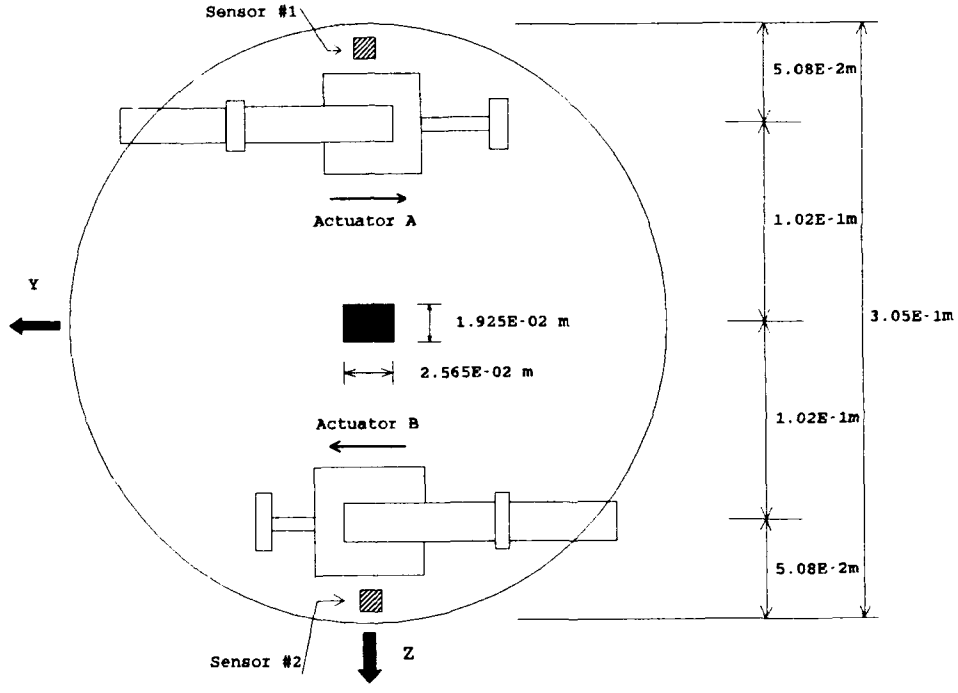

Figure 3.7 ABE Base Plate Configuration (7:53)

IV. Finite Element Modeling of the ABE

The finite element method can be thought of as a version of the assumed-mode method. Instead of defining a function which describes the deflected shape of an entire structure, the finite element method defines a shape function ψ over a small region in such a way so as to maintain the inter-element continuity of the ψ's for the entire structure. A brief review of the theory from Ref. 9 for beams in bending and torsion is presented in this Chapter. Ref. 10 contains a more detailed discussion of finite element theory. Also included in this Chapter is the development of the ABE finite element model using MSC/NASTRAN.

Theory

If we assume Bernoulli-Euler beam theory, the transverse displacements for a beam in bending can be approximated by (9:385-387)

$$v(x,t)=\sum_{i=1}^{4}\psi_i(x)v(t) \tag{4.1}$$

where the shape functions ψ satisfy the boundary conditions

$$\psi_1(0) = 1, \quad \psi'_1(0) = \psi_1(L) = \psi'_1(L) = 0 \tag{4.2}$$

$$\psi'_2(0) = 1 \quad \psi_2(0) = \psi_2(L) = \psi'_2(L) = 0 \tag{4.3}$$

$$\psi_3(L) = 1, \quad \psi_3(0) = \psi'_3(0) = \psi'_3(L) = 0 \tag{4.4}$$

$$\psi'_4(L) = 1, \quad \psi_4(0) = \psi'_4(0) = \psi_4(L) = 0 \tag{4.5}$$

For a beam in bending the general solution for static deflection v(x) is the cubic polynomial

$$v(x) = c_1 + c_2\left(\frac{x}{L}\right) + c_3\left(\frac{x}{L}\right)^2 + c_4\left(\frac{x}{L}\right)^3 \tag{4.6}$$

After substituting the given boundary conditions into equation 4.6, the beam element shape functions are found to be

$$\psi_1 = 1 - 3\left(\frac{x}{L}\right)^2 + 2\left(\frac{x}{L}\right)^3 \tag{4.7}$$

$$\psi_2 = x - 2L\left(\frac{x}{L}\right)^2 + L\left(\frac{x}{L}\right)^3 \tag{4.8}$$

$$\psi_3 = 3\left(\frac{x}{L}\right)^2 - 2\left(\frac{x}{L}\right)^3 \tag{4.9}$$

$$\psi_4 = -L\left(\frac{x}{L}\right)^2 + L\left(\frac{x}{L}\right)^3 \tag{4.10}$$

By applying equation 4.6 to the kinetic and potential energy expressions, terms for the stiffness and mass are

$$k_{ij} = \int_0^L EI\psi_i\psi_j dx \tag{4.11}$$

$$m_{ij} = \int_0^L \rho A\psi_i\psi_j dx \tag{4.12}$$

Substituting the shape functions into the expressions for the stiffness and mass results in the element stiffness and mass matrix

$$[k] = \left(\frac{EI}{L^3}\right)\begin{bmatrix} 12 & 6L & -12 & 6L \\ 6L & 4L^2 & -6L & 2L^2 \\ -12 & -6L & 12 & -6L \\ 6L & 2L^2 & -6L & 4L^2 \end{bmatrix} \tag{4.13}$$

$$[m] = \left(\frac{\rho AL}{420}\right)\begin{bmatrix} 156 & 22L & 54 & -13L \\ 22L & 4L^2 & 13L & -3L^2 \\ 54 & 13L & 156 & -22L \\ -13L & -3L^2 & -22L & 4L^2 \end{bmatrix} \tag{4.14}$$

The torsional stiffness and mass matrix for a beam element can be found in a similar manner (9:388-389). The rotation along the element is given by

$$\theta(x,t) = \psi_1(x)\theta_1(t) + \psi_2(x)\theta_2(t) \tag{4.15}$$

subject to boundary conditions

$$\psi_1(0)=1, \quad \psi_1(L)=0 \tag{4.16}$$

$$\psi_2(0)=0, \quad \psi_2(L)=1 \tag{4.17}$$

The shape functions are given by

$$\psi_1(x)=1-\frac{x}{L} \tag{4.18}$$

and

$$\psi_2(x)=\frac{x}{L} \tag{4.19}$$

Substituting equation 4.15 into the torsional expressions for potential and kinetic energy, the expressions for stiffness and mass become

$$k_{ij} = \int_0^L GJ\psi_i\psi_j dx \tag{4.20}$$

$$m_{ij} = \int_0^L \rho I_p \psi_i \psi_j dx \tag{4.21}$$

Inserting the shape functions from equations 4.18 and 4.19 into equations 4.20 and 4.21 gives the stiffness and mass matrix for a beam element in torsion.

$$[k] = \left(\frac{GJ}{L}\right)\begin{bmatrix} 1 & -1 \\ -1 & 1 \end{bmatrix} \tag{4.22}$$

$$[m] = \left(\frac{\rho I_p L}{6}\right)\begin{bmatrix} 2 & 1 \\ 1 & 2 \end{bmatrix} \tag{4.23}$$

For an undamped system, the element matrices can be formed into partitioned system mass and stiffness matrices (9:406-407). The matrices are partitioned into active and constrained degrees-of-freedom giving the equation of motion

$$\begin{bmatrix} M_{aa} & M_{ac} \\ M_{ca} & M_{cc} \end{bmatrix}\begin{Bmatrix} \ddot{U}_a \\ \ddot{U}_c \end{Bmatrix} + \begin{bmatrix} K_{aa} & K_{ac} \\ K_{ca} & K_{cc} \end{bmatrix}\begin{Bmatrix} U_a \\ U_c \end{Bmatrix} = \begin{Bmatrix} P_a \\ P_c \end{Bmatrix} \tag{4.24}$$

for the system. For $U_c = 0$, equation 4.24 can be reduced to

$$M_{aa}\ddot{U}_a + K_{aa}U_a = P_a \tag{4.25}$$

plus an additional equation of reaction constraints. Since M_{aa} and K_{aa} are sufficient to solve for the active displacement vector U_a, the second equation is not required.

Assume a solution of the form

$$(U) = (\psi)\cos\omega t \tag{4.26}$$

where (ψ) is a vector of real numbers and $\cos(\omega t)$ is a scalar multiplier. Substituting equation 4.26 into equation 4.25 gives

$$[K - \omega^2 M](\psi)\cos\omega t = 0 \tag{4.27}$$

For this equation to be valid for all time,

$$[K-\omega^2 M](\psi)=0 \qquad (4.28)$$

The solution to this equation gives the eigenvalues ω_i and their associated eigenvectors.

MSC/NASTRAN 66A Solution Solver

MSC/NASTRAN solution sequence "Real Eigenvalue Analysis" (SOL 3) was used for the preliminary modeling of the ABE. "Modal Transient Response" (SOL 112) was used in the optimization sequence so that initial conditions could be obtained. In all cases, the eigenvalue extraction method used was the Modified Givens Method with mass normalization. Unlike the Givens method, the Modified Givens Method does not require that the mass matrix be nonsingular. Instead of performing Cholesky decomposition on the mass matrix, a positive definite matrix [K + λM] is formed where λ is selected by the program to optimize the reliability and accuracy of the eigenvalue extraction. The Givens transformation method is used to convert the program defined [J] matrix to tridiagonal form. A modified Q-R algorithm is used to extract the eigenvalues from the tridiagonal matrix. The complete eigenvalue extraction procedure is contained in Reference (11:4.2-4 - 4.2-8).

Initial Beam Model

SDRC-IDEAS was used (12) as the pre/post-processor for the MSC/NASTRAN data file. The ABE finite element model consists of 11 grid points, or nodes, which are connected by NASTRAN CBAR elements. The CBAR element specifies the beam connecting nodes and references a physical and a material property table for the element. The SPC entry is used to specify the physical degrees of freedom for each grid point. For the ABE model in this thesis, the fixed end has no degrees of freedom. All other nodes are free to translate in the y-direction and rotate about the "x" and "y" axis.

The first run model consisted of a 10 element beam without the end disk or actuators. Results were computed in both SDRC-IDEAS and MSC/NASTRAN and compared to the numerical calculations performed in Chapter II. Table 4.1 gives the natural frequencies calculated by using both programs. For the simple beam without the end disk, MSC/NASTRAN quickly losses accuracy. This loss of accuracy for a simple cantilevered beam using MSC/NASTRAN is also shown in Reference (13:7.9). No reason is given in the reference for such a large error in the third and higher bending modes. The error is reduced considerably once the base disk is attached.

Table 4.1 Beam Without End Disk

Mode	Numerical	MSC/NASTRAN	Error	SDRC-IDEAS	Error
	Hz	Hz	%	Hz	%
XY-1	6.65	6.61	- 0.60	6.65	0.00
XY-2	41.72	40.88	- 2.01	41.65	- 0.17
XY-3	116.81	112.81	- 3.42	116.44	- 0.32
T-1	391.89	353.59	- 9.77	392.40	+ 0.13

The second step in the model construction was to construct a rigid body disk in SDRC-IDEAS and attach it to the beam. A concentrated mass model was also constructed using the inertia properties of the disk and as expected the dynamic results were identical. As a result, the concentrated mass model was used. Table 4.2 gives the natural frequencies of the beam with the end disk attached using both SDRC-IDEAS and MSC/NASTRAN and compares their results to the numerical results obtained in Chapter II.

Table 4.2 Beam With End Disk

Mode	Numerical	MSC/NASTRAN	Error	SDRC/IDEAS	Error
	Hz	Hz	%	Hz	%
XY-1	2.17	2.17	0.00	2.17	0.00
XY-2	28.01	27.92	0.32	27.99	- 0.07
XY-3	76.36	76.17	- 0.25	76.25	- 0.14
T-1	15.07	15.05	- 0.13	15.05	- 0.13

As mentioned earlier, the disk provides the primary component of rotatory inertia. From Table 4.2, it is apparent that the torsion mode is now well within the 0-100 Hz bandwidth of the modified ABE. Figures 4.1 - 4.4 show the mode shape comparisons for the first three bending modes and torsion. The top figure on each page is the mode shape of the beam without the end disk. The bottom figure is the mode shape for the beam with the end disk. Notice the mode shape for mode 2 and 3. The weight of the disk is causing the beam to act almost like a pinned beam at the free end. This was noticed in earlier work (7:4) on the ABE and was one of the reasons for poor control results for these modes. The modified ABE uses the structural dynamics shaker to overcome this problem.

The third step was to add the actuator non-moving mass components to the beam. Tables 3.2, 3.3, and 3.4 contain the mass and inertia properties of the actuator components. Once again, these were added to the finite element model as concentrated masses with inertial properties. The results of this step are listed in Table 4.4. This step is referred to by Jacques as the "clean configuration."

The final configuration includes the actuator mass. This configuration was not developed in SDRC-IDEAS. The natural frequencies for this configuration are presented in a later section in Table 4.4.

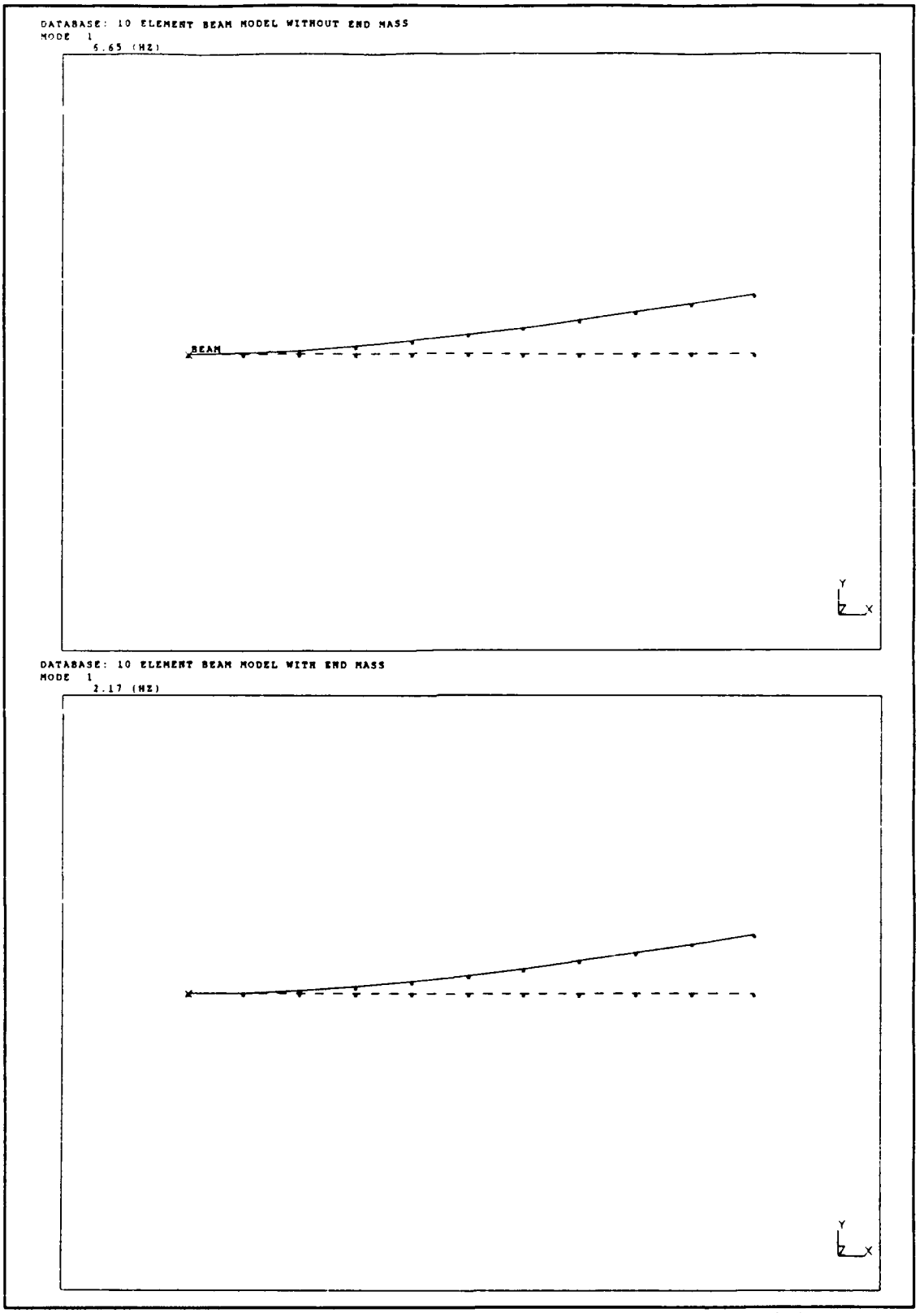

Figure 4.1 Mode 1 Bending For Beam and Beam With Disk

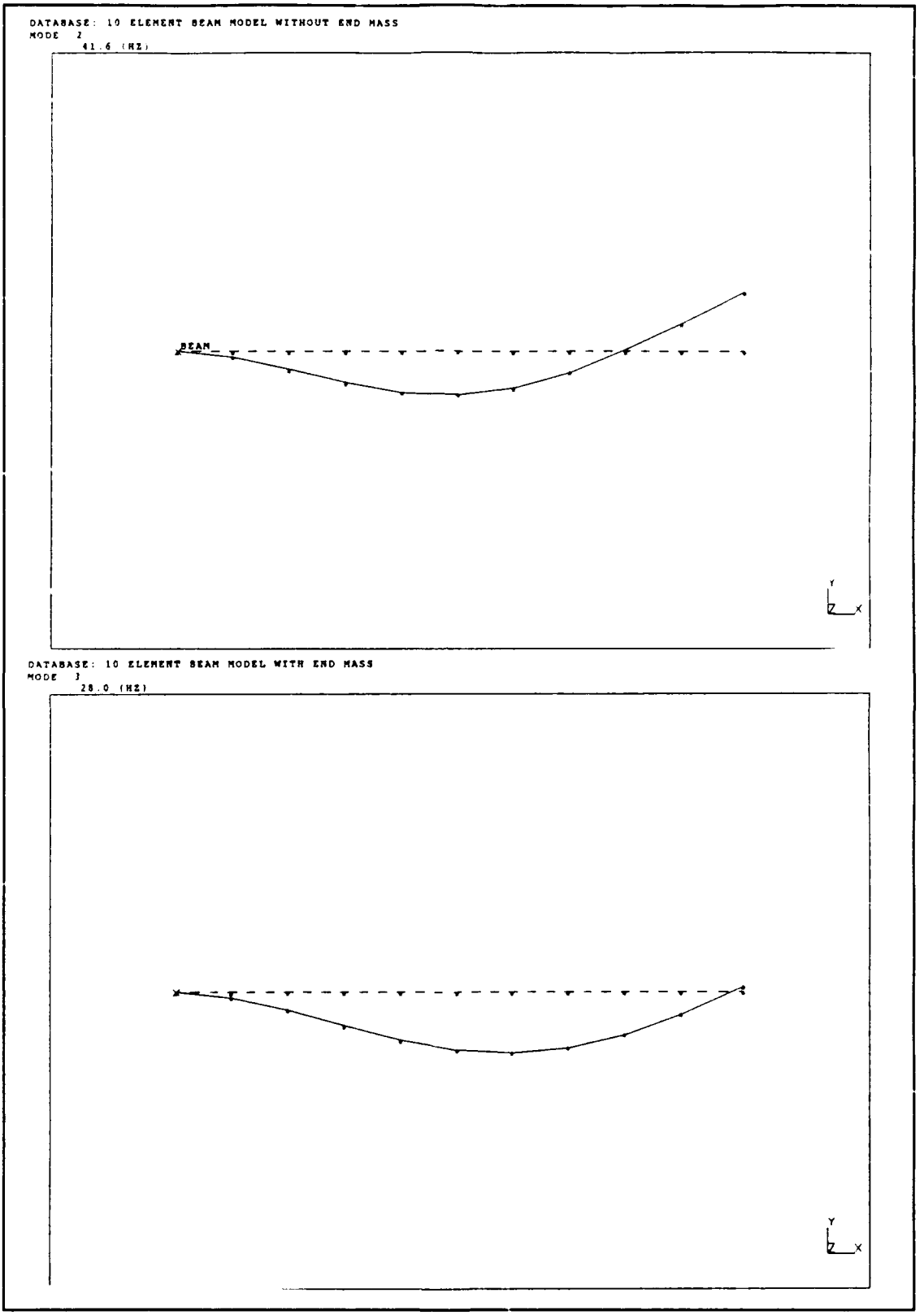

Figure 4.2 Mode 2 Bending For Beam And Beam With Disk

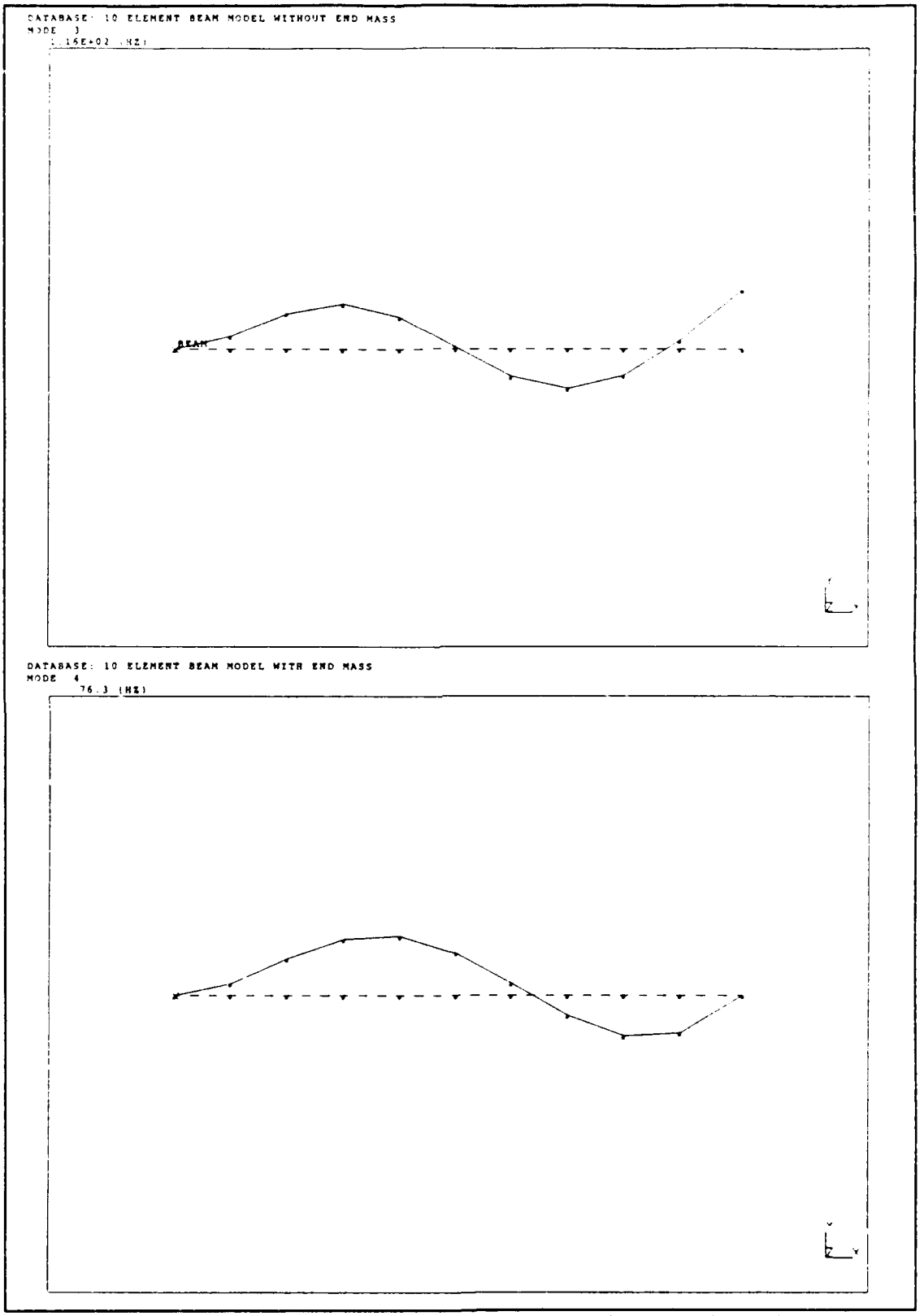

Figure 4.3 Mode 3 Bending For Beam And Beam With Disk

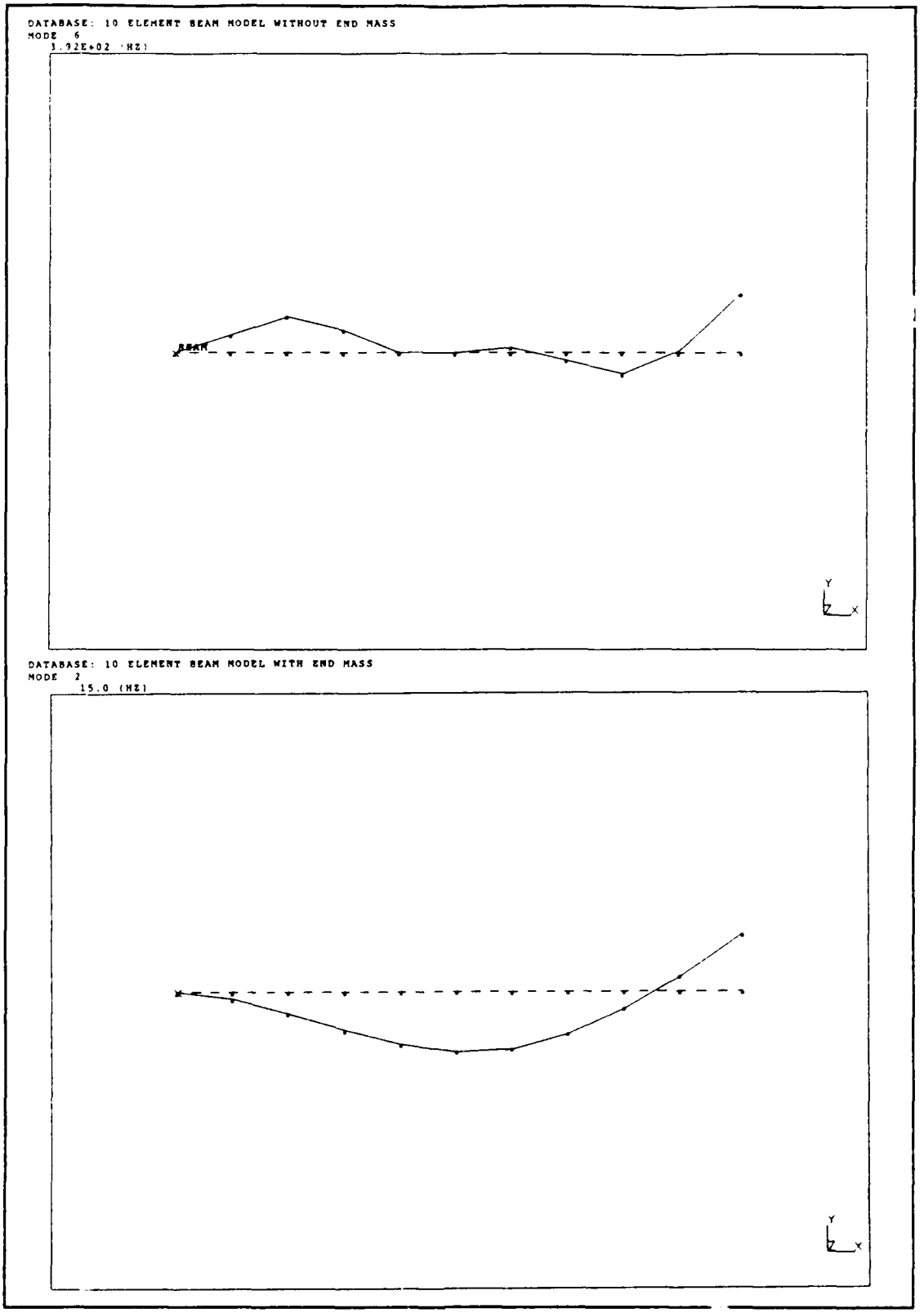

Figure 4.4 Torsion Mode For Beam And Beam With Disk

Table 4.3 Clean Configuration

Mode	MSC/NASTRAN (Hz)	SDRC/IDEAS (Hz)
XY-1	2.08	2.08
XY-2	27.74	27.81
XY-3	74.20	74.29
T-1	14.14	14.13

Model Verification

Even though the ABE is a very simple structure, the finite element model created in MSC/NASTRAN still contains modeling errors. The equations of motion from the finite element model only represent a mathematical model of the real structure. The goal in modeling is to match as closely as possible the behavior of the physical structure in the realm of interest. The realm of interest for the ABE is the dynamic behavior of the first three bending modes and the first torsion mode.

Convergence. To determine if 10 elements were sufficient, 10 beam models were created with different numbers of elements to test for convergence of the natural frequencies. Table 4.4 contains the results of this test.

Table 4.4 Convergence Test Results

Beam - Number of Elements	XY-1	XY-2	XY-3	T-1
B-2	2.174	28.182	79.088	15.045
B-3	2.174	28.029	76.848	15.045
B-4	2.174	28.000	76.447	15.045
B-5	2.174	27.992	76.333	15.045
B-6	2.174	27.989	76.290	15.045
B-7	2.174	27.988	76.271	15.045
B-8	2.174	27.987	76.262	15.045

Beam - Number of Elements	XY-1	XY-2	XY-3	T-1
B-9	2.174	27.987	76.256	15.045
B-10	2.174	27.986	76.253	15.045
B-35	2.174	27.986	76.246	15.045
Numerical	2.174	28.010	76.360	15.072
Error B-10 (%)	0.00	-0.09	-0.14	-0.18

The finite element model converges from above to a solution below the numerical results. For the 10-element beam, the accuracy is quite good for the first three bending modes and the first torsion mode.

Effects of Shear Deformation. The theoretical model was based on Bernoulli-Euler beam assumptions. These assumptions neglected shear deformation and rotatory inertia. From (9:204), the theoretical equation of motion for a short, stubby beam (Timoshenko Beam Theory) which includes these effects is

$$\left[EI\frac{\partial^4 v}{\partial x^4} - \left(p - \rho A\frac{\partial^2 v}{\partial t^2}\right)\right] - \left[\rho I\frac{\partial v^4}{\partial x^2 \partial t^2}\right] + \left[\frac{EI}{\kappa GA}\frac{\partial^2}{\partial x^2}\left(p - \rho A\frac{\partial^2 v}{\partial t^2}\right)\right] - \left[\frac{\rho I}{\kappa GA}\frac{\partial^2}{\partial t^2}\left(p - \rho A\frac{\partial^2 v}{\partial t^2}\right)\right] = 0 \tag{4.29}$$

The first term in brackets is from Bernoulli-Euler beam theory. The principal rotatory inertia is in the second term while the principal shear deformation is in the third term. The fourth term includes combined rotatory inertia and shear deformation. SDRC-IDEAS accounts for the effects of shear by the definition of a shear area ratio term. The shear area ratios are defined in SDRC-IDEAS to be (12:2.18)

$$S_{ry} = \frac{A}{Iy^2} \int_0^{a/2} \frac{Q_y^2}{a} dy \qquad (4.30)$$

$$S_{rz} = \frac{A}{I_z^2} \int_0^{b/2} \frac{Q_y^2}{b} dz \qquad (4.31)$$

where, the Q's, shown in figure 4.5, are

$$Q_y = \int_{-a/2}^{a/2} \int_0^{b/2} z dz dy \qquad (4.32)$$

$$Q_z = \int_{-b/2}^{b/2} \int_0^{a/2} y dy dz \qquad (4.33)$$

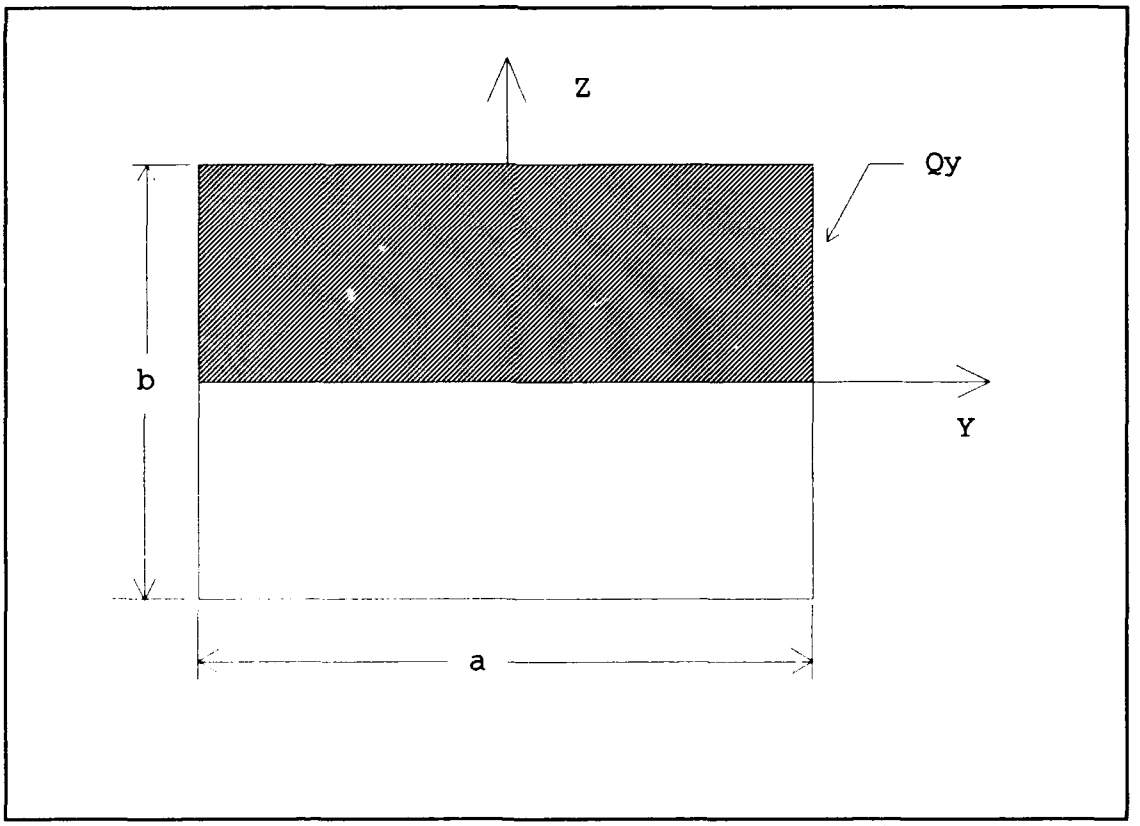

Figure 4.5 Q Area For Shear Area Ratio Calculation

Results from the 10-element beam model were computed with and without the effects of shear. Table 4.5 presents the results of these computations. The data suggests that the Bernoulli-Euler assumption was a good assumption. For the final model, however, the effects of shear and rotatory inertia will be included.

Table 4.5 Effects of Shear

Mode	B-10 W/O Shear (Hz)	B-10 With Shear (Hz)	Comparison (%)
XY-1	2.174	2.174	0.00
XY-2	27.993	27.986	-0.03
XY-3	76.280	76.246	-0.04
T-1	15.045	15.045	0.00

Comparison With Modal Test Data. The final "test" of the mathematical finite element model is to compare it to experimental data. In structural dynamics modeling, finite element analysis and modal analysis take different approaches to obtain a system model (14:86). Modal analysis models are derived experimentally while finite element models are derived mathematically. This difference makes modal analysis a good check of the finite element model. Jacques performed modal analysis on the ABE to determine its response to vibration. Table 4.6 gives the comparison between Jacques modal analysis model of the final configuration (7:39) and the MSC/NASTRAN finite element model with actuators and disk. One reason for the large difference in second and third mode bending may be because displacements in the x-direction were constrained in MSC/NASTRAN. Another reason for the difference is because of the exclusion of the actuator dynamics from the finite element model. The section on damping will address the actuator dynamics.

Modal Transformation

The finite element model equation of motion which includes the mass, stiffness, and damping matrices as well as the control inputs is

Table 4.6 Final Configuration Model Comparison

Mode	Jacques Modal Test (Hz)	MSC/NASTRAN (Hz)	Error (%)
XY-1	1.97	1.93	- 2.03
XY-2	23.43	27.74	+ 18.40
XY-3	62.92	73.62	+ 14.53
T-1	13.35	13.07	- 2.10

$$[m](\ddot{q}) + [c](\dot{q}) + [k](q) = [b](u) \tag{4.34}$$

where q is a vector of generalized coordinates, [b] is the control input distribution matrix, and u is a vector of control forces. Assuming that only the first two bending modes and the first torsion mode are present in the response, then q is a 3x1 vector and the generalized coordinates are defined as

q1 = displacement of node 11.

q2 = rotation of node 11.

q3 = displacement of node 5.

In terms of the physical coordinates, the generalized coordinates are

$$q_1 = \frac{1}{2}(-y_{11a} + y_{11b}) \tag{4.35}$$

$$q_2 = \frac{1}{2}(y_{11a} + y_{11b}) \tag{4.36}$$

$$q_3 = y_5 \tag{4.37}$$

In terms of the generalized coordinates, the measured coordinates are then

$$\dot{y}_{11a} = -\dot{q}_1 + \dot{q}_2 \tag{4.38}$$

$$\dot{y}_{11b} = \dot{q}_1 + \dot{q}_2 \tag{4.39}$$

$$\dot{y}_5 = \dot{q}_3 \tag{4.40}$$

If we assume the modes are uncoupled and assume modal damping, equation 4.34 can be decoupled by using modal coordinates η and the modal matrix of right eigenvectors Φ to define a transformation such that

$$[q] = \Phi\,[\eta] \tag{4.41}$$

where the eigenvectors have been normalized such that

$$\Phi^T[m]\Phi = [M] = [I] \tag{4.42}$$

Equation 4.34 can then be written as

$$(\ddot{\eta}) + [2\zeta\omega](\dot{\eta}) + [\omega^2](\eta) = \Phi^T[b](u) \tag{4.43}$$

The matrix $[2\zeta\omega]$ is a diagonal matrix where the i^{th} element represents damping for the i^{th} mode. The matrix $[\omega^2]$ is a diagonal matrix where the diagonal entries are the eigenvalues for equation 4.43.

Damping

Damping is inherent in any structure, but predicting how much damping is in a structure is difficult. Modal testing provides a good approach to help understand the effects damping has on a structure. From modal analysis data, Jacques estimated how much damping was present in the ABE. Table 4.6 gives the experimentally determined damping values for both the "clean configuration" and the final configuration with actuators attached. The viscous damping factor ζ is the ratio

c/c_{cr} where c_{cr} is the critical damping factor. For large space structures, the damping factor is typically very small.

By including the actuator damping with the beam damping, the stability effects of the actuators cannot be determined. Inman (15:508-

Table 4.6 Modal Analysis Damping Values (7:39,41)

Mode	Clean Configuration (ζ)	Final Configuration (ζ)
XY-1	0.00129	0.0640
XY-2	0.00375	0.0236
XY-3	0.00086	0.0121
T-1	Not Determined	0.00839

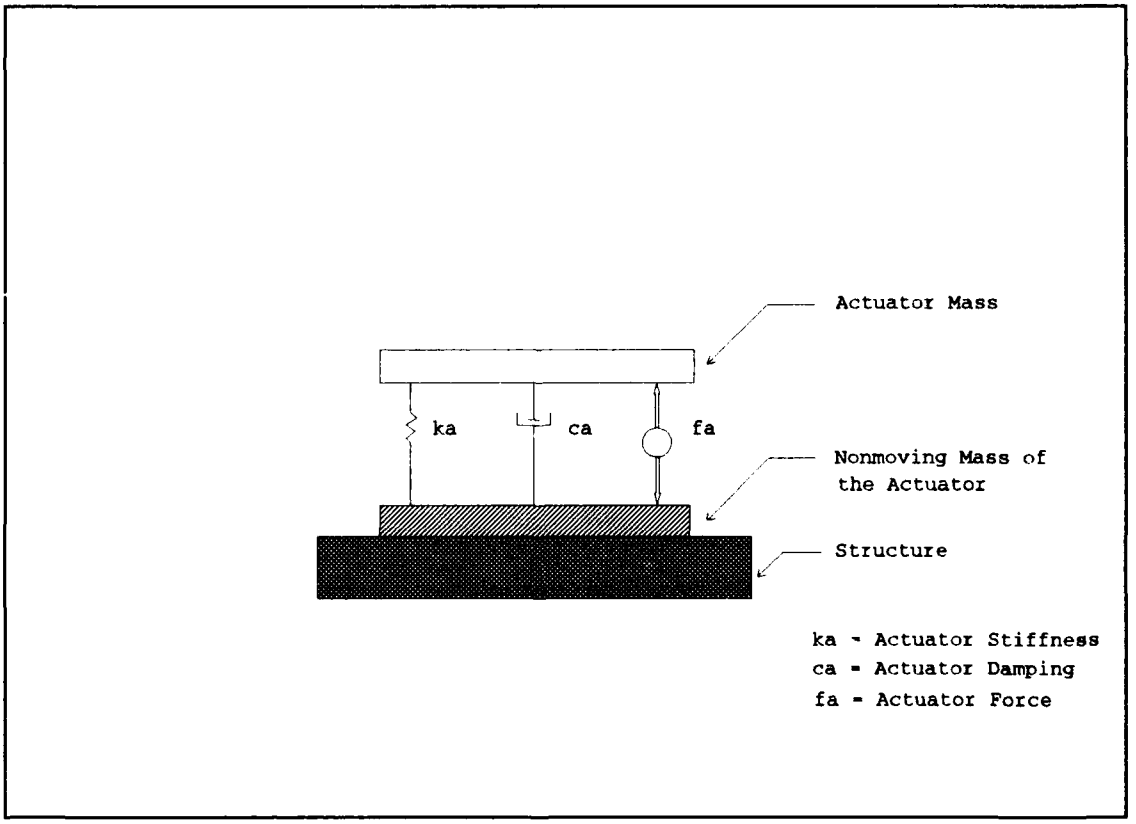

Figure 4.6 Simple Model of Actuator Dynamics (15:508)

513) shows the effects of actuator dynamics on the overall system stability. Figure 4.6 shows a simple model of the actuator dynamics. If actuator dynamics are neglected, the mathematical "answer" to how much velocity feedback gain should be added to achieve a desired response is as much as is necessary. Inman presents examples which show how the system can go unstable as the gain is increased. When the actuator dynamics are introduced in the single-degree-of-freedom model shown in Figure 4.6, the [C] and [K] matrices in the equations of motion become coupled. If velocity feedback is used like it is in the ABE, the [C] matrix becomes coupled and unsymmetric. This limits the amount of gain that can be added before the actuators cause the system to destabilize.

Since this thesis is modeling the modified ABE, actuator damping will be treated as viscous modal damping. Proportional, or Rayleigh, damping can be used to model the damping where

$$[C] = \alpha[K] + \beta[M] \tag{4.44}$$

Matrix [C] is an orthogonal damping matrix (10:377) because it permits modes to be uncoupled by the eigenvectors associated with the undamped eigenvalue problem. The damping ratio is related to the stiffness and mass proportional damping constants α and β by

$$\zeta = \frac{1}{2}\left(\alpha\omega + \frac{\beta}{\omega}\right) \tag{4.45}$$

α and β can be found in terms of ω and ζ by

$$\alpha = 2(\zeta_2\omega_2 - \zeta_1\omega_1)/(\omega_2^2 - \omega_1^2) \tag{4.46}$$

$$\beta = 2\omega_1\omega_2(\zeta_1\omega_2 - \zeta_2\omega_1)/(\omega_2^2 - \omega_1^2) \tag{4.47}$$

Using data in Table 4.6, α = 2.2072E-04 and β = 1.5219. The graph for $0 \leq \omega \leq 400$ rad/sec is shown in Figure 4.7 where the Rayleigh damping

curve is the sum of the mass proportional damping curve and the stiffness proportional damping curve.

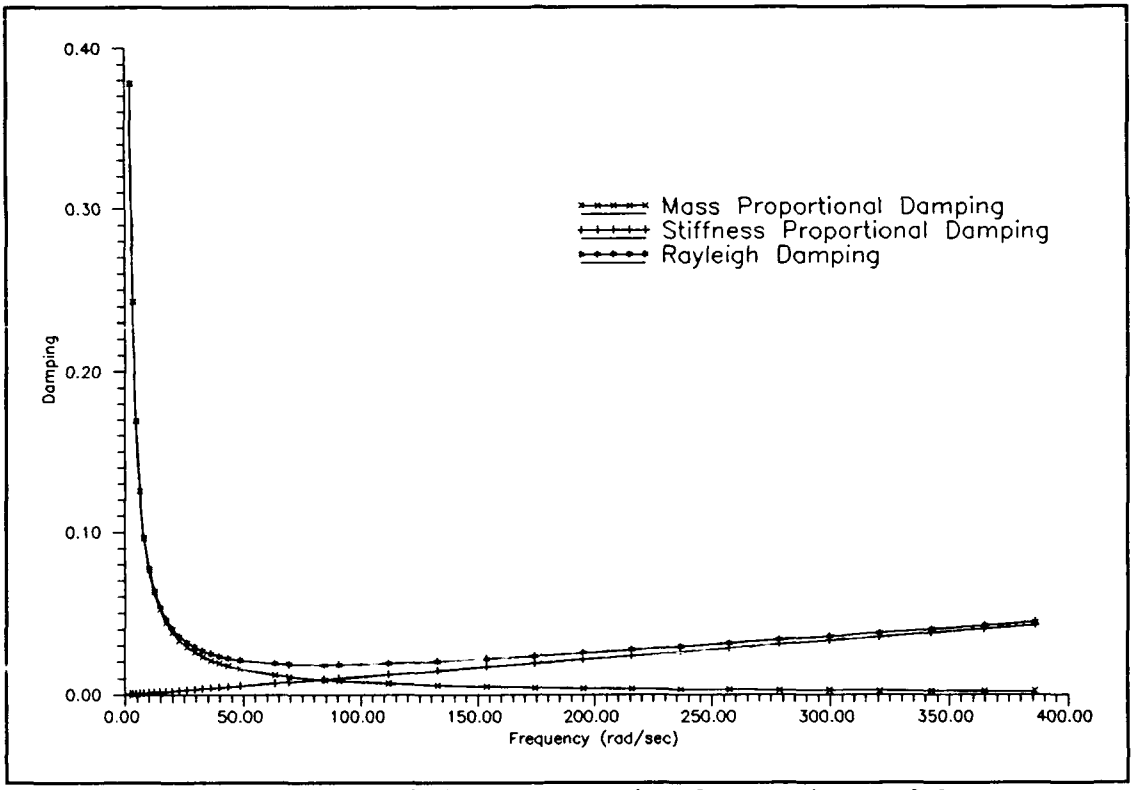

Figure 4.7 Rayleigh (Proportional) Damping Model

Initial Conditions

Structures are normally designed to withstand some given design conditions. When the design conditions are applied, dynamical systems will exhibit a response. This response is needed as initial conditions for each structural iteration in the structural/control optimization. Miller, Vipperla and Venkayya (3:928) demonstrated that it is not adequate to specify the initial response conditions for a structure being optimized and then hold these constant for the iteration process. As the structural property is varied (cross-sectional area) in the

optimization process, each iterated structure will exhibit different initial conditions. Therefore, it is necessary to specify the design conditions, such as the applied load, and then solve for the initial conditions for each iteration of the structure.

An impact load was included in the MSC/NASTRAN finite element solution process. To obtain the initial conditions, the TLOAD data entry is used to specify a load table TABLED1 and a scale factor entry DAREA. The equation for the force input in MSC/NASTRAN is

$$P(t) = A[F(t-\tau)] \tag{4.48}$$

where the time delay τ=0. The scale factor A was selected to be 1000 N. The load table is shown graphically in Figure 4.7. The table is shown graphically to illustrate how MSC/NASTRAN reads input tables. If the three points at t=0.001, t=0.002, and t=0.003 where the only points

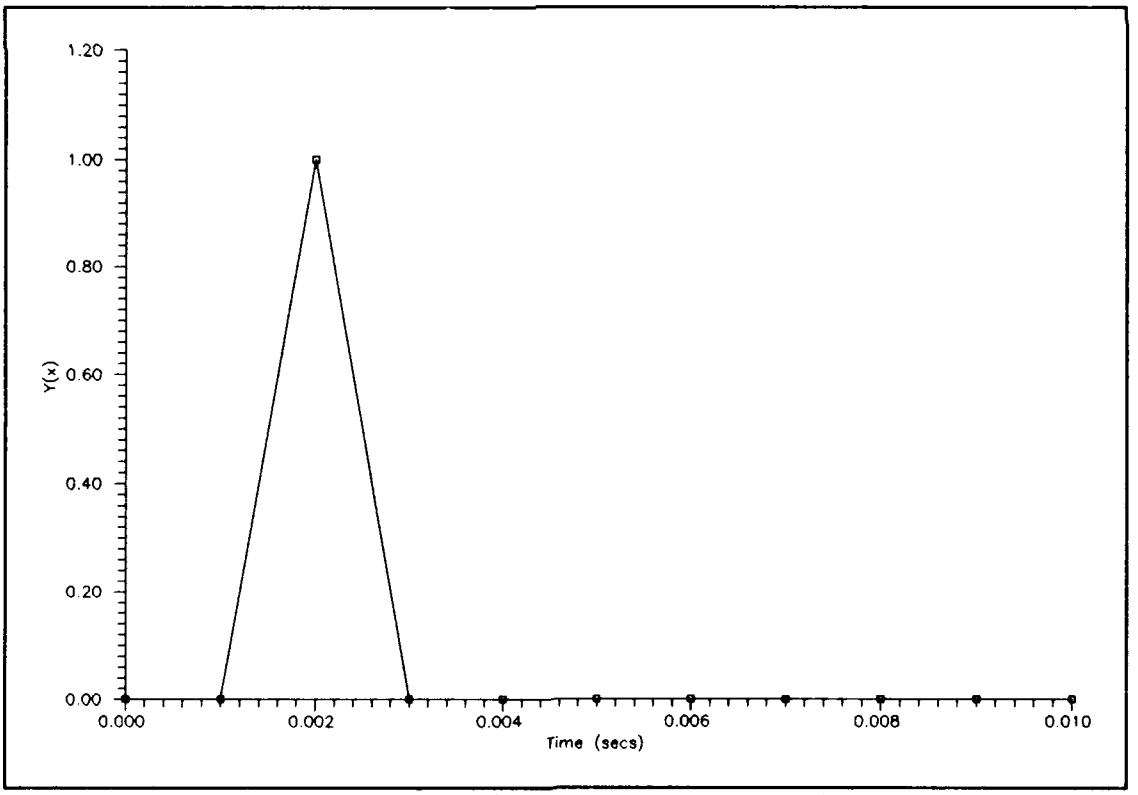

Figure 4.8 MSC/NASTRAN Force Area Chart

specified, an infinite load would be applied. This is because MSC/NASTRAN extrapolates tables. Since no value is specified after t=0.003, the slope from t=0.002 to t=0.003 would be continued after t=0.003. To prevent an infinite load, values of zero must be specified on both sides of the load. The initial conditions for the structure/control optimization were chosen at t=0.003. This has the effect of "turning on" the control system at t=0.003. The ABE undamped and damped response to the initial conditions are shown in Figures 4.9 and 4.10.

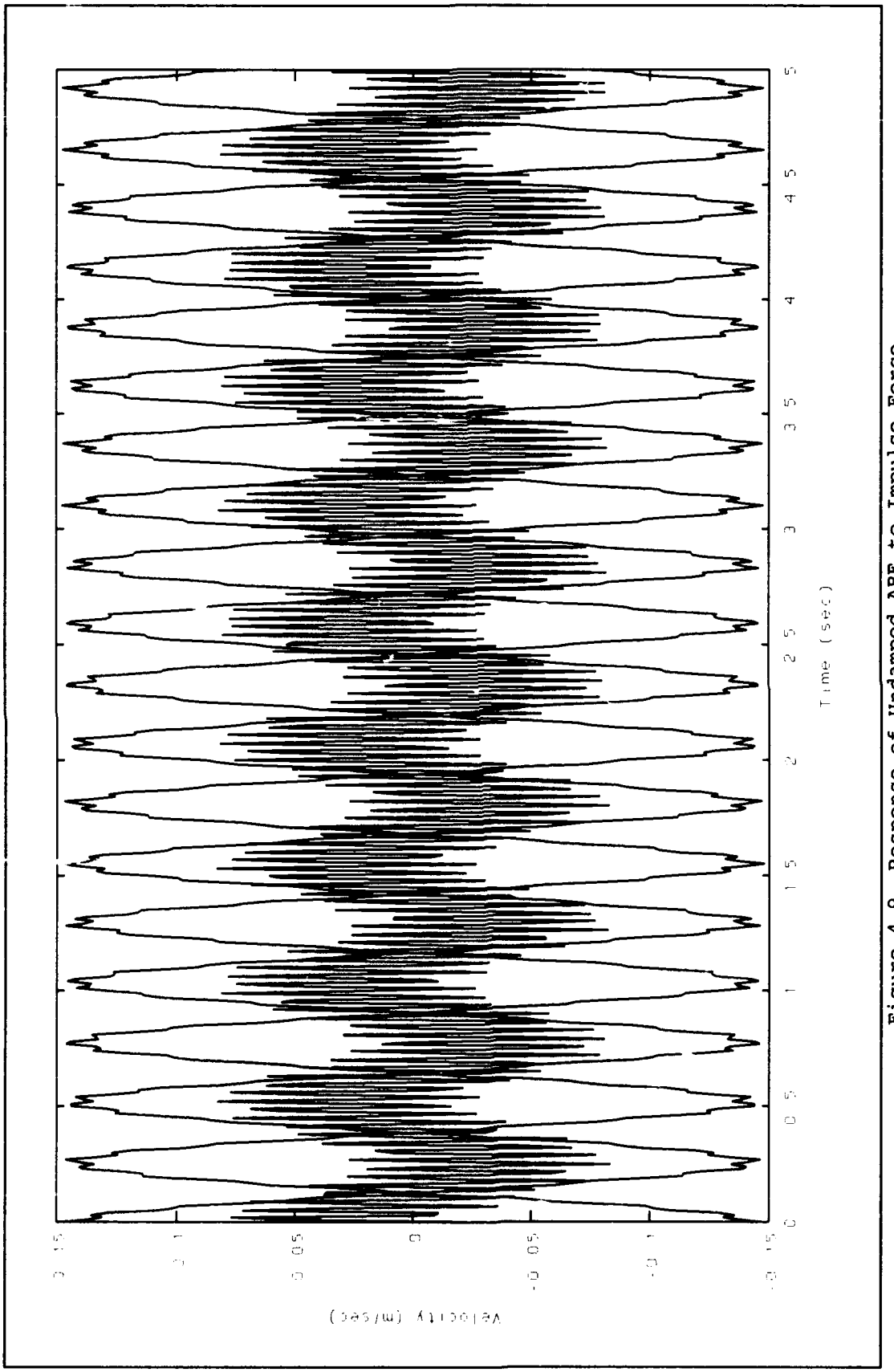

Figure 4.9 Response of Undamped ABE to Impulse Force

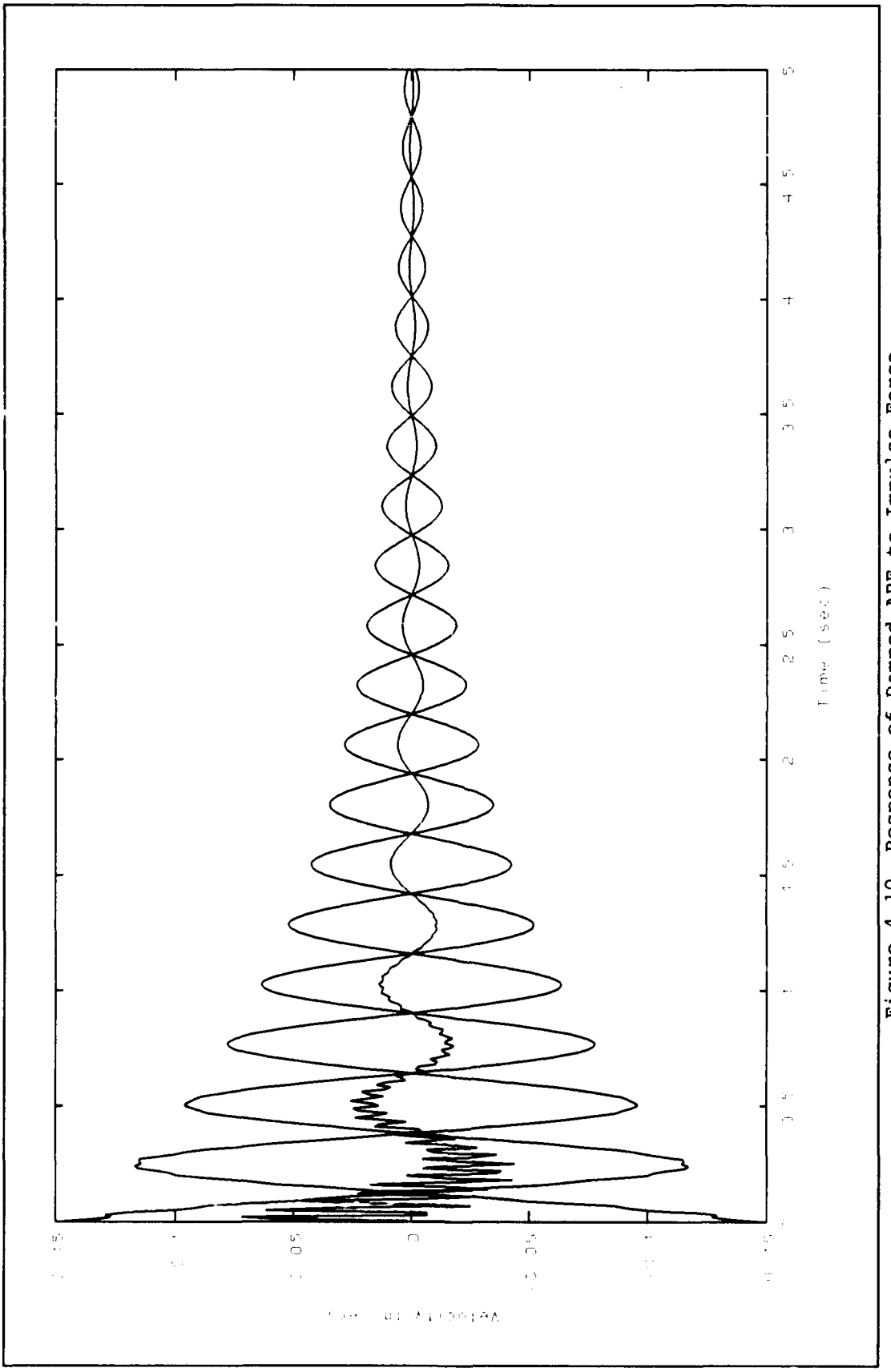

Figure 4.10 Response of Damped ABE to Impulse Force

V. Control Theory

The state-space formulation is detailed in this Chapter. LQR theory and the selection of the Q and R weighing matrices are presented.

State-Space Formulation

After normalizing the eigenvectors with respect to the mass matrix, the linear differential equations of motion from equation 4.43 can be written in state-space form. The standard state-space format for the state equation is

$$[\dot{x}] = A[x] + B[u] + [w] \tag{5.1}$$

where the state vector is

$$[x]^T = [\eta_1, \eta_2, \eta_3, \dot{\eta}_1, \dot{\eta}_2, \dot{\eta}_3] \tag{5.2}$$

and the input vector is

$$[u]^T = [F_A, F_B, F_C] \tag{5.3}$$

The plant matrix A and the input distribution matrix B are

$$A = \begin{bmatrix} 0 & I \\ -\omega^2 & -2\xi\omega \end{bmatrix} \tag{5.4}$$

$$B = \begin{bmatrix} 0 \\ \Phi^T b \end{bmatrix} \tag{5.5}$$

and [w] is a process noise or input disturbance vector.

The output equation can be written as

$$[y] = C[x] + D[u] + [v] \tag{5.6}$$

The output distribution matrix C is

$$C=[C_p\Phi \,|\, C_V\Phi] \tag{5.7}$$

where the partitions C_p and C_V are the position and velocity sensor distributions respectively. The matrix D allows the output variables to be controlled by [u] while [v] is a measurement noise term. The schematic of the state-space model is shown in Figure 5.1.

This thesis will assume that the plant disturbance or process noise term [w] is negligible. In addition, the sensors are assumed to be perfect and there is no control over the output vector. The implies that [v]=0 and D=0. The input distribution matrix [b] is defined to be

$$b=\begin{bmatrix} -1 & 1 & 0 \\ 1 & 1 & 0 \\ 0 & 0 & 1 \end{bmatrix} \tag{5.8}$$

Since position feedback is not used, C_p=0. C_V is given by

$$C_V=\begin{bmatrix} -1 & 1 & 0 \\ 1 & 1 & 0 \\ 0 & 0 & 1 \end{bmatrix} \tag{5.9}$$

thus, for collocated sensors and controllers, $B=C^T$. The final state-space formulation is

$$[\dot{x}]=A[x]+B[u] \tag{5.10}$$

$$[y]=C[x] \tag{5.11}$$

Linear Quadratic Regulator Theory

Ref. 16 covers LQR theory (16:6.1-6.9) in detail. A brief review of the theory is presented.

If full state feedback is used, the control input can be defined as a linear combination of the state variables
that make the closed-loop system

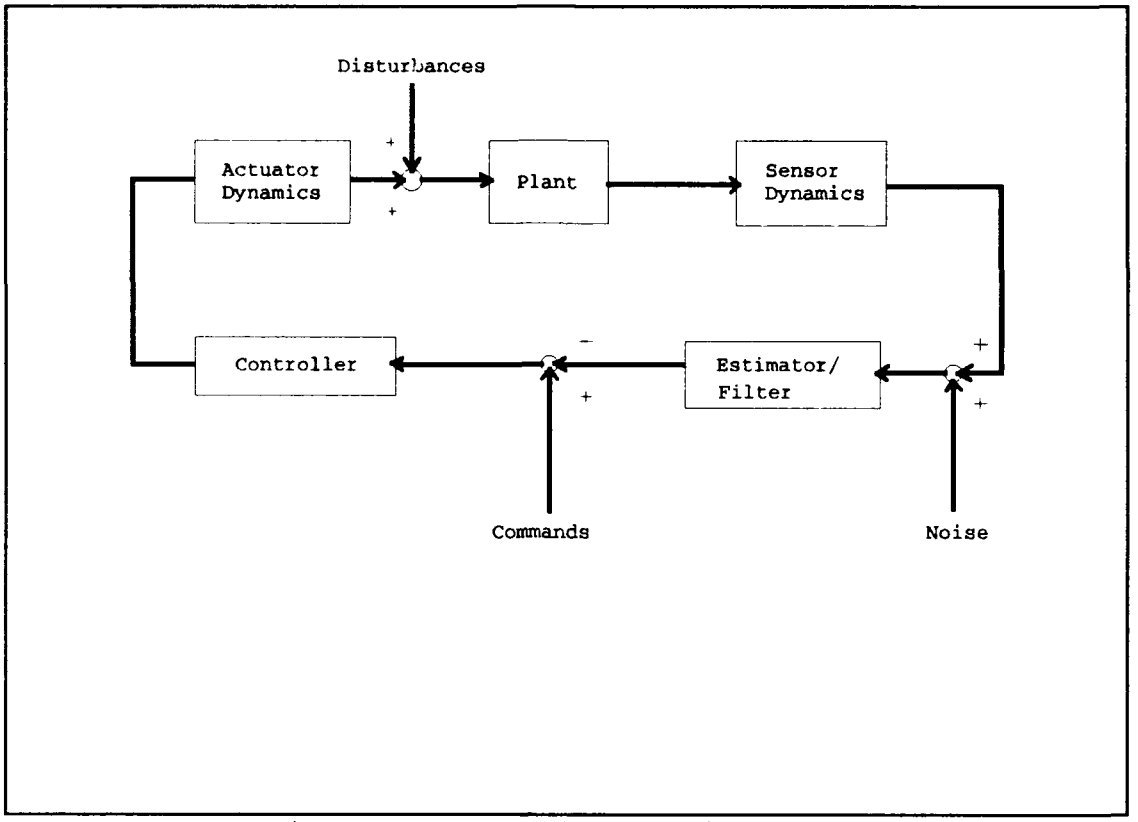

Figure 5.1 Control Schematic (1:519)

$$u(t) = -K_c x(t) \tag{5.12}$$

$$\dot{x}(t) = Ax(t) + B[-K_c x(t)] \tag{5.13}$$

$$\dot{x}(t) = [A - BK_c]x(t) \tag{5.14}$$

asymptotically stable. The control gain K_c can be found by minimizing the performance index

$$J_c = \int_0^\infty [x^T(t) Q_c x(t) + u^T(t) R_c u(t)] dt \tag{5.15}$$

where Q_c and R_c are symmetric, real, positive definite matrices chosen by the design engineer according to the importance of the state and of the controls. From (16:6.1-6.2), this can be interpreted as "we wish to find a control law u(t) such that the integral-squared-error of the

deviation of the state trajectories from their nominal are kept small without using a great deal of control energy." From optimal control theory, the gain matrix K_c in equation 5.12 which minimizes equation 5.14 is given by

$$K_c = R_c^{-1} B^T S \tag{5.16}$$

where S is the solution to the algebraic Riccati equation

$$A^T S + SA - SBR_c^{-1} B^T S + Q_c = 0 \tag{5.17}$$

Since position feedback is not used for this work, however, the gain matrix K_c is not guaranteed to be optimal. This is the basis of a Linear Quadratic Regulator.

Generally, the state variables cannot be measured directly. An estimator is required to reconstruct the states from the sensor outputs. The estimator has the form

$$[\dot{\hat{x}}] = A[\hat{x}] + B[u] + K_o[y - \hat{y}] \tag{5.18}$$

$$[\hat{y}] = C[\hat{x}] \tag{5.19}$$

where [x] and $[\hat{y}]$ are the estimated state vector and the estimated output vector. The observer gain K_o must be chosen so that the error defined by

$$[e] = [\hat{x}] - [x] \tag{5.20}$$

is stable. Since the state vector is not available, the control input is also based on the estimated state vector

$$[u] = -K_o[\hat{x}] \tag{5.21}$$

K_o is selected to minimize the estimator cost function

$$J_o=\int_0^\infty [x^T(t)Q_o x(t)+y^T(t)R_o y(t)]dt \qquad (5.22)$$

where Q_o represents the process noise covariance and R_o represents the measurement noise covariance. This is the basis of a Kalman filter. When a Kalman filter is added to a Linear Quadratic Regulator, the result is a Linear Quadratic Gaussian compensator.

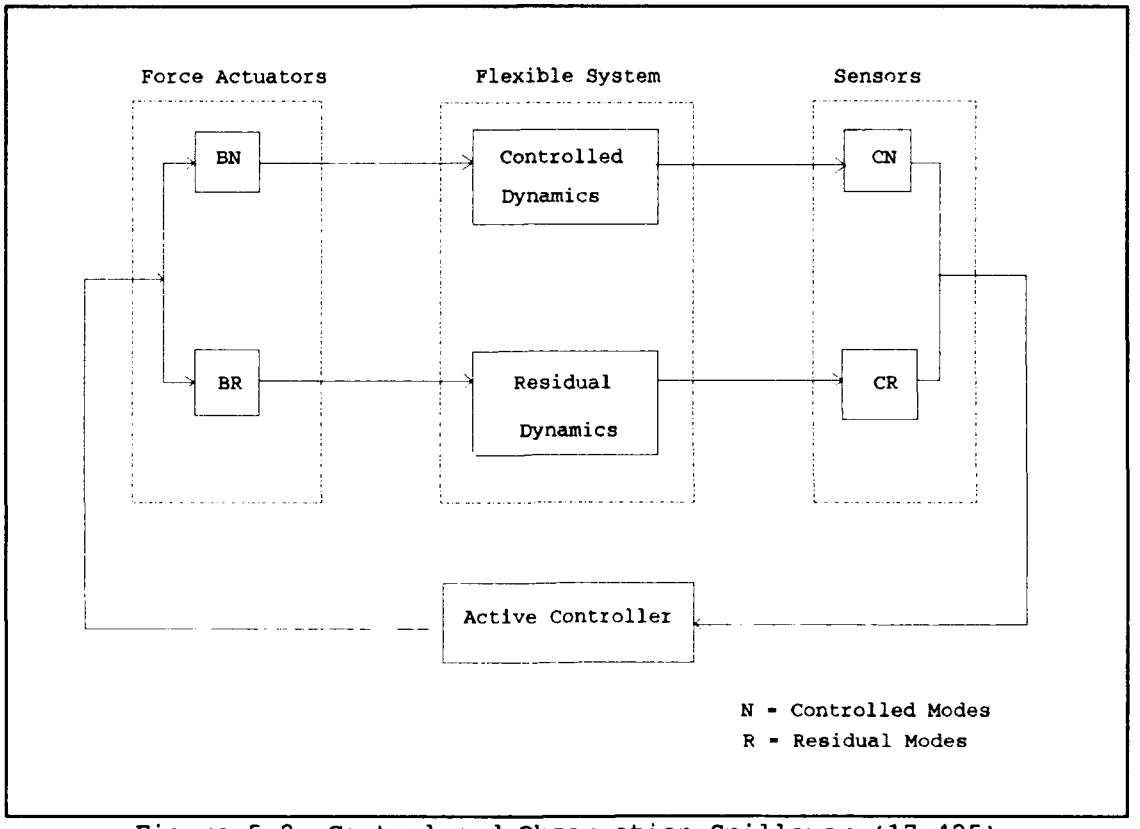

Figure 5.2 Control and Observation Spillover (17:425)

If residual modes are present, they will result in spillover. Figure 5.2 shows a schematic of spillover. If the sensor outputs are contaminated by the residual modes through C_R, the effect is known as observation spillover. If the control actuators are excited by the residual modes through B_R, the effect is known as control spillover. The effects of spillover can be detrimental. Calico and Janiszewski (18) showed that eliminating either observation or control spillover was

sufficient to ensure stability of the suppressed modes. Jacques (7) attempted to demonstrate modal suppression on the ABE by eliminating observation spillover. The results achieved while trying to suppress bending mode 2 were partially successful. The reason for the partial success was attributed to the estimator model. Balas (17:421) presents two estimator designs. The first is based on the Kalman filter. The Kalman filter is used by Balas if the system signal-to-noise ratios are not very high. If the system signal-to-noise ratios are sufficiently high, the system is treated as deterministic and the estimator used is a Luenberger observer. The reason for this is the estimator error term in equation 5.19 will contain additive noise terms with the Kalman filter but these terms are absent with the Luenberger observer. Since system noise was attributed in part to poor estimator performance, additional work on the ABE should examine the effect of estimator choice on the control model.

For the integrated structure/control optimization procedure implemented in this thesis, it is assumed that the state is completely observable. LQR theory will be used as the optimal control law without the introduction of a Kalman filter. MATLAB uses eigenvector decomposition of an associated Hamiltonian matrix to solve the LQR problem (19:CR-38,CR-39). For convenience, the "c" and "o" subscript will dropped. Parameters used for the remainder of this work refer to the controller.

Choice of Weighing Matrices Q and R

In the past, an optimized structure was given to a control engineer to design an optimal control system. The engineer selected Q and R subject to the importance of the state or the control system so that a desired dynamic response was achieved. Venkayya and Tischler (20:433-434) have proposed that the selection of Q and R should not be arbitrary, but that their selection should ensure that the cost function

J provides a measure of some appropriate physical quantity, such as total system energy.

From Chapter IV, the finite element equation of motion is

$$m\ddot{q}(t)+c\dot{q}(t)+kq(t)=bu(t) \tag{5.23}$$

If J is defined as

$$J=\int_0^\infty [\theta_m \dot{q}^T m\dot{q}+\theta_k q^T kq+\theta_R u^T b^T k^{-1} bu]\,dt \tag{5.24}$$

for positive scaling parameters θ_m, θ_k, and θ_R, then J is the absolute sum of the kinetic, strain, and potential energies. Total system energy is thus minimized to satisfy the LQR control law. Considering the modal coordinate transformation 4.41 and the mass normalization 4.42, Q and R can be written as

$$Q=\begin{bmatrix} \theta_m \bar{I} & \bar{0} \\ \bar{0} & \theta_k[\omega_i^2] \end{bmatrix} \tag{5.25}$$

$$R=\left[\theta_R b^T k^{-1} b\right] \tag{5.26}$$

For the optimization in Chapter VI,

$$\theta_m = \theta_k = \theta_Q \tag{5.27}$$

VI. Integrated Structure/Control Optimization

This Chapter introduces the structure/control optimization procedure. The effects of Q/R selection on the control system specifications are examined. In addition, two optimization approaches are presented. The first approach is based on minimizing mass and total system energy. The second approach, Onada's method, develops a relationship between control system energy and control system mass. The combined mass of the structure and the control system are then minimized. Finally, the ABE is optimized using the constraints of the existing control system.

Optimization Algorithm

The combined optimization of a structure and its control system can be divided into three distinct phases as shown in Figure 6.1. An initial structure is specified to start the first phase. A finite element program is used to solve for the eigenvalues and eigenvectors of the structure. With the eigenvalues and eigenvectors determined, the plant matrix [A] can be constructed for the state-space equations. The state-space equations are used in the second phase to solve the optimal control problem. Depending on the output from the second phase, the third phase would use an optimization procedure to determine a "direction" to iterate the first phase input parameters.

This thesis will not use a true optimization procedure. Instead, a range of structural parameters will be used in a form of "sensitivity analysis." The structural parameter which is varied is the cross-sectional area. To maintain a proportional cross-section, the side dimension "b" is defined in terms of "a" based on the current ABE. "a" is then varied in 10% increments. Table 6.1 lists the cross-sectional areas and the moment's of inertia for the 17 beam iterations. Figure

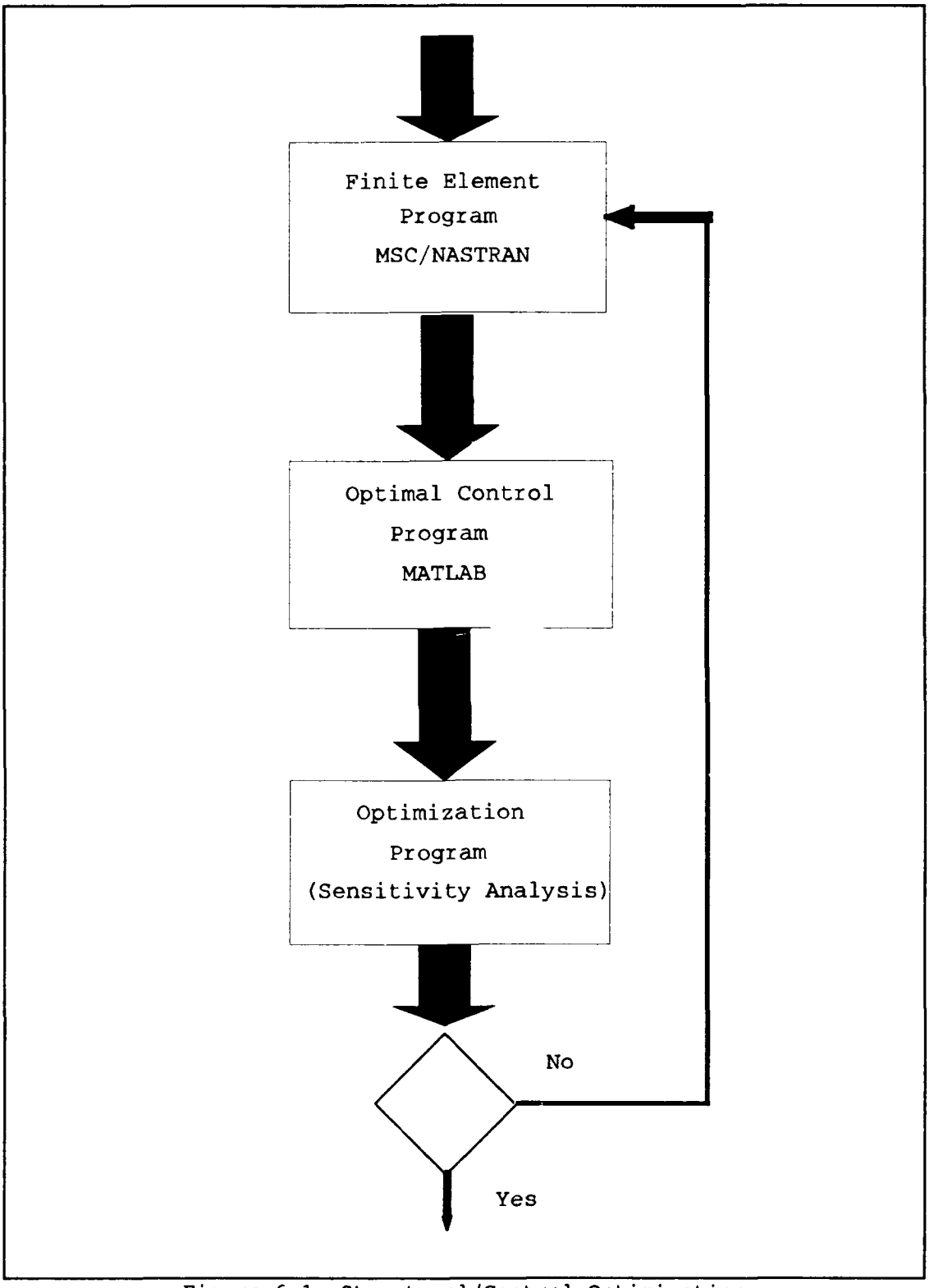

Figure 6.1 Structural/Control Optimization

6.2 shows the linear relationship between the structural mass and the cross-sectional area.

The finite element procedure outlined in Chapter IV was used for each of the design iterations. The output obtained from MSC/NASTRAN included:

1. The natural frequencies.
2. The mass normalized eigenvectors.
3. The [k] matrix.
4. The initial conditions subject to a 1000 N force.

Table 6.1 Structural Iteration Properties

Number	Area (m^2)	I_y (m^4)	I_z (m^4)	J (m^4)
1	7.900E-05	3.903E-10	6.930E-10	8.426E-10
2	1.234E-04	9.530E-10	1.692E-09	2.057E-09
3	1.778E-04	1.976E-09	3.508E-09	4.266E-09
4	2.419E-04	3.661E-09	6.500E-09	7.903E-09
5	3.160E-04	6.245E-09	1.109E-08	1.348E-08
6	3.999E-04	1.000E-08	1.776E-08	2.160E-08
7	4.938E-04	1.525E-08	2.707E-08	3.292E-08
8	5.975E-04	2.232E-08	3.964E-08	4.819E-08
9	7.110E-04	3.162E-08	5.614E-08	6.825E-08
10	8.345E-04	4.355E-08	7.732E-08	9.401E-08
11	9.678E-04	5.857E-08	1.040E-07	1.264E-07
12	1.111E-03	7.719E-08	1.370E-07	1.666E-07
13	1.264E-03	9.993E-08	1.774E-07	2.157E-07
14	1.427E-03	1.273E-07	2.261E-07	2.749E-07
15	1.600E-03	1.601E-07	2.842E-07	3.455E-07
16	1.782E-03	1.987E-07	3.528E-07	4.290E-07
17	1.975E-03	2.440E-07	4.331E-07	5.267E-07

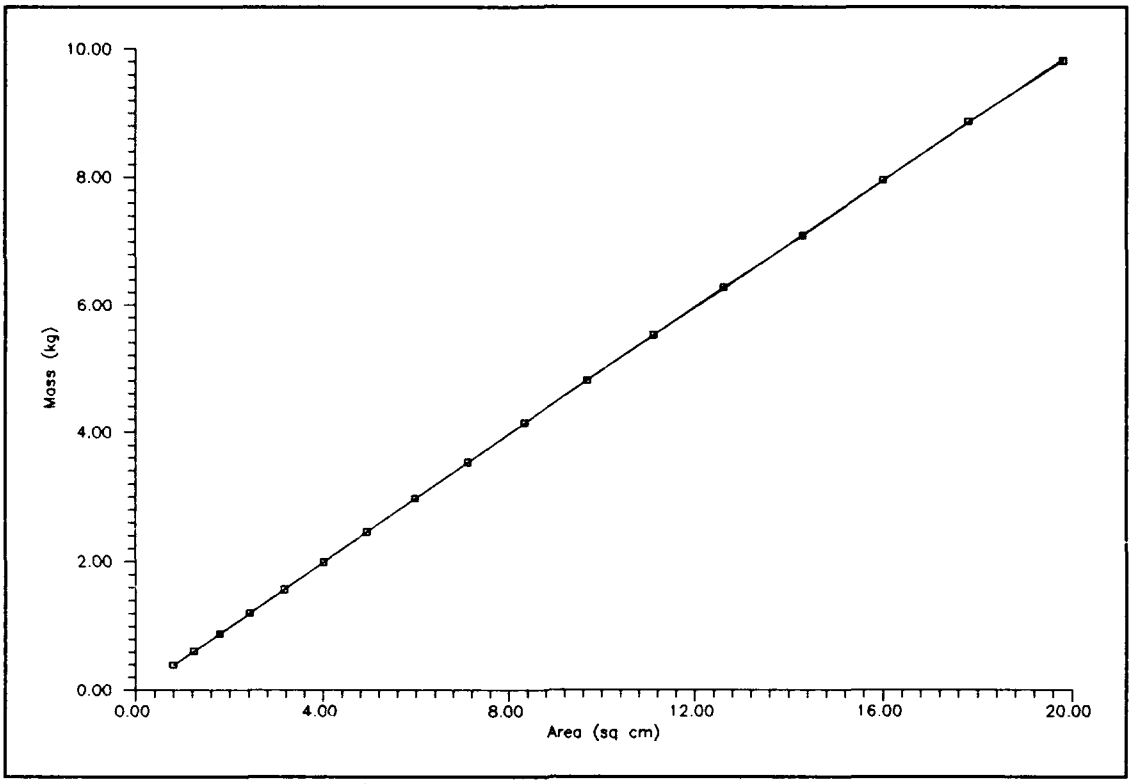

Figure 6.2 Mass versus Area

The control optimization phase was solved using MATLAB. A MATLAB .M file (Appendix D) was written to apply Linear Quadratic Regulator theory to the finite element output data. The MATLAB .M file produced data files containing the following information:

1. The optimum gain matrix K.
2. The Riccati solution matrix S.
3. The cost function J.
4. The initial control force for each actuator.
5. The control energy function C.
6. The closed-loop damping ratios.
7. The closed-loop frequencies.

Each iteration was performed using Q and R values as defined is Chapter V as well as constant Q and R values. In addition, a weighing value was applied to the Q and R values to determine the effect weighing has on the optimization. The basic nomenclature scheme used is

Q ## = Variable Q as defined in Equation 5.25

R ## = Variable R as defined in Equation 5.26

QI ## = Constant Q as defined in Equation E.1

RI ## = Constant R as defined in Equation E.2

The first # in the scheme represents the weight applied to θ_Q. The second # represents the weight applied to θ_R. The weighing #'s used were combinations of 1.0 and 0.3. Table E.1 in Appendix E provides the weighing used in the optimization.

The final phase of the combined optimization procedure uses data from the second phase to select a search direction in which to vary the input structural parameters. As mentioned earlier, a search direction is not used. Instead, a range of structural parameters are used to chart the effects of the various optimization methods. The data needed from the second phase depends on the optimization method chosen. In the following sections, the cost function J and the control energy function C are used. Other methods contained in the literature have demonstrated the use of the initial control force, the closed-loop damping ratios, and the closed-loop eigenvalues to find a search direction to iterate the structural parameters.

Relationship of Q and R Selection To Control Response

To show the effects of Q and R selection on the optimization process, viscous damping from the structure and actuators will be neglected. With viscous damping neglected, only damping from the velocity feedback control law will effect the system. Figures 6.3 and 6.4 show the simulated undamped response of beam iteration #1 and #17 to the applied impulse force. The measurements are taken from positions 11a, 11b, and 5 on the beam.

From the velocity feedback control law, damping is added to the closed loop response. The amount of damping depends on the gain K which

is selected by LQR theory. The closed-loop plant matrix from equation 5.14 is repeated here.

$$A_{CL} = [A - B*K] \tag{6.1}$$

The effect of selecting Q and R by Equations 5.24 and 5.25 on control theory is to keep the closed-loop damping ratio and the percent overshoot constant throughout the structure/control iteration. Figures 6.5 and 6.6 show the closed loop damping ratios and the percent overshoot for Q and R selected by Equations 5.24 and 5.25. Figures 6.7 and 6.8 show the damping ratios and the percent overshoot when Q and R are held constant. From these figures, it is easy to see how the weighing parameters θ on Q and R can be selected to achieve a desired control response. If we plot the damped closed-loop frequency versus σ

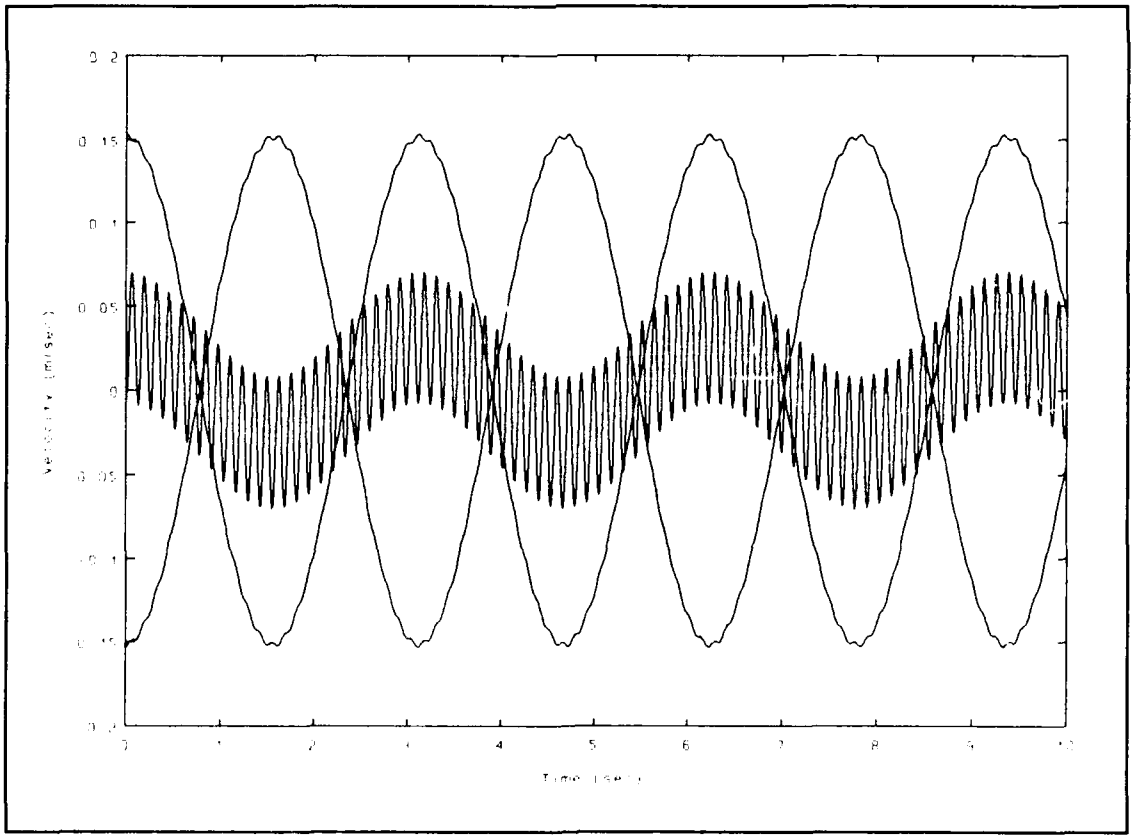

Figure 6.3 Beam #1 Undamped Response

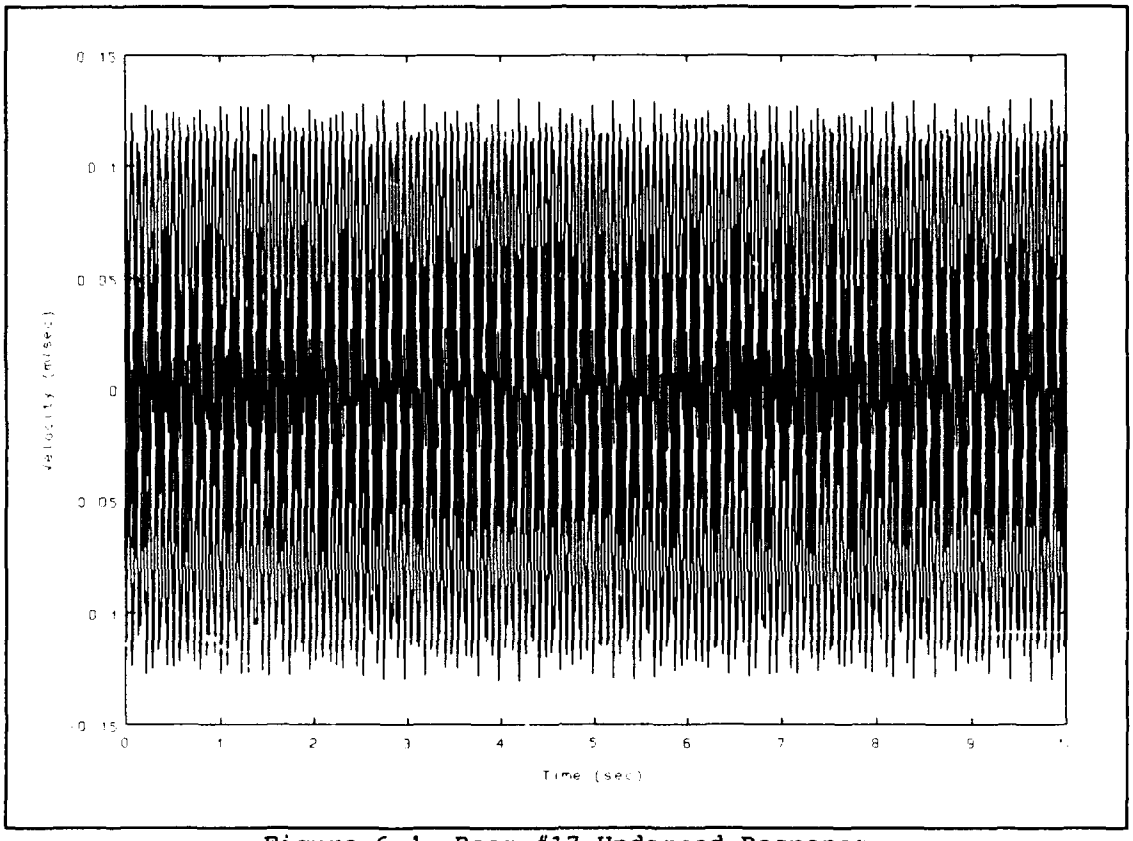

Figure 6.4 Beam #17 Undamped Response

= $\zeta\omega_n$, we see in Figure 6.9 that when the Q and R values vary, a negatively sloped line is produced in the s-plane which is indicative of maintaining a constant overshoot requirement (21:61). A constant settling time requirement, on the other hand, would produce a vertical line in the s-plane. With Q and R held constant, Figure 6.10 shows a slope slightly right of a vertical line.

The settling time can be found from (21:61)

$$t_s = \frac{4.6}{\zeta\omega_n}$$

for a settling-time specification of 1%. The settling time is plotted in Figure 6.11 for Q and R which vary and Figure 6.12 for Q and R held constant. The settling time starts out high but then decreases for the Q and R which vary. The settling time gradually increases for the constant Q and R.

Figures 6.13 - 6.16 show the initial control force required from each actuator for each iteration. In order to maintain a constant percent overshoot, more force is needed as the structure gets heavier. This is shown for actuator A in Figure 6.13 and for actuator C in Figure 6.14. When a "constant" settling time is desired, more control force is needed as the structure gets lighter. This is shown in Figure 6.15 for actuator A and in Figure 6.16 for actuator C.

Optimization Using Cost Function J

The optimization of space structures can be formulated (8:63) as

$$\begin{aligned} &\text{minimize} && m(v) \\ &\text{such that} && g_j(v) \geq 0,\ j = 1, \ldots, n_g \end{aligned}$$

where [v] is a vector of structural sizes, and m is the structural objective function, typically mass. The function $g_j(v)$ represents constraints on the structural design. To integrate structural optimization with the control system design, the mass objective function can be combined with the control quadratic performance index J, so that the optimization becomes (3:928)

$$\text{minimize} \quad m^* = q_1 m(v) + q_2 J(K,v) \tag{6.3}$$

$$\begin{aligned} \text{such that} \quad & g_j(v) \geq 0, && j = 1, \ldots, n_g \\ & h_i(K,v) \geq 0, && i = 1, \ldots, n_h \end{aligned}$$

where h_i are constraints on the closed-loop control system. For numerical optimization, the gradient of m^* is required. Miller and Shim

(22:292) present a numerical optimization solution technique to solve equation 3.

Values of J versus cross-sectional area are plotted in Figures 6.17 - 6.20 for the different weighing parameters θ on Q and R. Figure 6.17 shows the J values plotted for Q and R selected by equations 5.24 and 5.25. These J values were computed without viscous damping ($\zeta = 0$). To show the effects of damping on the J values, Figure 6.18 uses the same Q and R values but includes viscous damping. For the lighter structures, the total minimum energy J increases significantly. Figure 6.19 is a plot of J for the undamped structure when Q and R are held constant. Figure 6.20 is the same plot except the effects of damping are included. When Q and R are held constant, damping inherent to the structure does not have much effect on the minimum system energy as shown in Figure 6.19 and Figure 6.20. The reason for this can be seen in Figures 6.15 and 6.16. For fixed Q and R, the control system expends more energy to quickly dampen out vibrations for the lighter structures. Even though more control energy is expended, the total system energy is less because the control system does not allow the structure to vibrate long enough to dominate the total energy.

From equation 6.3, the optimal value for m^* is clearly dependent on the choice of q_1 and q_2. How do we select q_1 and q_2 when J(K,v) represents total system energy and m(v) represents structural mass? Clearly the units of energy and mass are incompatible, but the literature avoids this question. Presumably in the design process, q_1 and q_2 would be design values which are adjustable. q_2, for example, could be a measure of mass/energy for a given control system. On the other hand, it may not matter. Since this is multiobjective optimization, q_1 and q_2 are weighing parameters which may simply be selected by decision makers to achieve some overall goal.

Figure 6.21 and Figure 6.22 show the optimization of m(v) and J(K,v) for ($q_1 = 1$, q_2 100), and ($q_1 = 1$, $q_2 = 385$), respectively. For

$q_1 = q_2 = 1.0$, the mass dominates the optimization and the curve slopes up to the right with no minimum. For $q_1 = 1.0$ and $q_2 > 1000$, the control system dominates and the curve slopes down to the right with no minimum. Somewhere in between the two extremes is an optimal value for q_1 and q_2 of whose selections are another nested optimization problem. $q_2 = 385$ was selected to show a trend. As q_2 is increased, the minimum m^* moves to the right. The same observation can be made on Figures 6.23 and 6.24 except that a higher value of q_2 is required for the system energy to influence the curve minimum.

Optimization Using Onada's Formulation

Haftka (8:64) points out two shortcomings of the above procedure. First, the effect of the control system on the mass of the structure and the structural constraints is neglected. Second, the Q and R matrices are somewhat arbitrary and are tuned by the control engineer to achieve the desired dynamic response. It is therefore unreasonable to select them before the optimization procedure starts and then leave them unchanged. Problems with the meaning of q_2 in the equation for minimizing the mass and total system energy were discussed above. Onada's formulation provides a physical meaning in a format which can be modeled. By selecting Q and R from equations 5.25 and 5.26 which allow them to vary, the second shortcoming that Haftka points out with the above procedure is satisfied.

Onada's formulation assumes (8:64) that the mass of the control system is related to the control effort as

$$m_c = \alpha [C_E]^{\beta} \tag{6.4}$$

where α and β are constants and C_E is the quadratic measure of the control effort

$$C_E = u_o^T R u_o \tag{6.5}$$

The optimization problem is to minimize the total mass of the system subject to a constraint on the magnitude of the response. The total mass of the system is the sum of the control mass and the structural mass. The response of the system is

$$r = x_o^T Q x_o \tag{6.6}$$

The optimization problem is formulated as:
Find [v] and [K] to minimize

$$m = m_s(v) + m_c(v,K) \tag{6.7}$$

subject to the constraint $r[v,K] \leq \sigma$ where σ is the response magnitude allowable.

For a beam structure, Onada and Haftka showed (23:1136) that as the mass of the beam was decreased, the mass of the control system became very large in order to control the vibration modes in the lighter structure. This was also demonstrated for the ABE optimization when the values of Q and R were held constant.

Figure 6.25 is a plot of the C values for the undamped structure when Q and R vary. The energy of the control system remains fairly constant. In Figure 6.17 then, the sharp increase in J for the lighter structures can be contributed to the increase of structural kinetic and strain energy. Figure 6.26 shows the effect of damping on the C values. When Q and R are held constant, the control energy increases as the structural size decreases. This is shown in Figures 6.27 and 6.28. Once again, structural viscous damping does not effect C significantly.

Figures 6.29 - 6.32 show the plot of equation 6.7 where $m_c(v,K)$ is determined by equation 6.4 for $\alpha = 50$ and $\beta = 1$. Figures 6.25 and 6.26 are for Q and R which vary. Since C remains fairly constant when Q and R vary, the optimal choice for m is the smallest structural size which

satisfies any given structural constraints. When Q and R remain constant, however, C becomes large as the structural size of the beam is decreased. The optimization formulation of equation 6.7 produces a minimum on Figures 6.31 and 6.32 for α = 50. The total mass of the system increases significantly for the smaller structural sizes as shown by Onada and Haftka. This is reasonable since a larger control would be required to provide the higher energy levels.

Comparison of Optimization Methods and Q/R Selection

The direct relationship shown in Figures 6.5 - 6.14 to control specification parameters gives an indication of how to select Q and R and their weighing parameters. To maintain constant overshoot and closed-loop damping requirements, Q and R are chosen by Equation 5.24 and 5.25. The weights on Q and R are varied to select the control response desired. For a near constant settling time, Q and R can be fixed with minor adjustments to their weighing parameters.

The effect on the control system is shown in Figures 6.33 to 6.37. Comparing beam #1 in Figures 6.33 to 6.34, more initial actuator force is required when Q and R are held constant to achieve a constant settling time. When Q and R vary, the initial actuator force is smaller but the time interval over which it is applied is longer. For actuator A, the square-root of the squared forces for both Q/R selections are plotted in Figure 6.35 to compare the force magnitudes with their applied time intervals. As the structure gets larger, more control force is required to maintain a constant overshoot and closed-loop damping ratio. Figure 6.36 shows this increase in initial force when Q and R are varied. For the larger structure, less initial control force is needed to achieve a constant settling time as shown in Figure 6.37.

It is interesting to examine the structural response to these control inputs. Figures 6.38 and 6.40 compare beam #1 and beam #17 when Q and R are varied. In Figure 6.40, the structural response is damped

out very quickly to maintain the overshoot requirements. The response in Figure 6.38 is allows to vibrate for some time (3+ sec) because the overshoot requirement is not violated. Figures 6.39 and 6.41 compare beam #1 and beam #17 when Q and R are held constant. In both cases, the vibration is damped out in less than 1 sec. Less control input is required to achieve this response, however, because of the increased damping present in the larger structure.

It is also of interest to compare the J and C values for the different Q and R selections. Figures 6.42 and 6.43 are plots of J versus area and C versus area, respectively, for both choices of Q and R. The total system energy starts out lower when Q and R are fixed than when Q and R are varied. At some point on the curve, the total system energy becomes less when Q and R are varied. The same pattern emerges in Figure 6.43 when we compare C values except that the trend is reversed for the Q and R selection. Notice that the cross-over point for J and C values are not the same. At the point of cross-over on the J curve, our expected value for C is less for the case when Q and R are constant.

Selection of Structure By Sensitivity Analysis

A true optimization was not performed on the ABE, but we can use the trends presented in this Chapter to examine the current ABE structure. Since the values of α and β are not known for the ABE, the minimization of the total system energy will be used.

From Chapter III and Appendix B, the limits on the proof mass actuators and the structural dynamics shaker can be found. These limits are

Actuators: 8.9 N * 80% = 7.12 N each

Shaker: 45 N

In addition, the actuators are limited to the bandwidth 0-100 Hz. Figure 6.44 shows the initial control force required for actuator A (and B) for the different parameters θ when Q and R are varied. Figure 6.45 shows the initial control force required for actuator C under the same conditions. A constraint line based on the above limits is drawn on the diagrams.

The plot of equation 6.3 with $q_1 = 1.0$ and $q_2 = 385.0$ is shown in Figure 6.46. For the top three curves, there are two minimums on the graph. Which minimum to select depends on the limits of our control system. From Figures 6.44 and 6.45, we see that the Q0/R0 and the Q0/R3 curve require initial control forces beyond the limits of our actuators. The required initial control forces for Q3/R0 are within our limits. Q3/R0 is selected as the minimum. For the selection of $q_1 = 1.0$ and $q_2 = 385$, the minimum for happens to coincide with the existing ABE structure. A plot of the required controller response is shown in Figure 6.47 and a plot of the structural response is shown in Figure 6.48. Of course other θ and q_i parameters for the ABE will also produce minimums within the limits of our controllers. These parameters can be adjusted to determine a control law which produces the desired system response with the limits of the control system. The control law for Q3/R0 is presented in Appendix F.

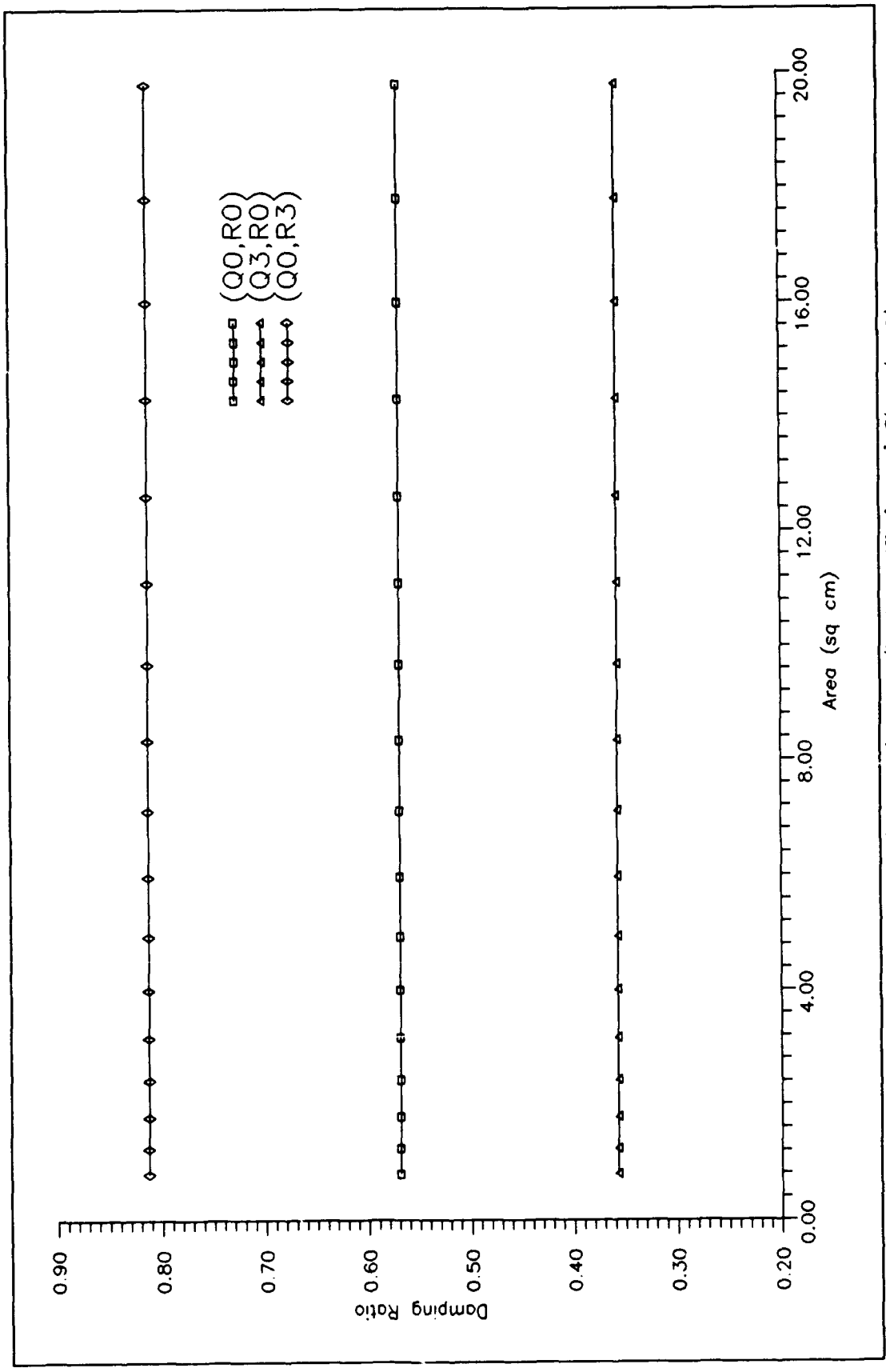

Figure 6.5. Damping Ratios - Q/R Vary (Undamped Structure)

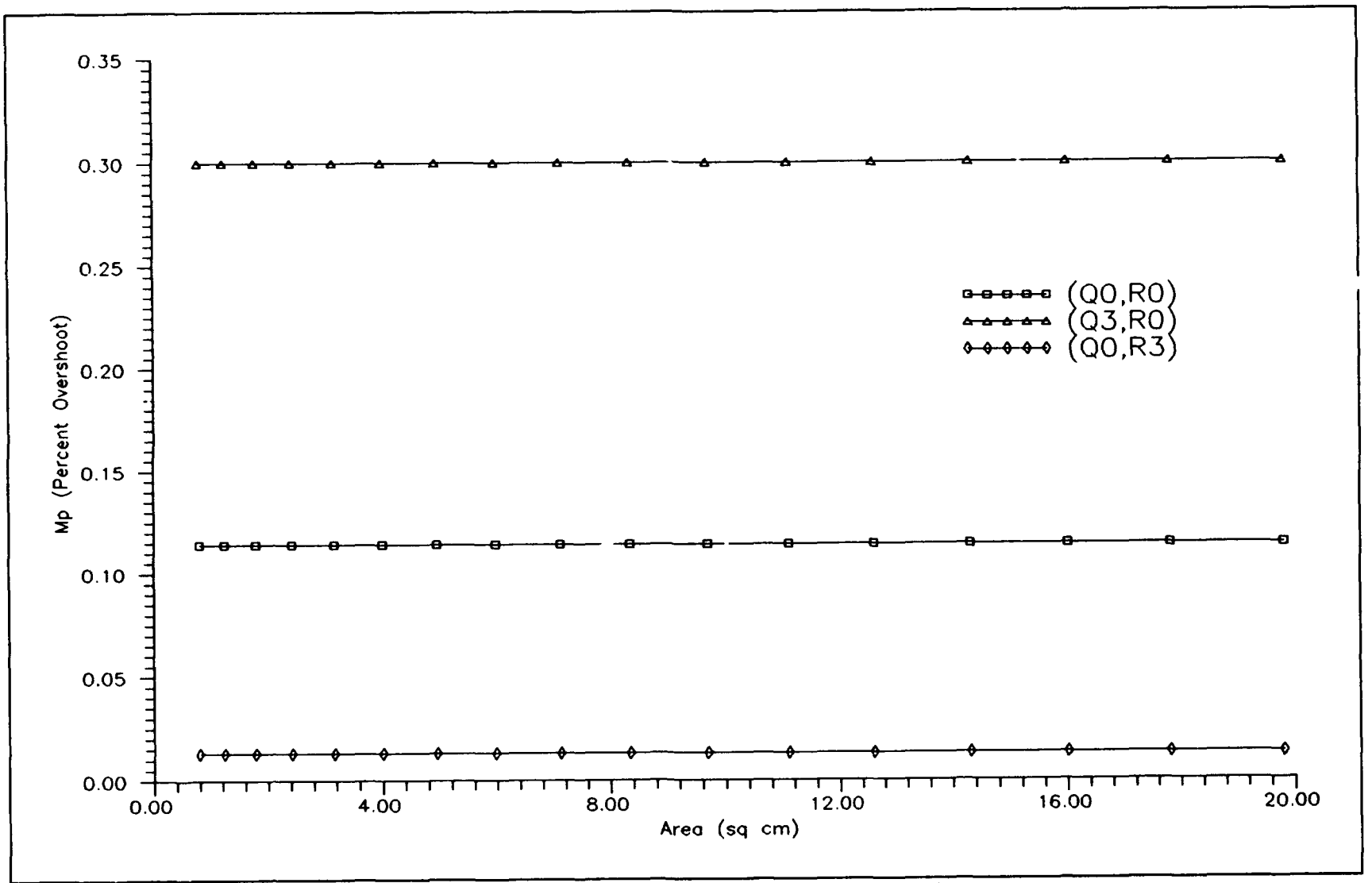

Figure 6.6. Percent Overshoot - Q/R Vary (Undamped Structure)

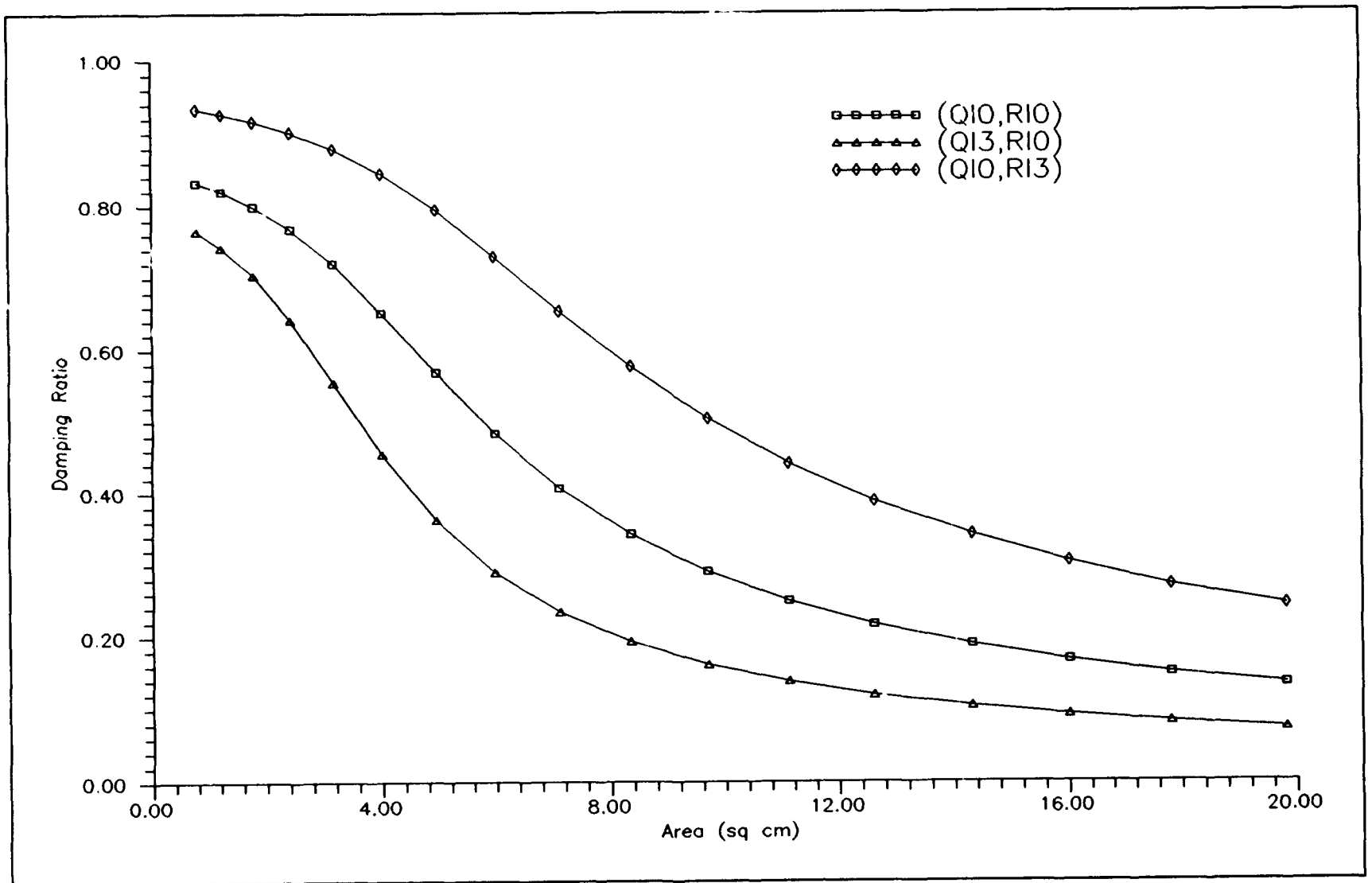

Figure 6.7. Damping Ratios - Q/R Constant (Undamped Structure)

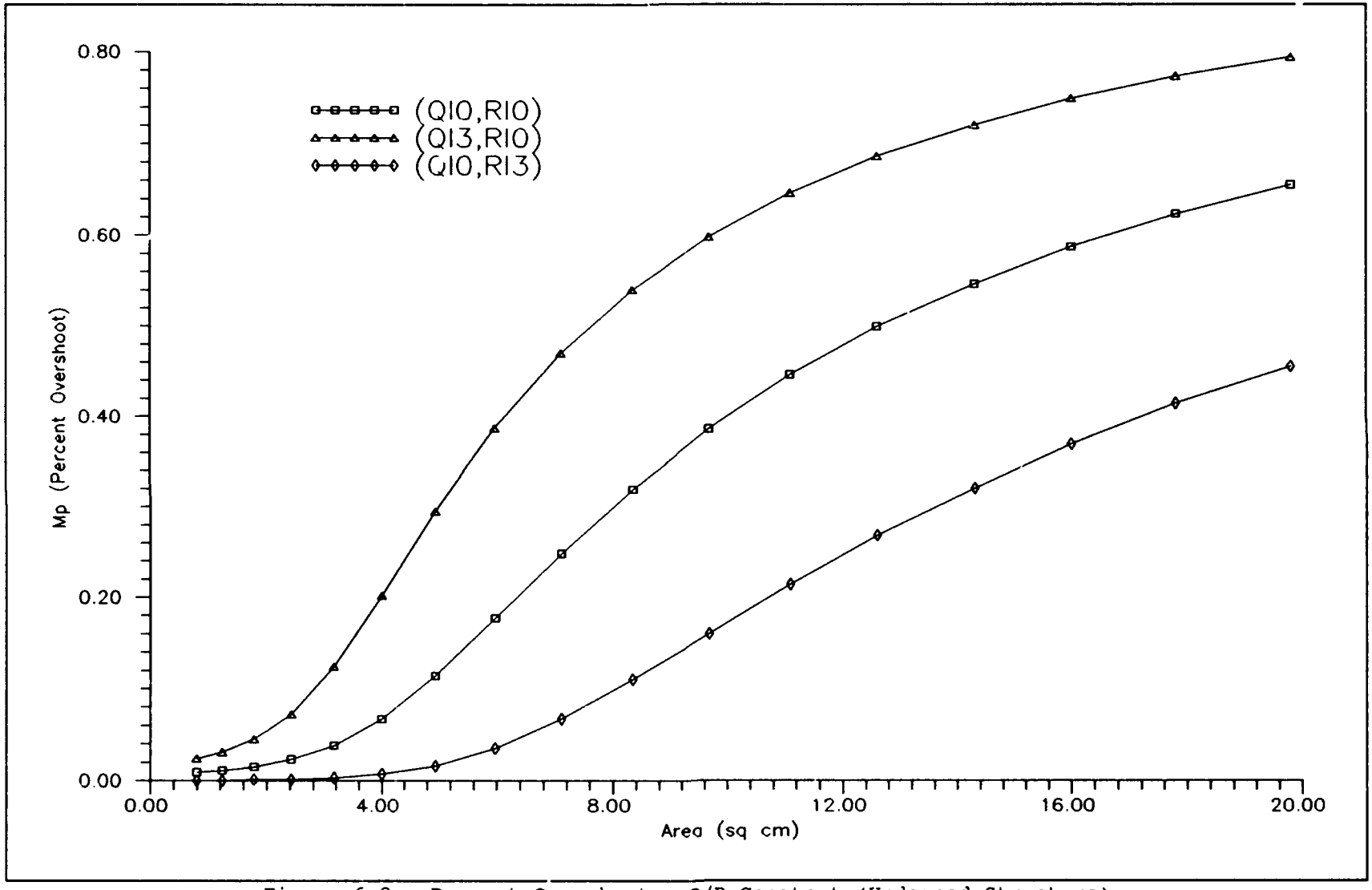

Figure 6.8. Percent Overshoot - Q/R Constant (Undamped Structure)

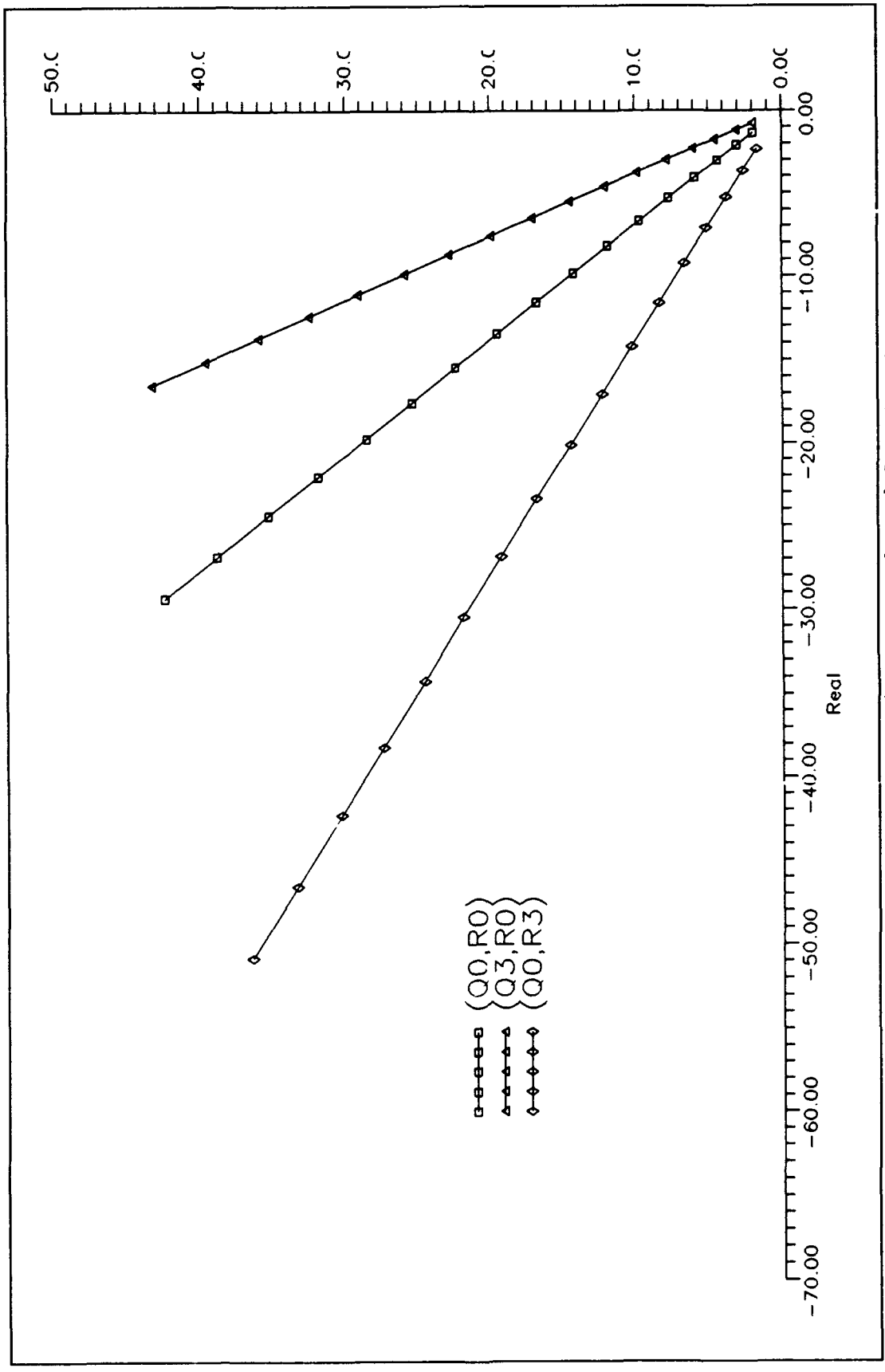

Figure 6.9. S-Plane - Q/R Vary (Undamped Structure)

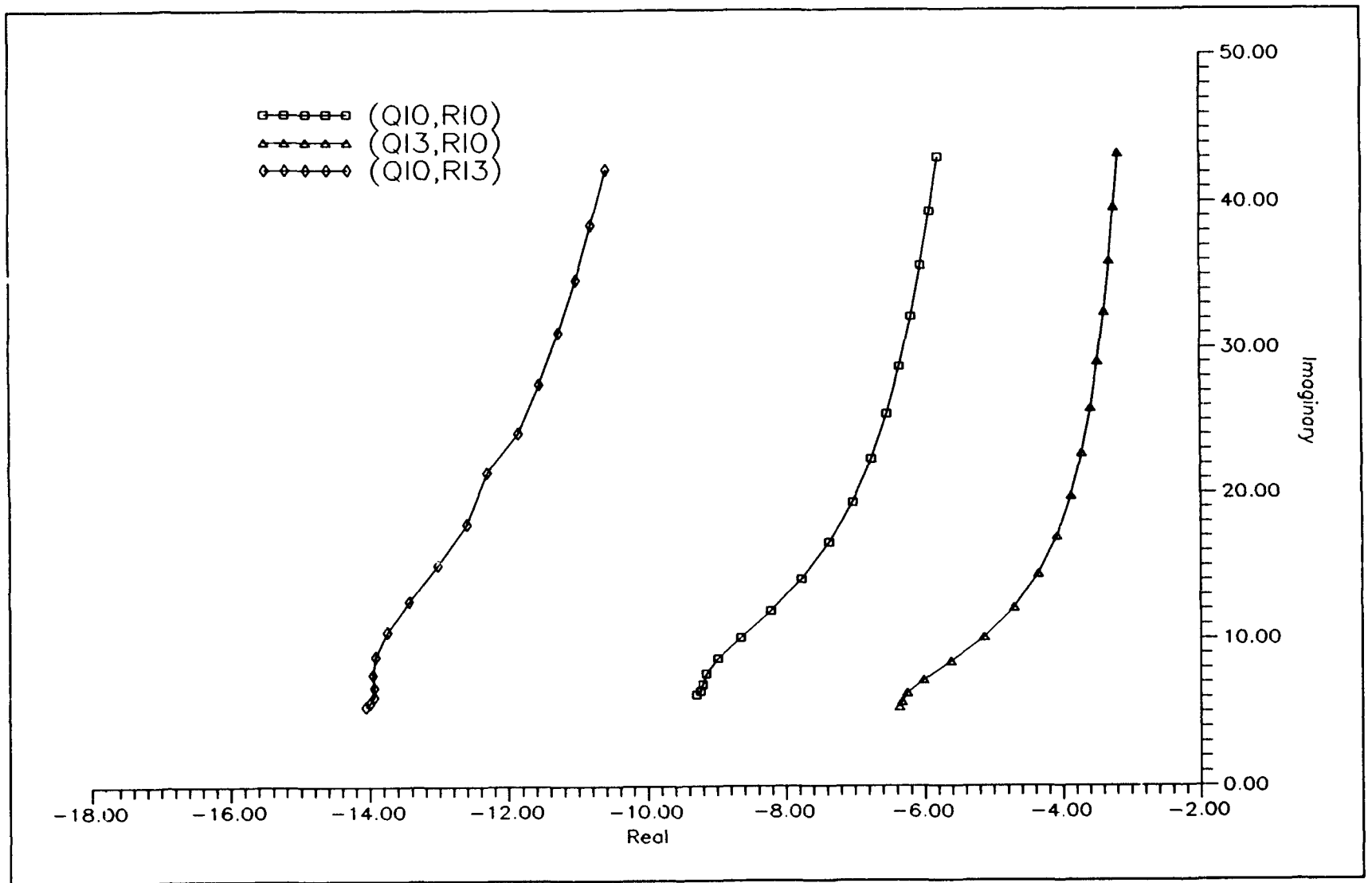

Figure 6.10. S-Plane - Q/R Constant (Undamped Structure)

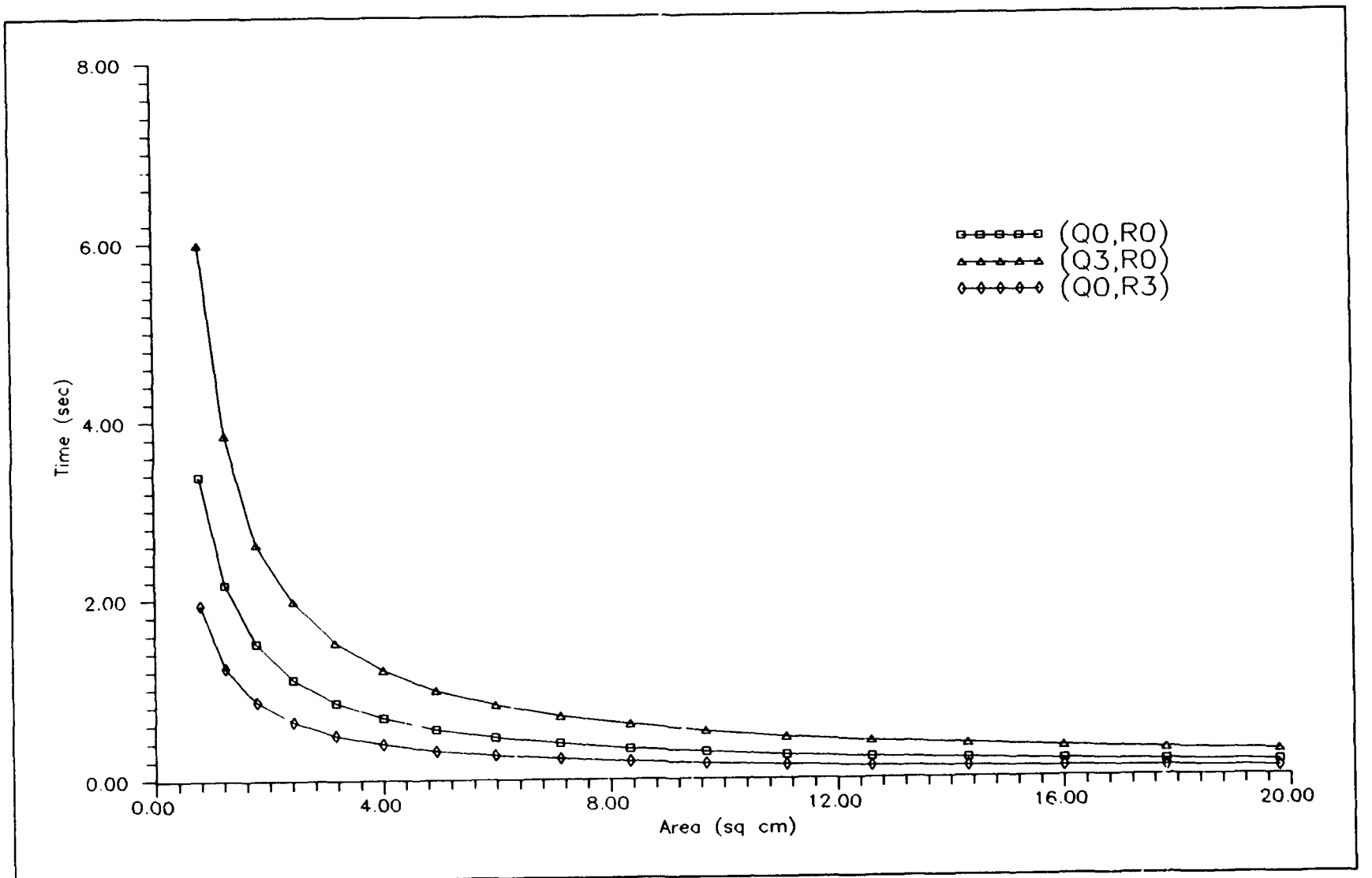

Figure 6.11 Settling-Time - Q/R Vary (Undamped Structure)

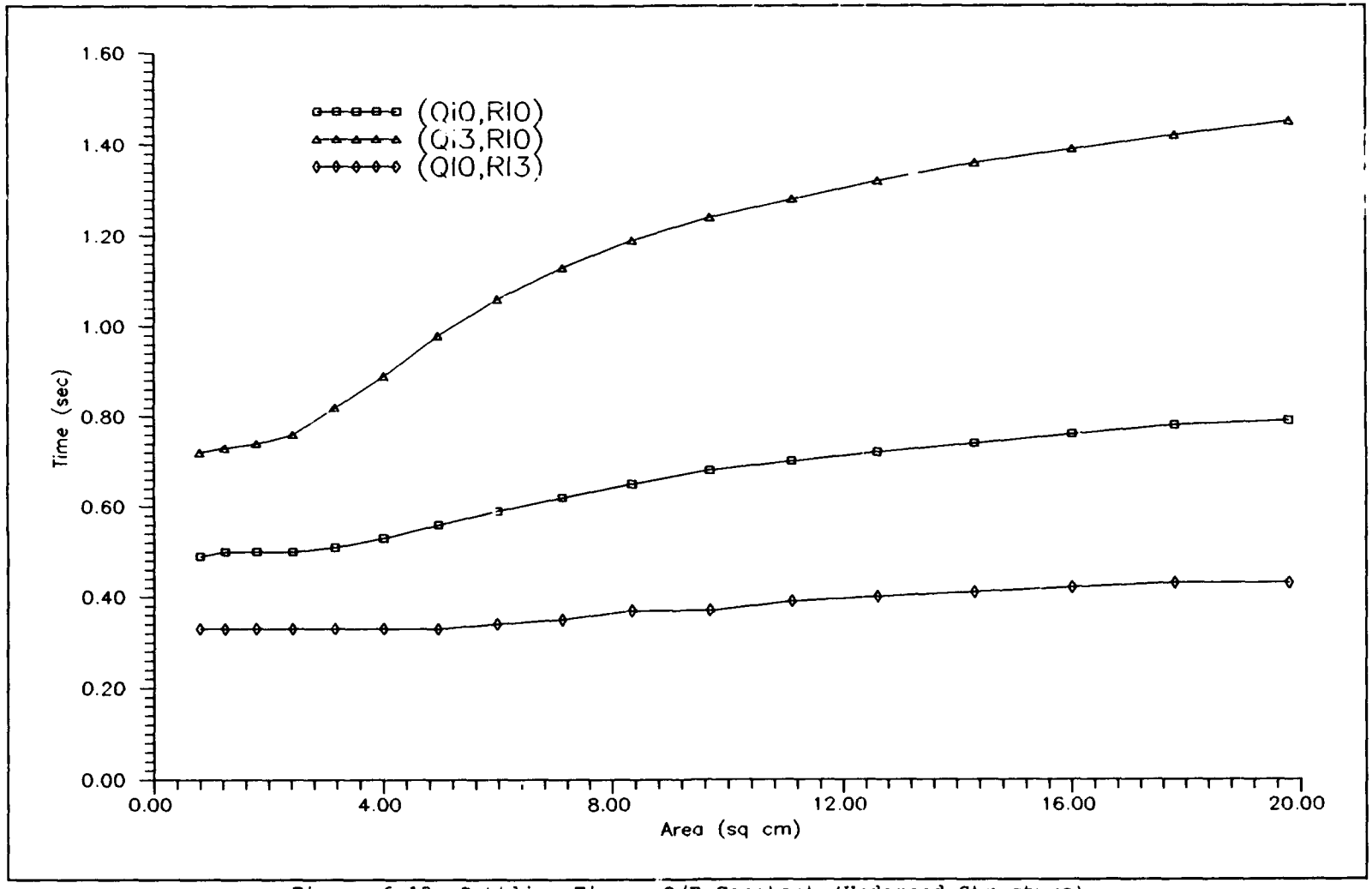

Figure 6.12 Settling-Time - Q/R Constant (Undamped Structure)

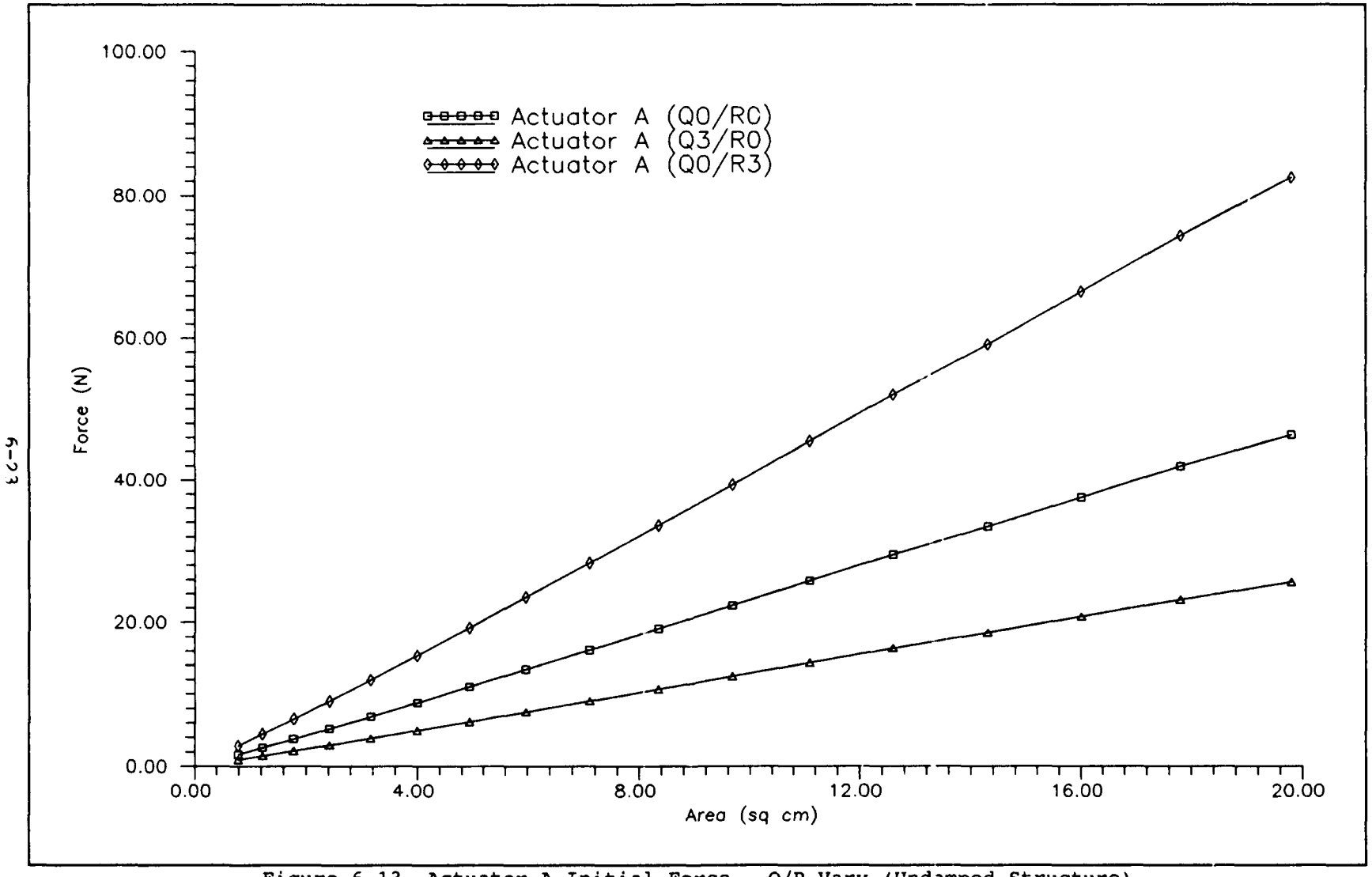

Figure 6.13 Actuator A Initial Force - Q/R Vary (Undamped Structure)

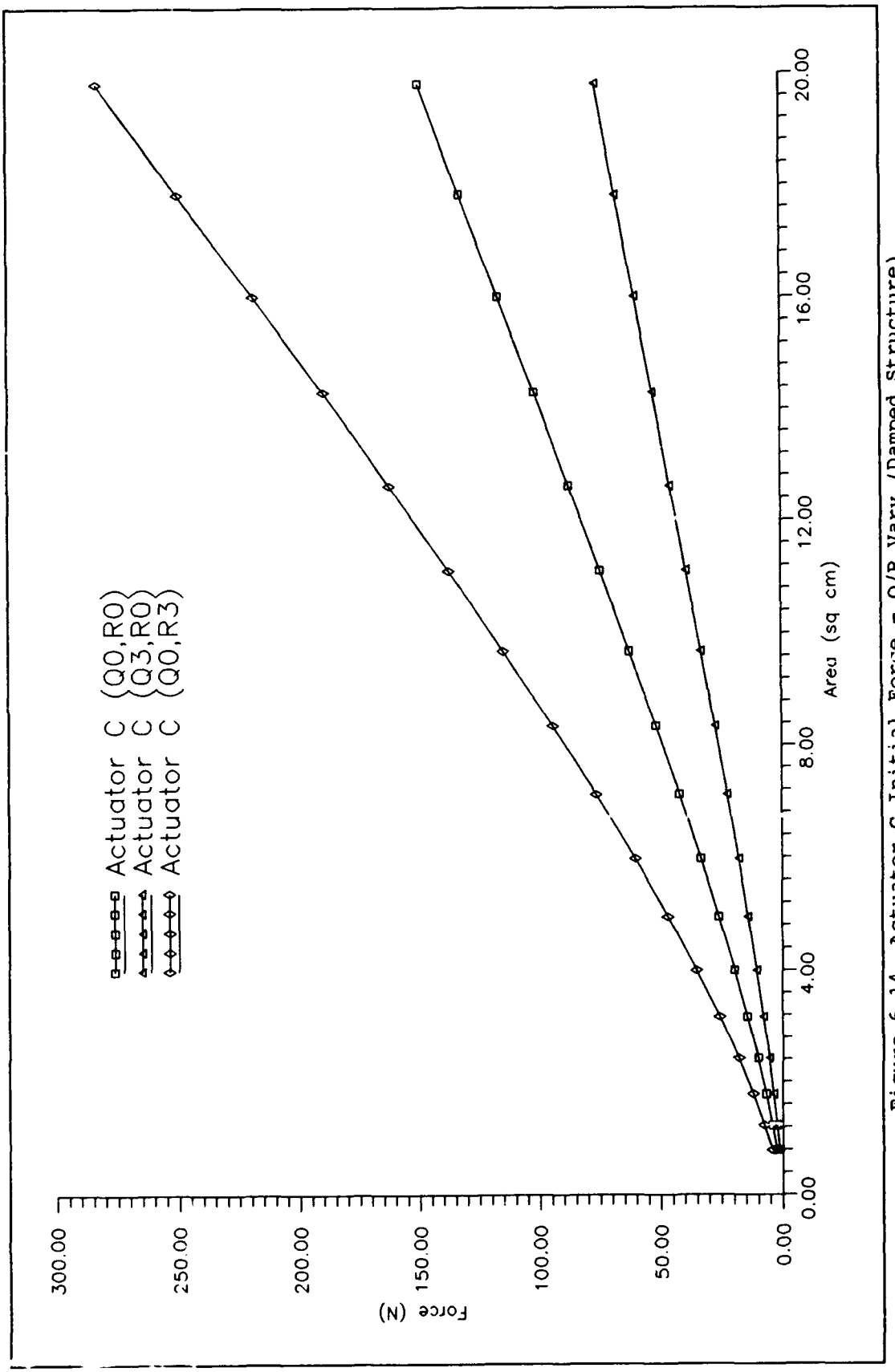

Figure 6.14 Actuator C Initial Force - Q/R Vary (Damped Structure)

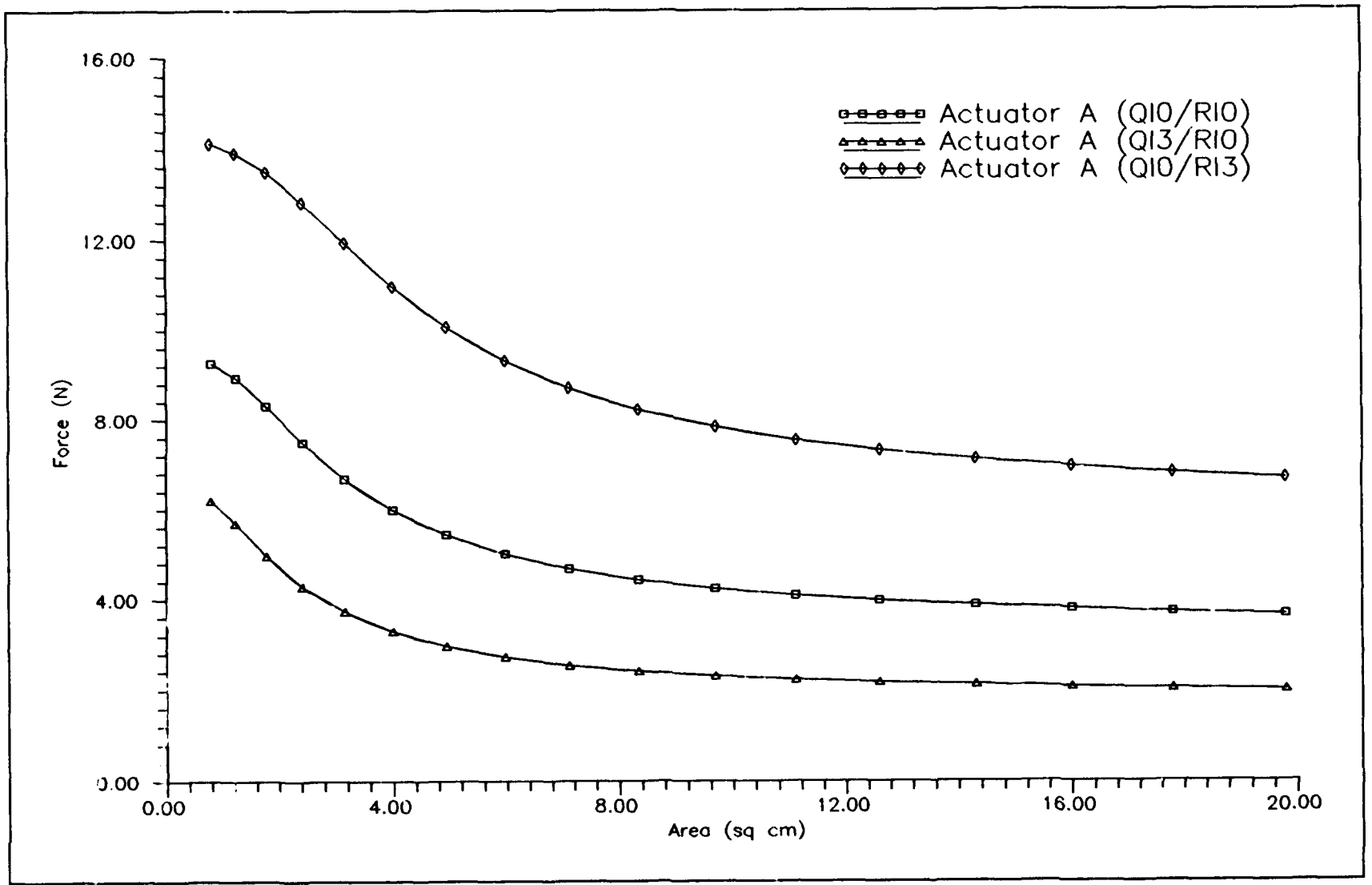

Figure 6.15 Actuator A Initial Force - Q/R Constant (Undamped Structure)

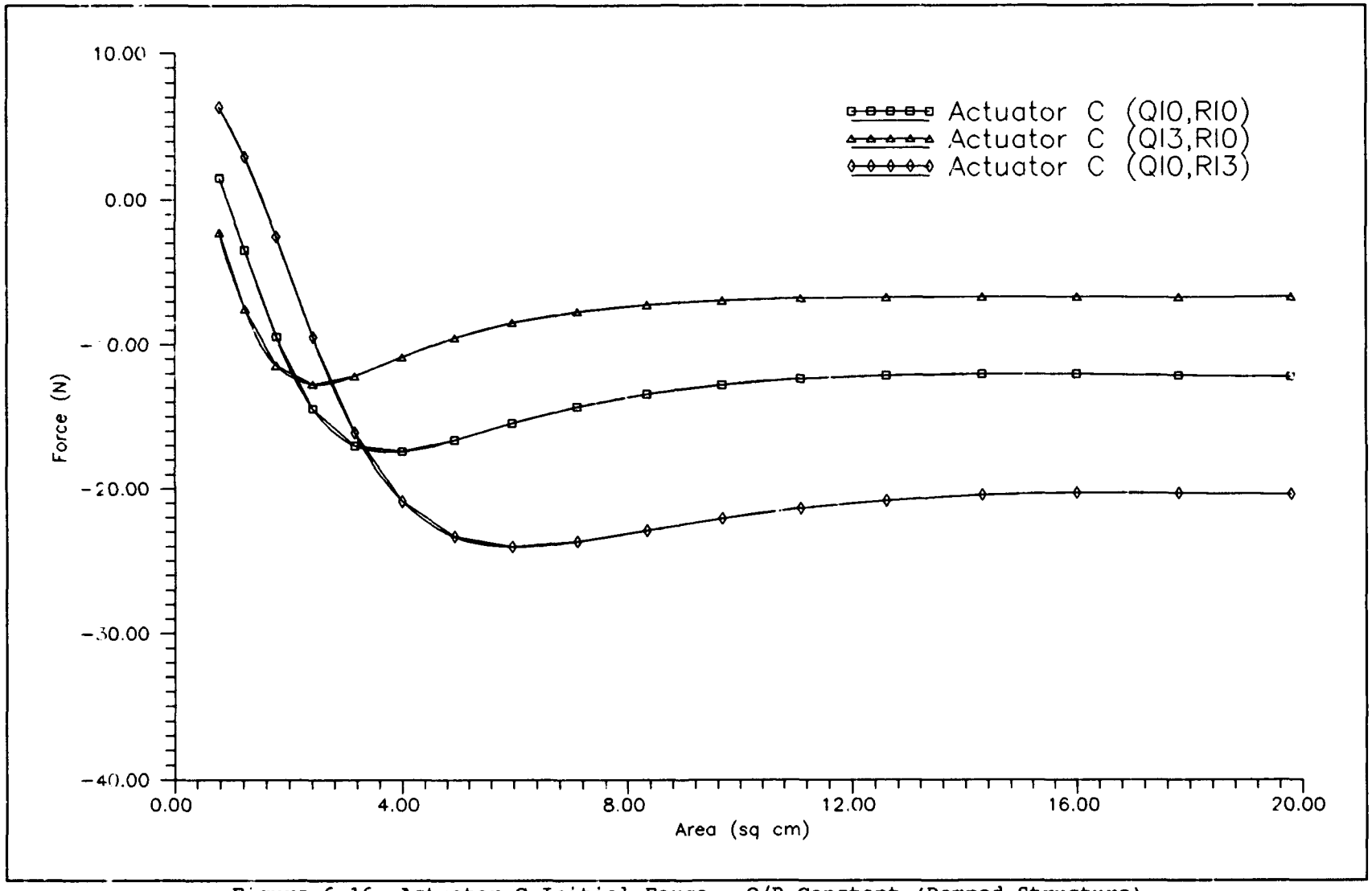

Figure 6.16 Actuator C Initial Force - Q/R Constant (Damped Structure)

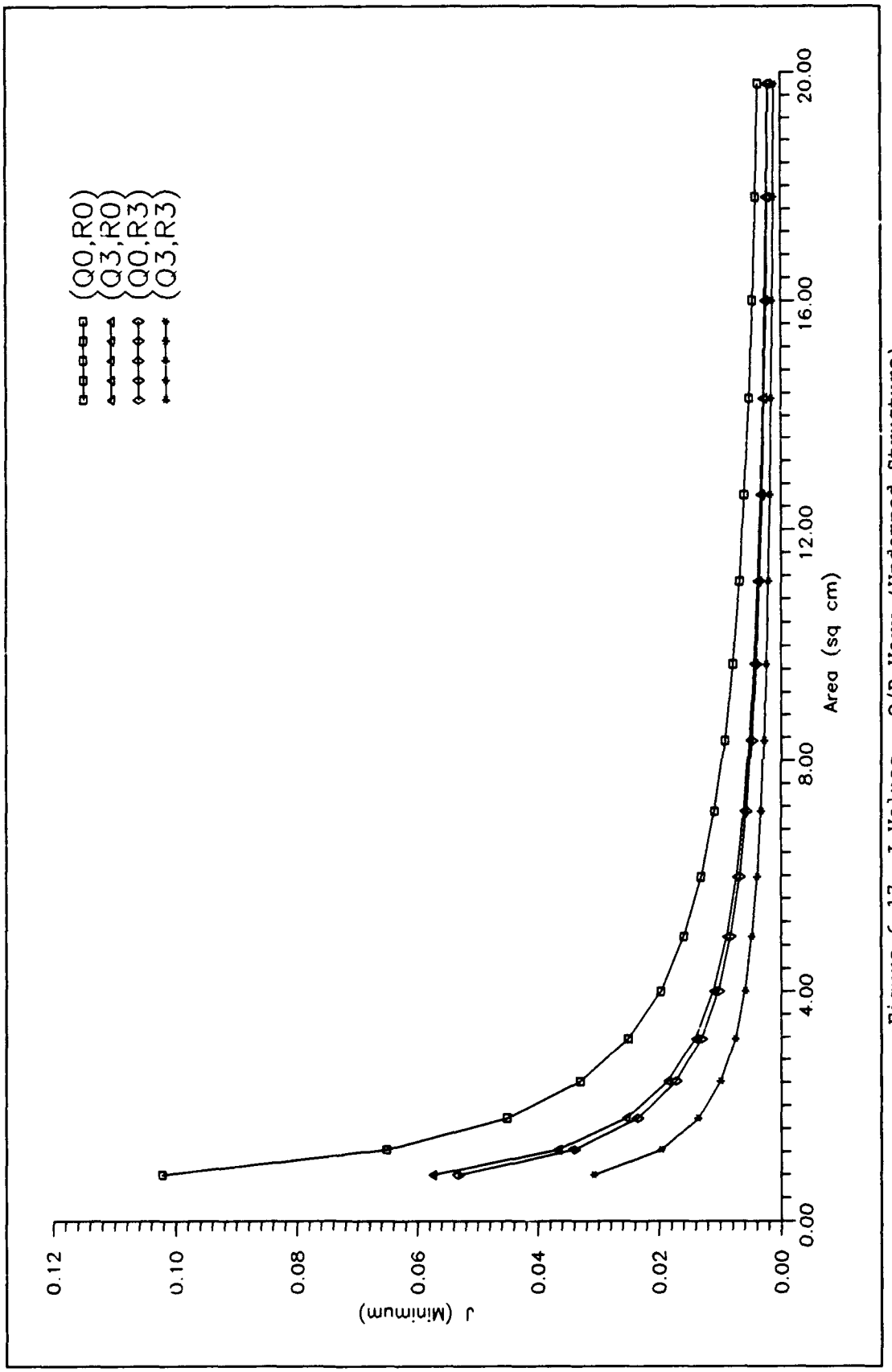

Figure 6.17 J Values - Q/R Vary (Undamped Structure)

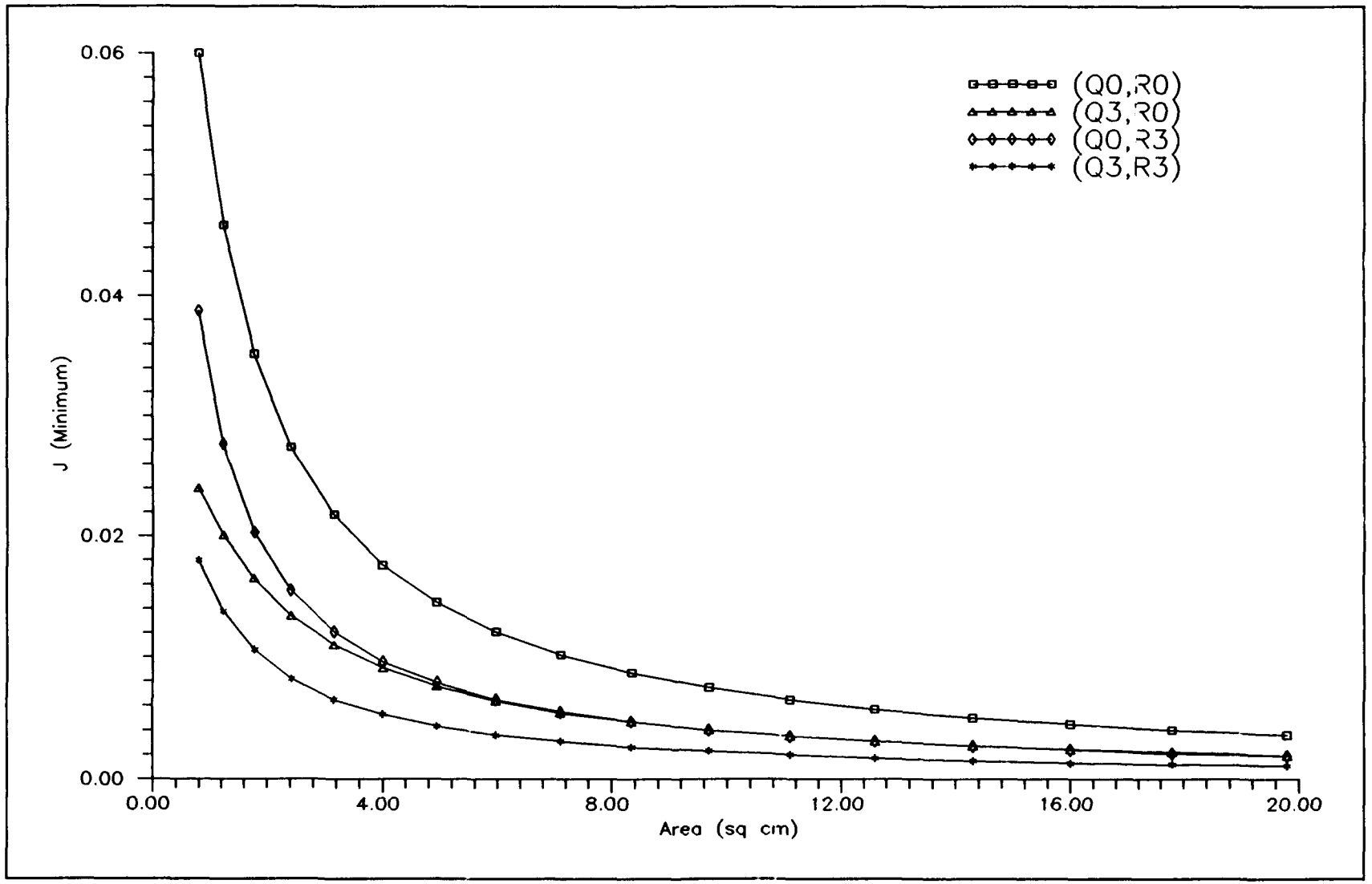

Figure 6.18 J Values - Q/R Vary (Damped Structure)

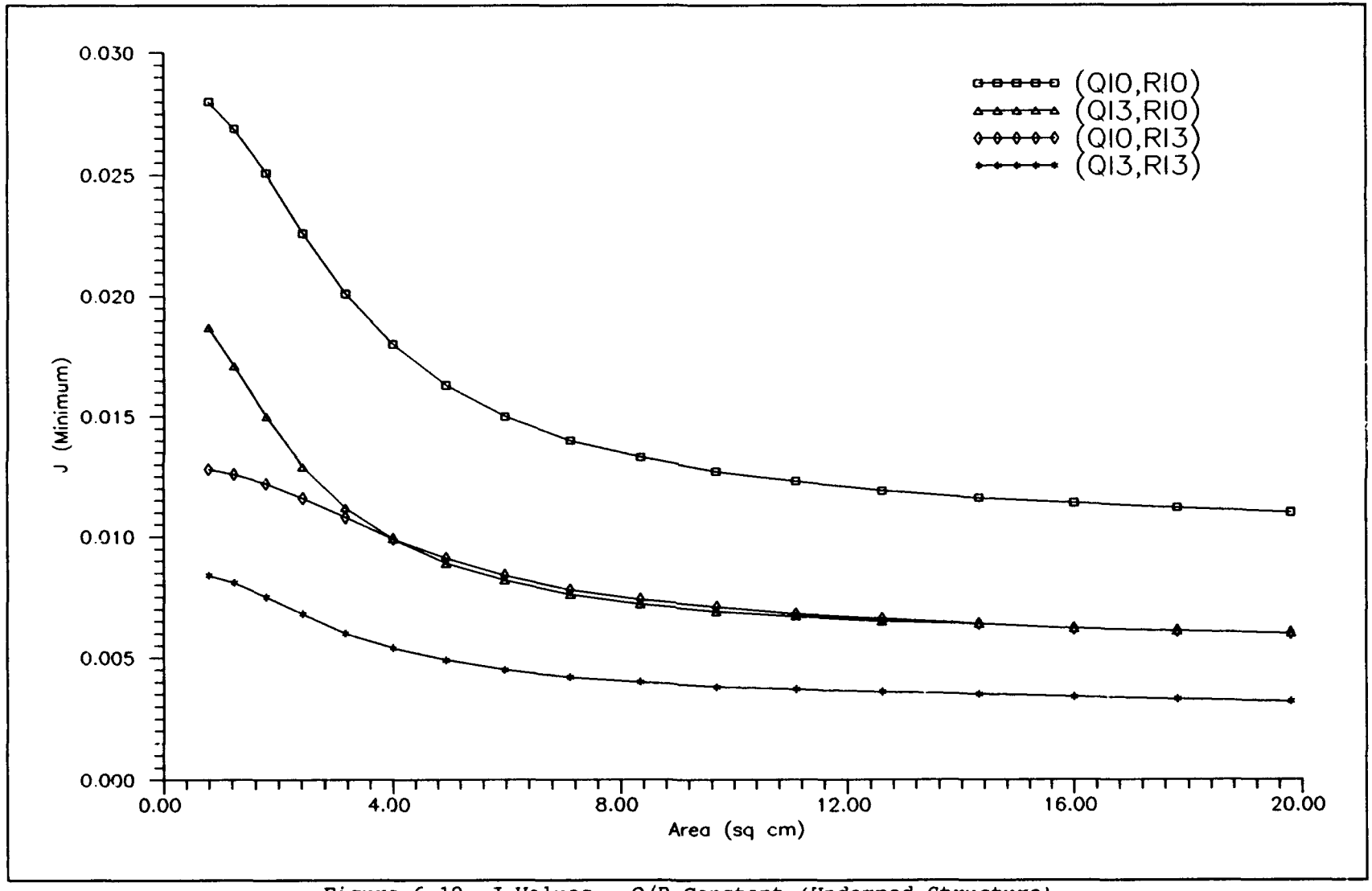

Figure 6.19 J Values - Q/R Constant (Undamped Structure)

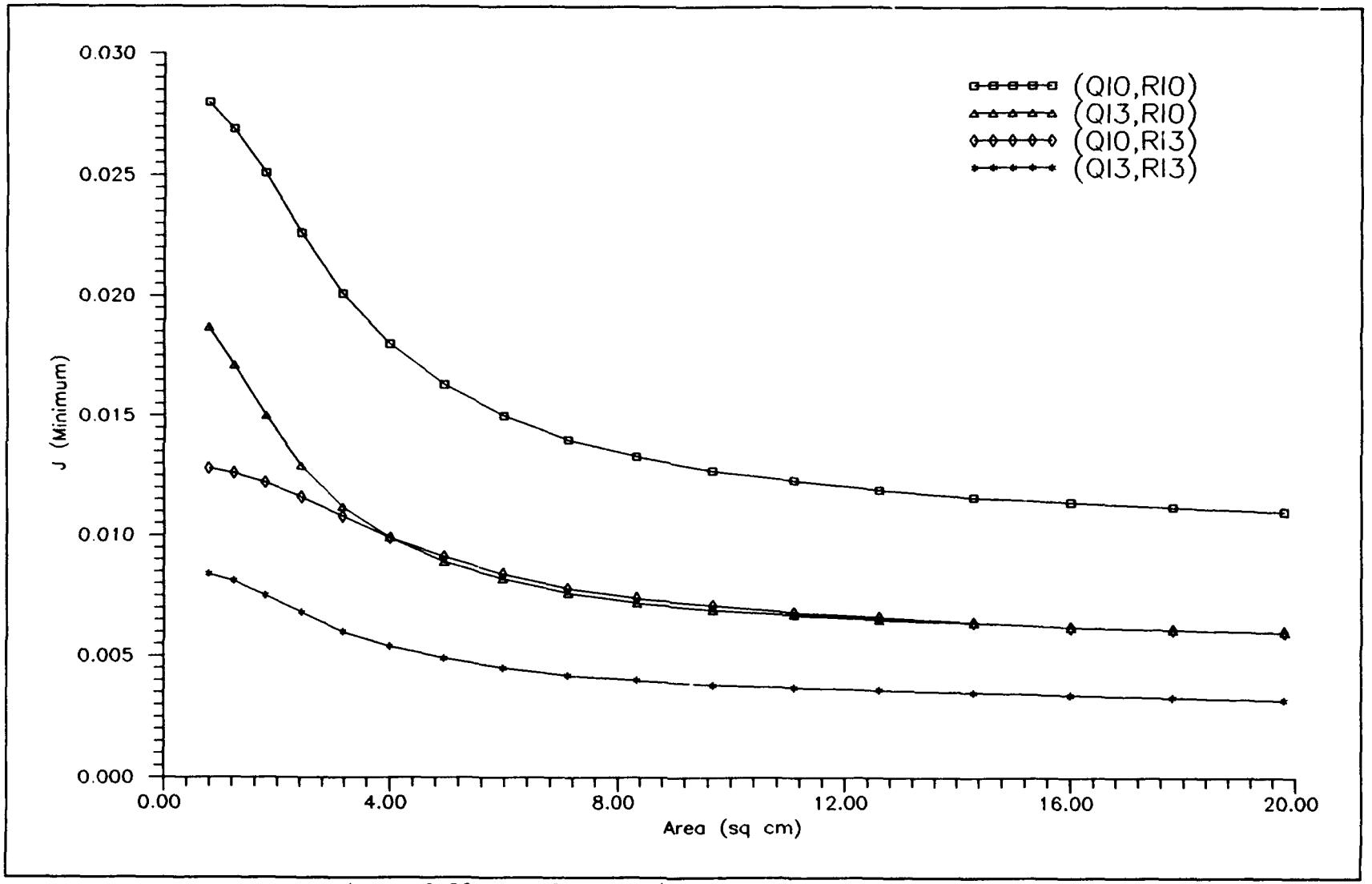

Figure 6.20 J Values - Q/R Constant (Damped Structure)

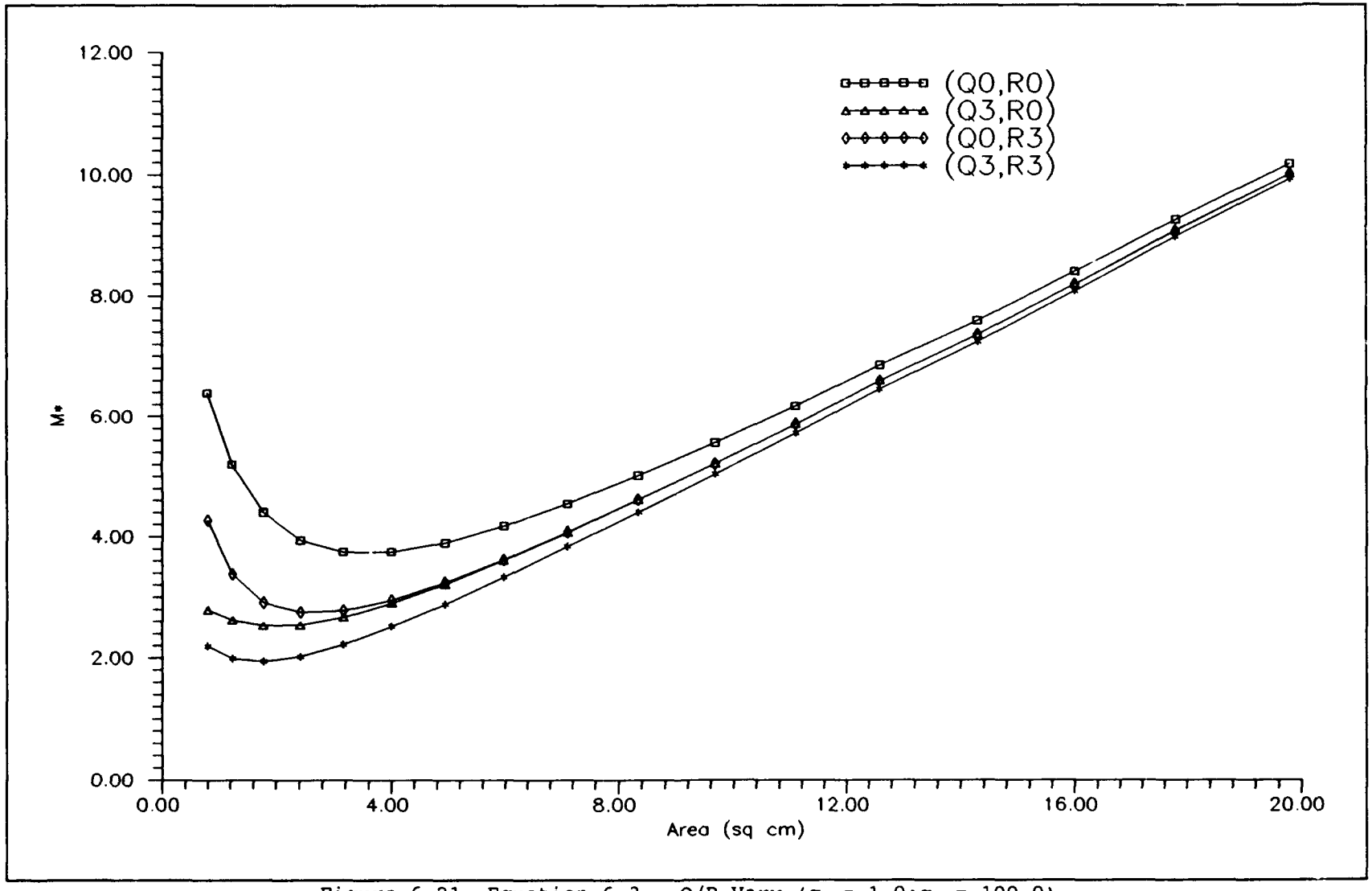

Figure 6.21 Equation 6.3 - Q/R Vary (q_1 = 1.0;q_2 = 100.0)

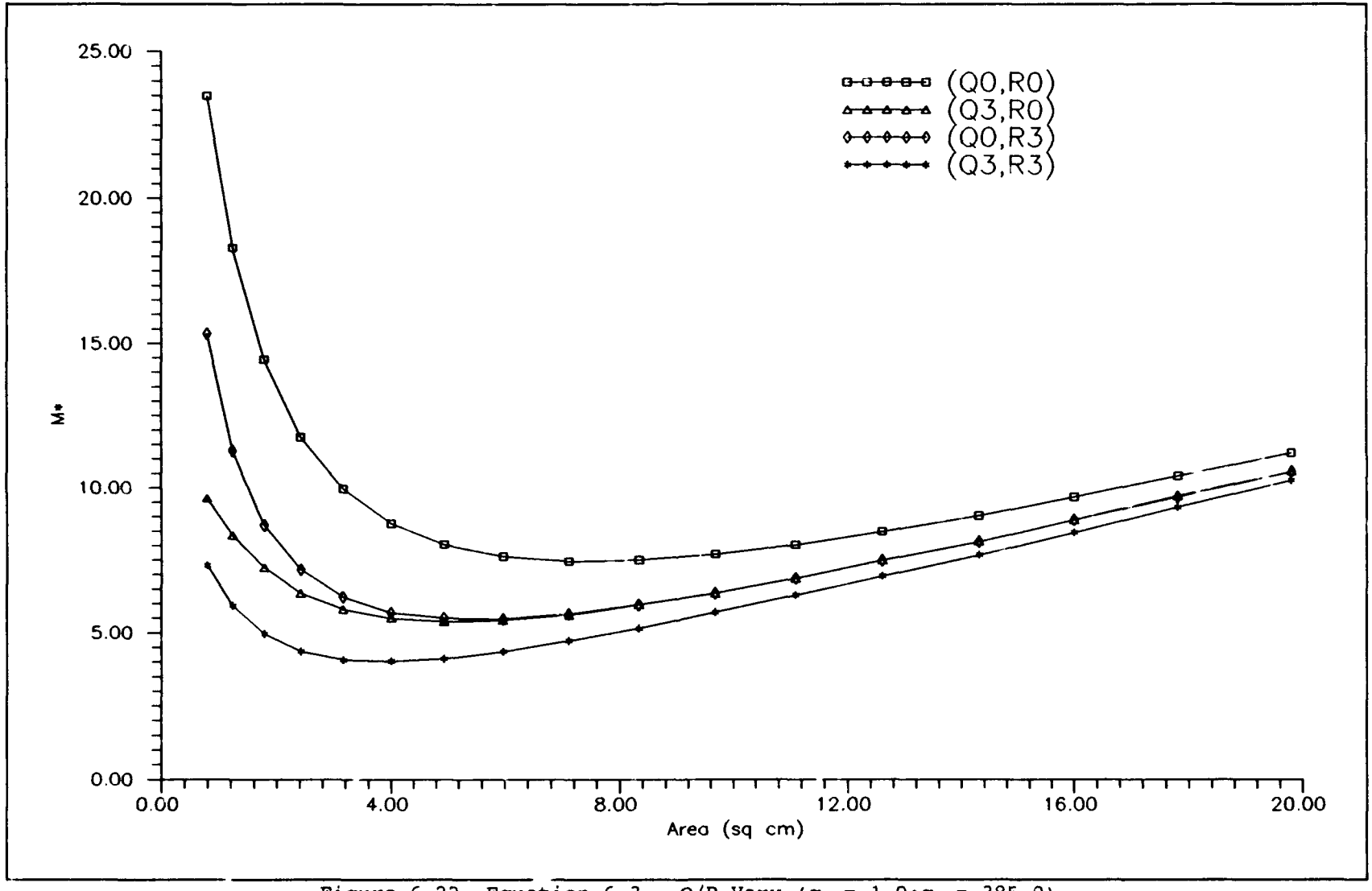

Figure 6.22 Equation 6.3 - Q/R Vary (q_1 = 1.0;q_2 = 385.0)

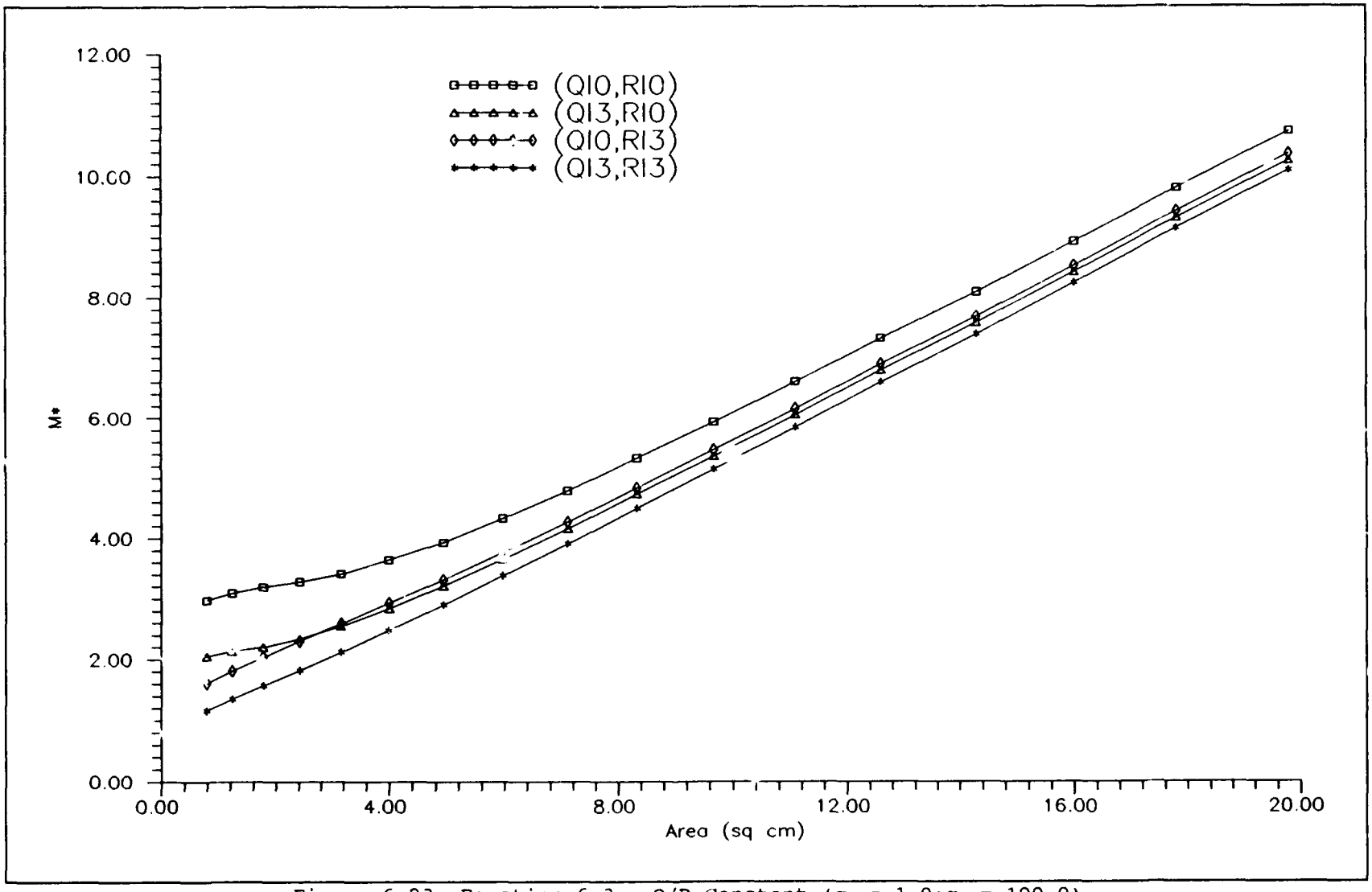

Figure 6.23 Equation 6.3 - Q/R Constant (q_1 = 1.0; q_2 = 100.0)

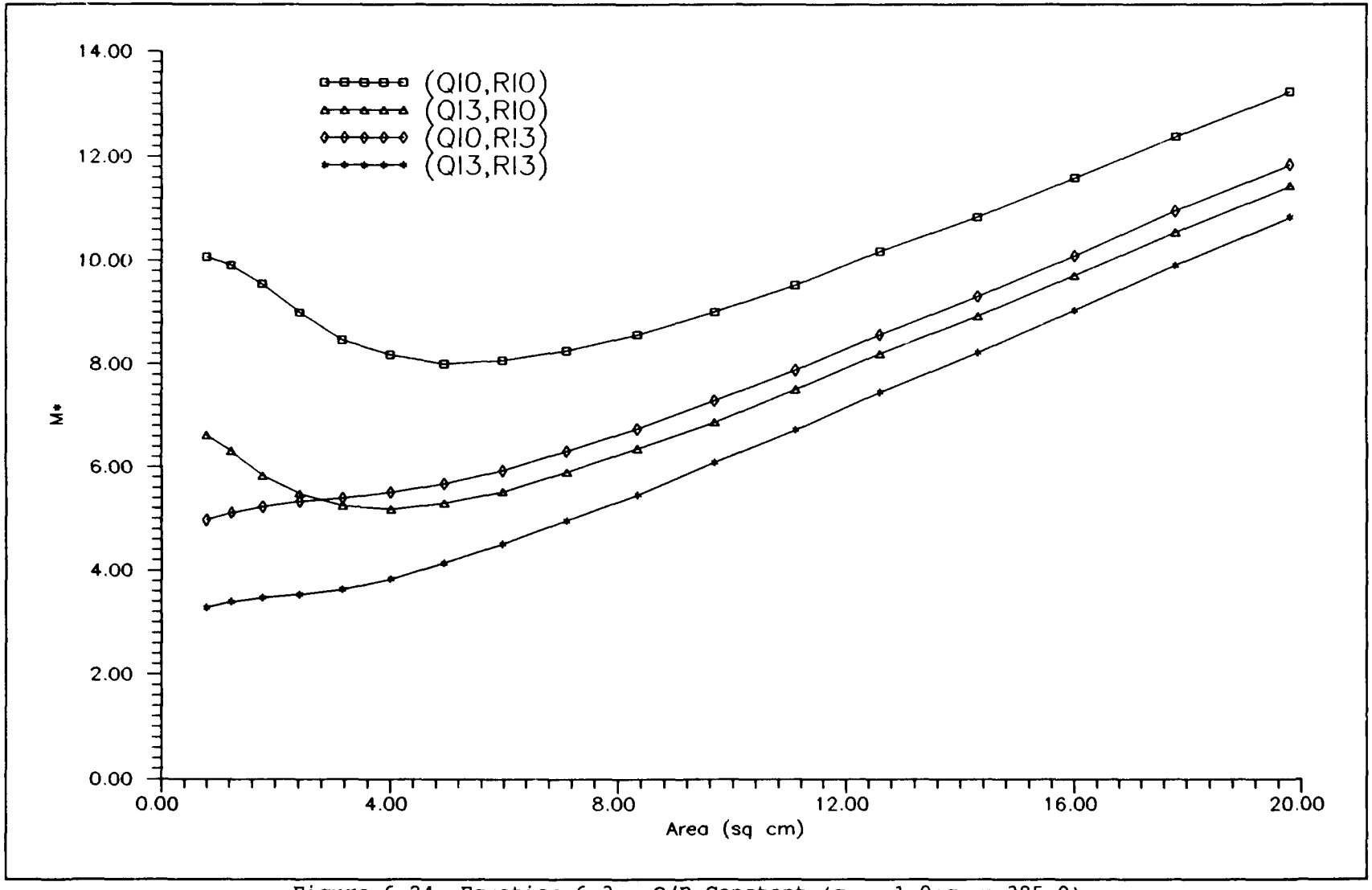

Figure 6.24 Equation 6.3 - Q/R Constant (q_1 = 1.0;q_2 = 385.0)

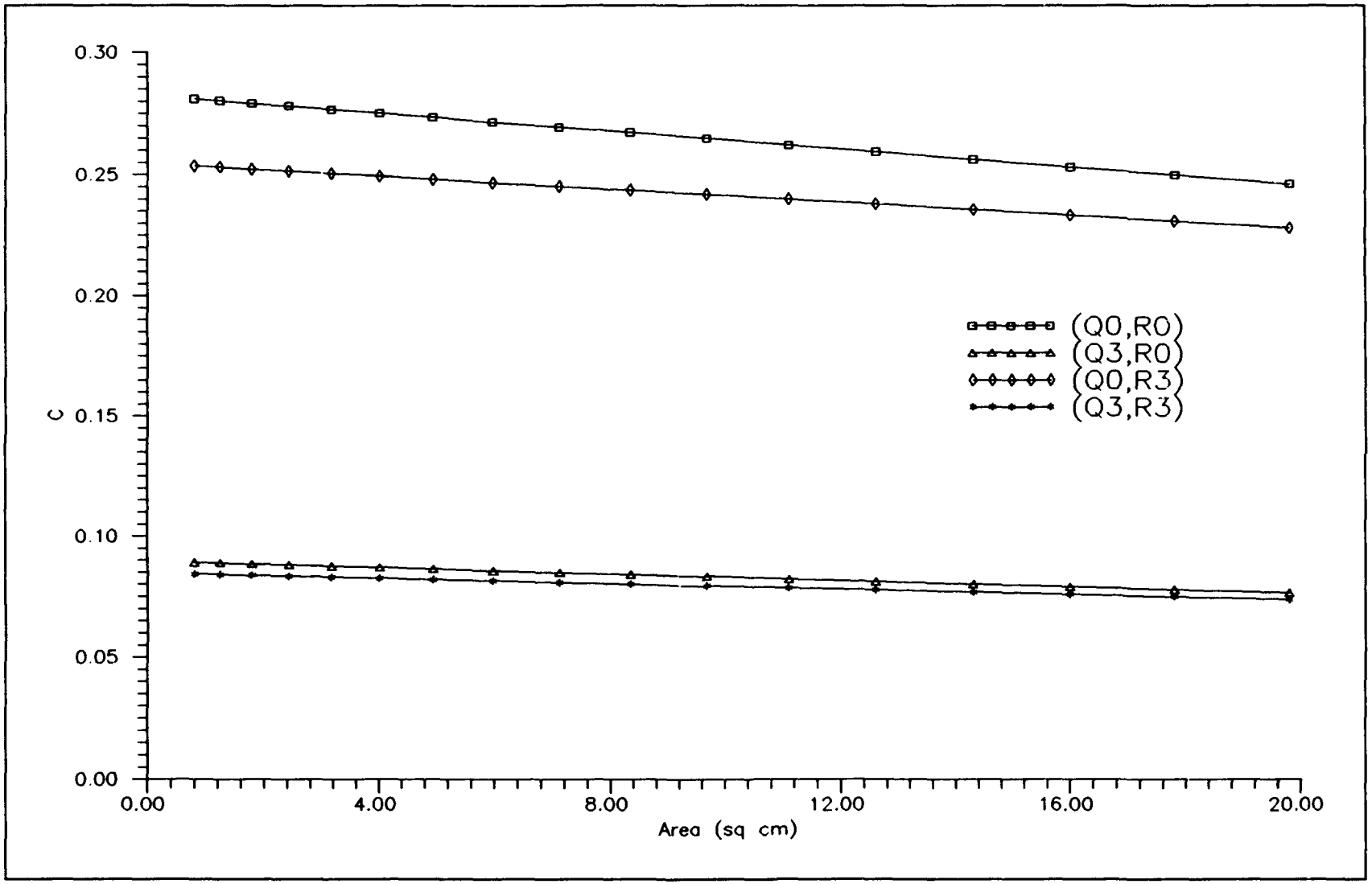

Figure 6.25 C Values - Q/R Vary (Undamped Structure)

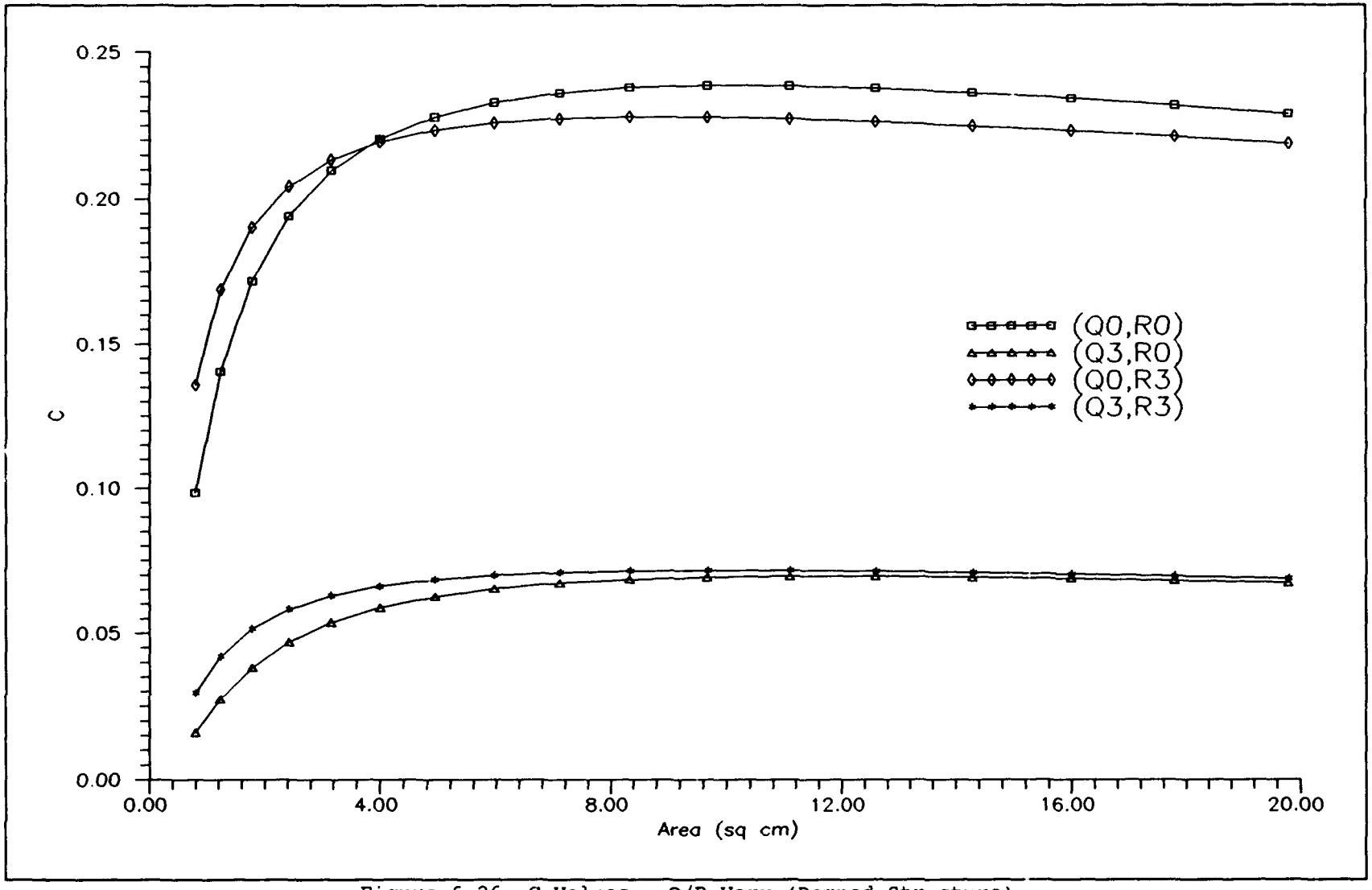

Figure 6.26 C Values - Q/R Vary (Damped Structure)

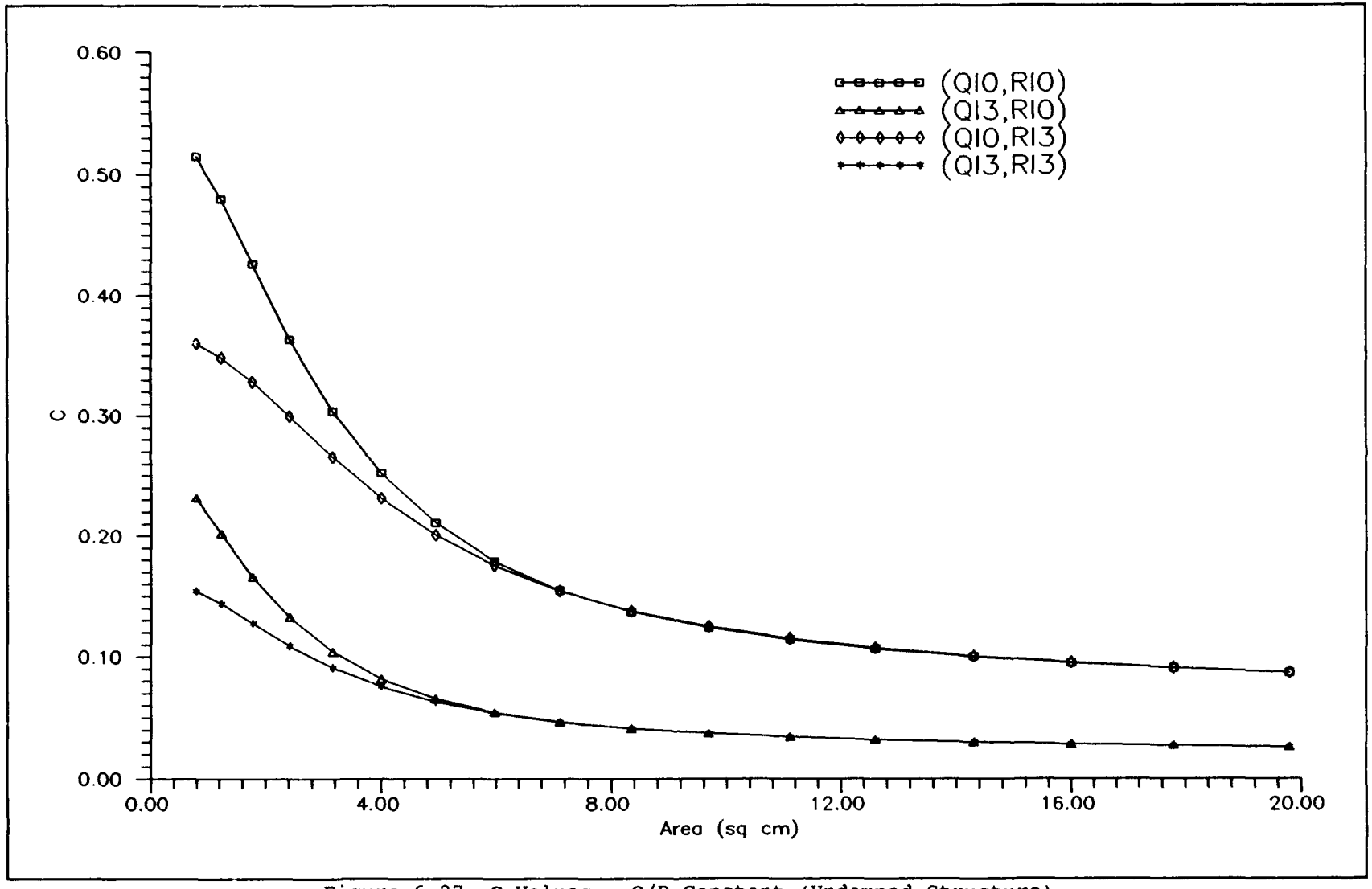

Figure 6.27 C Values - Q/R Constant (Undamped Structure)

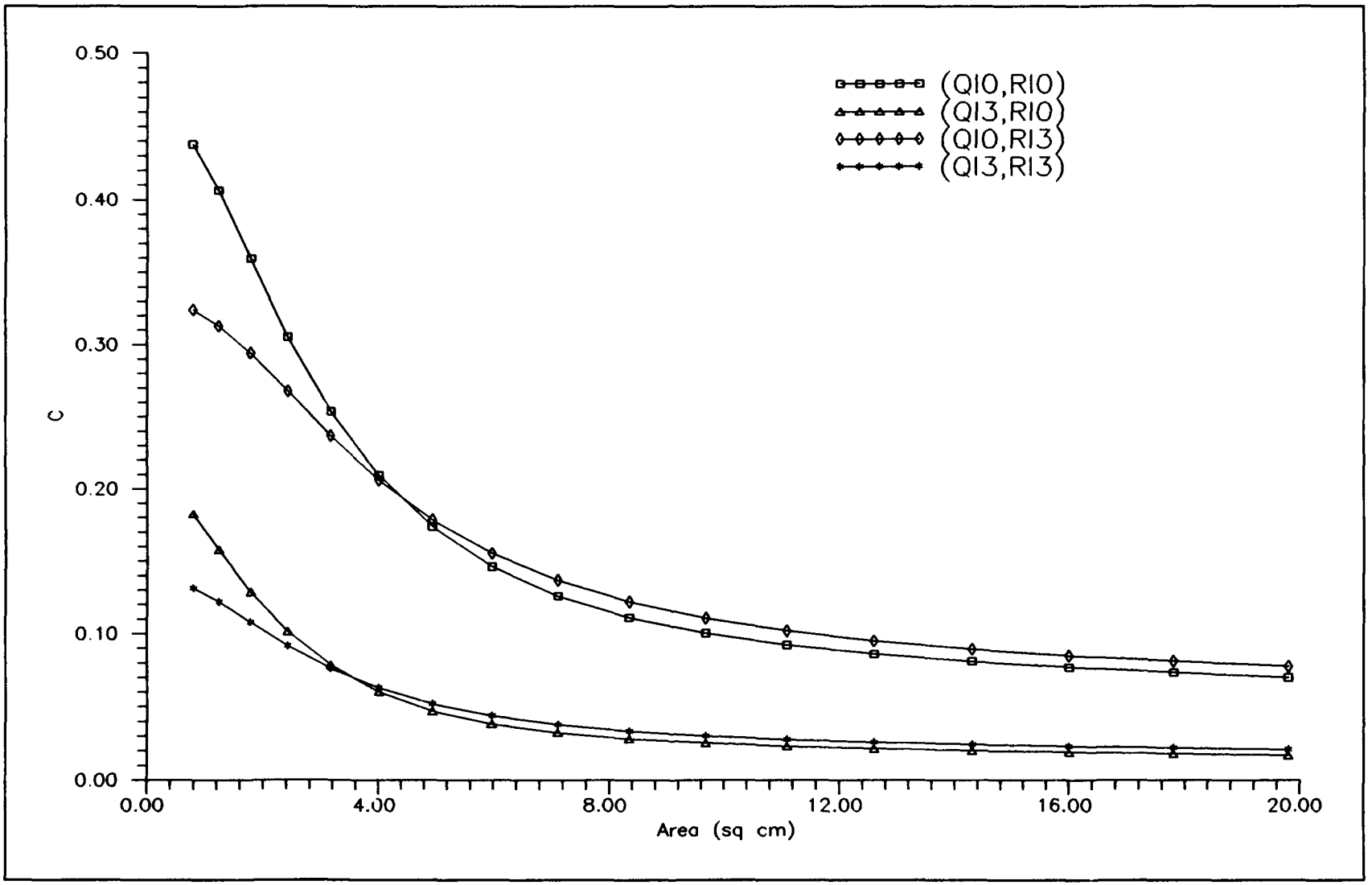

Figure 6.28 C Values - Q/R Constant (Damped Structure)

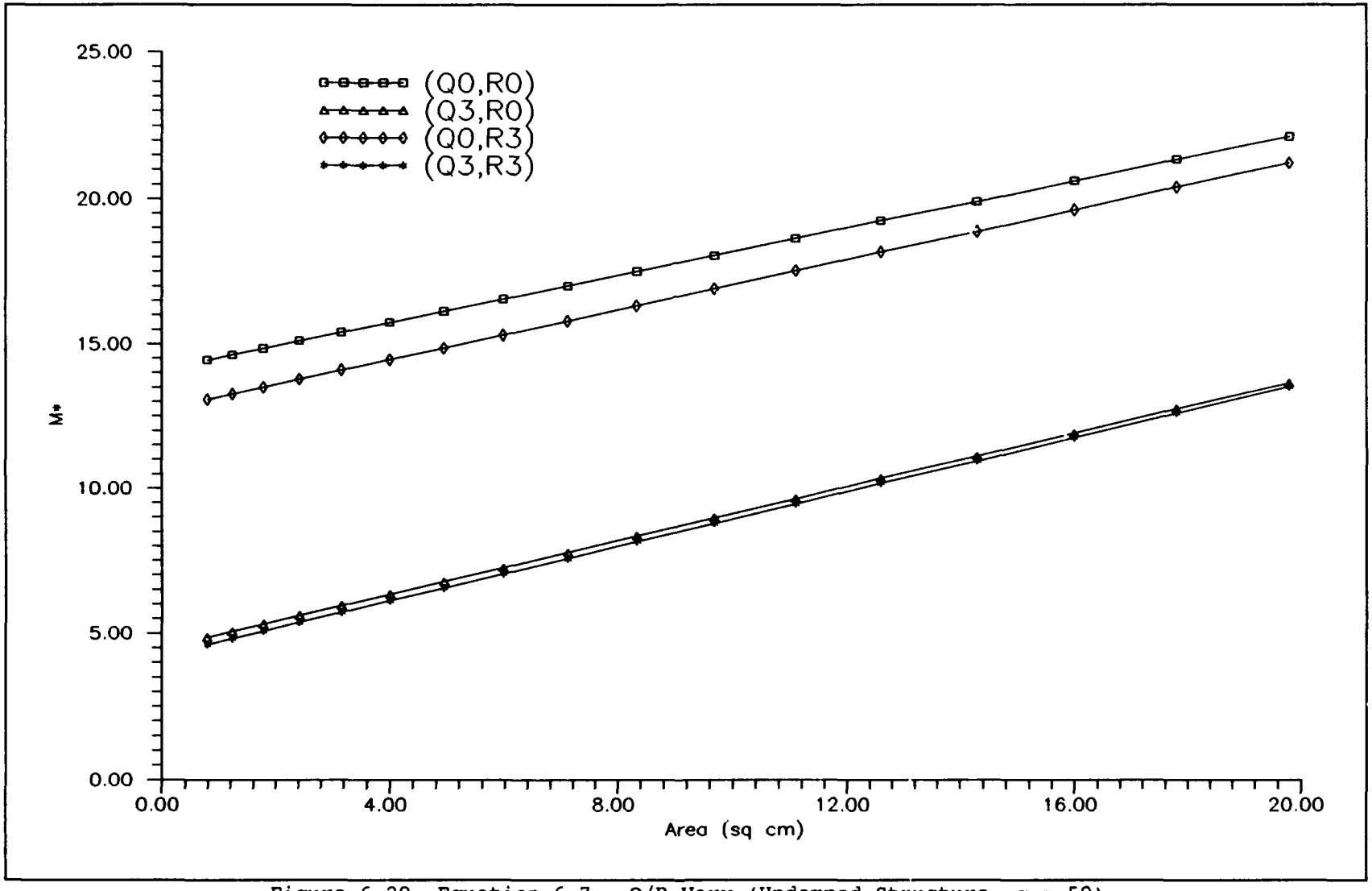

Figure 6.29 Equation 6.7 - Q/R Vary (Undamped Structure, α = 50)

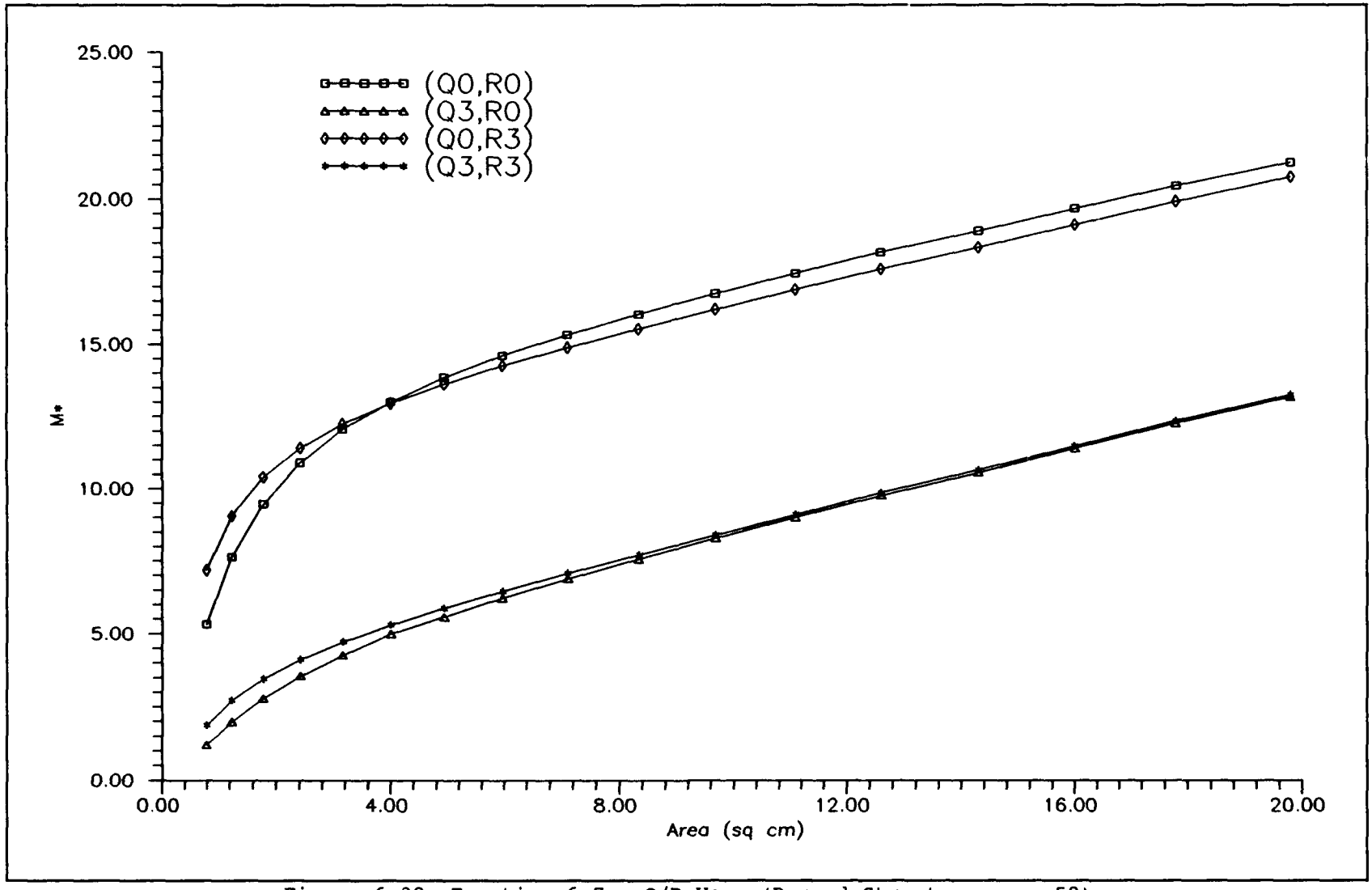

Figure 6.30 Equation 6.7 - Q/R Vary (Damped Structure, α = 50)

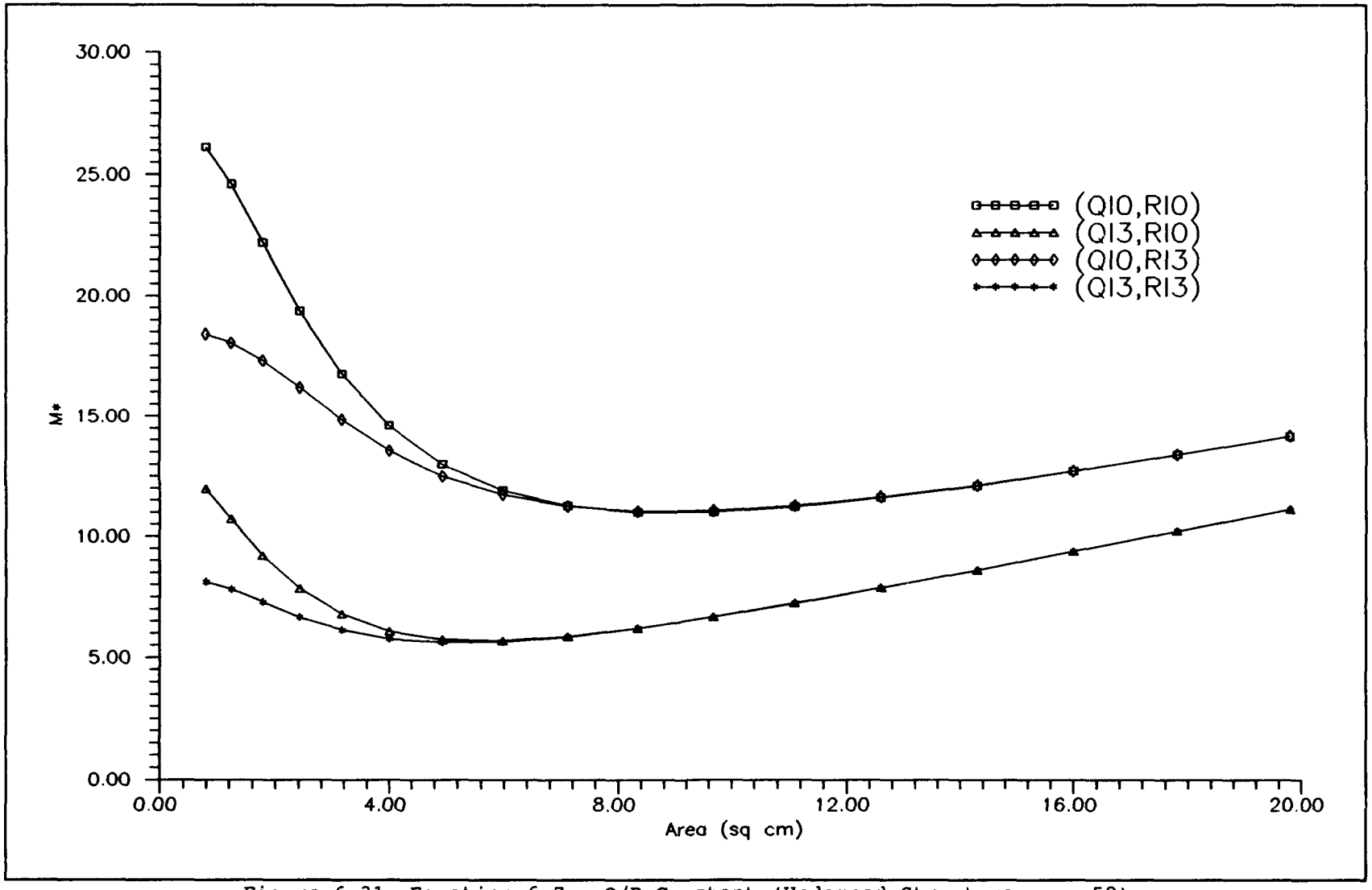

Figure 6.31 Equation 6.7 - Q/R Constant (Undamped Structure, α = 50)

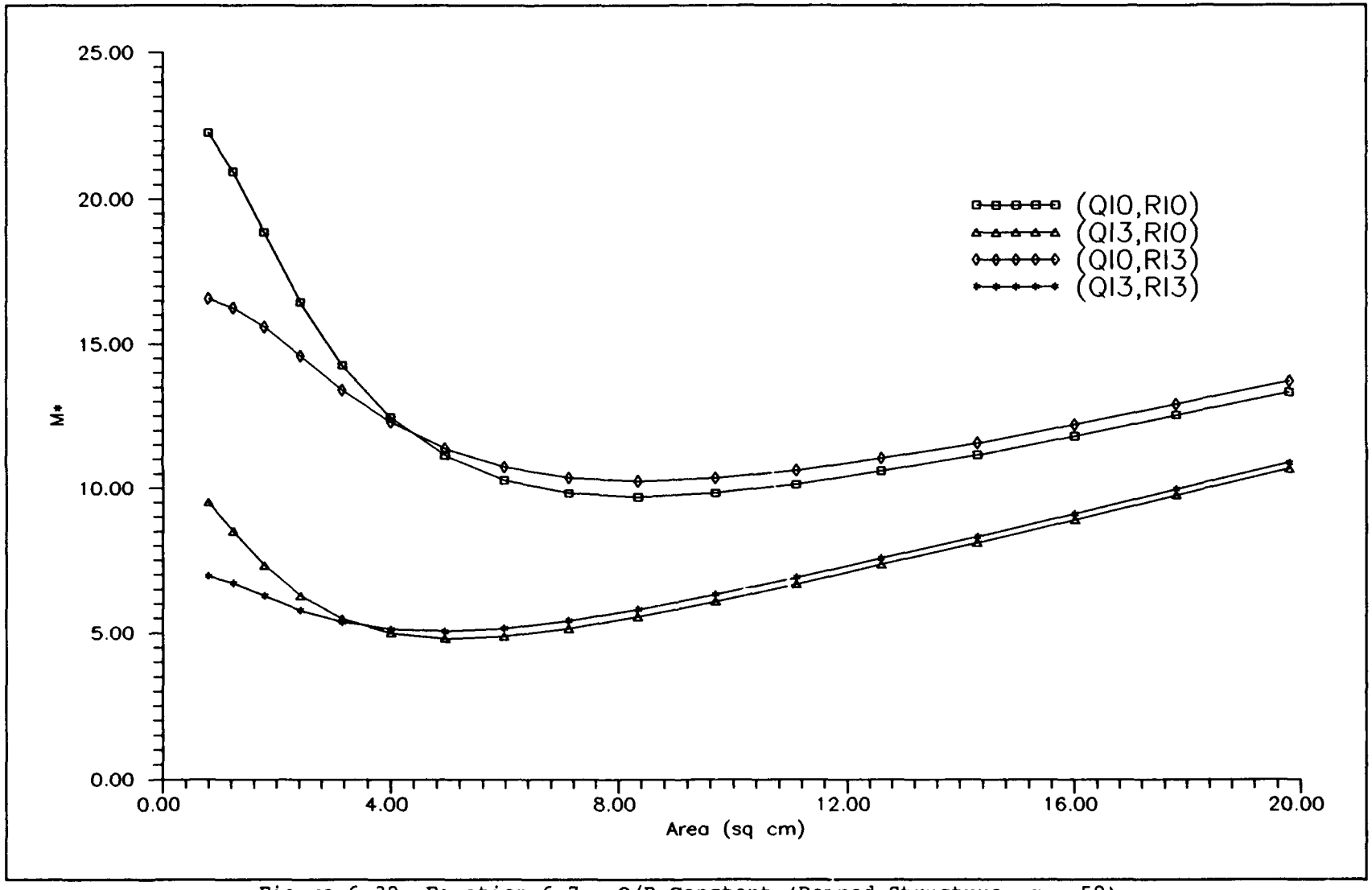

Figure 6.32 Equation 6.7 - Q/R Constant (Damped Structure, α = 50)

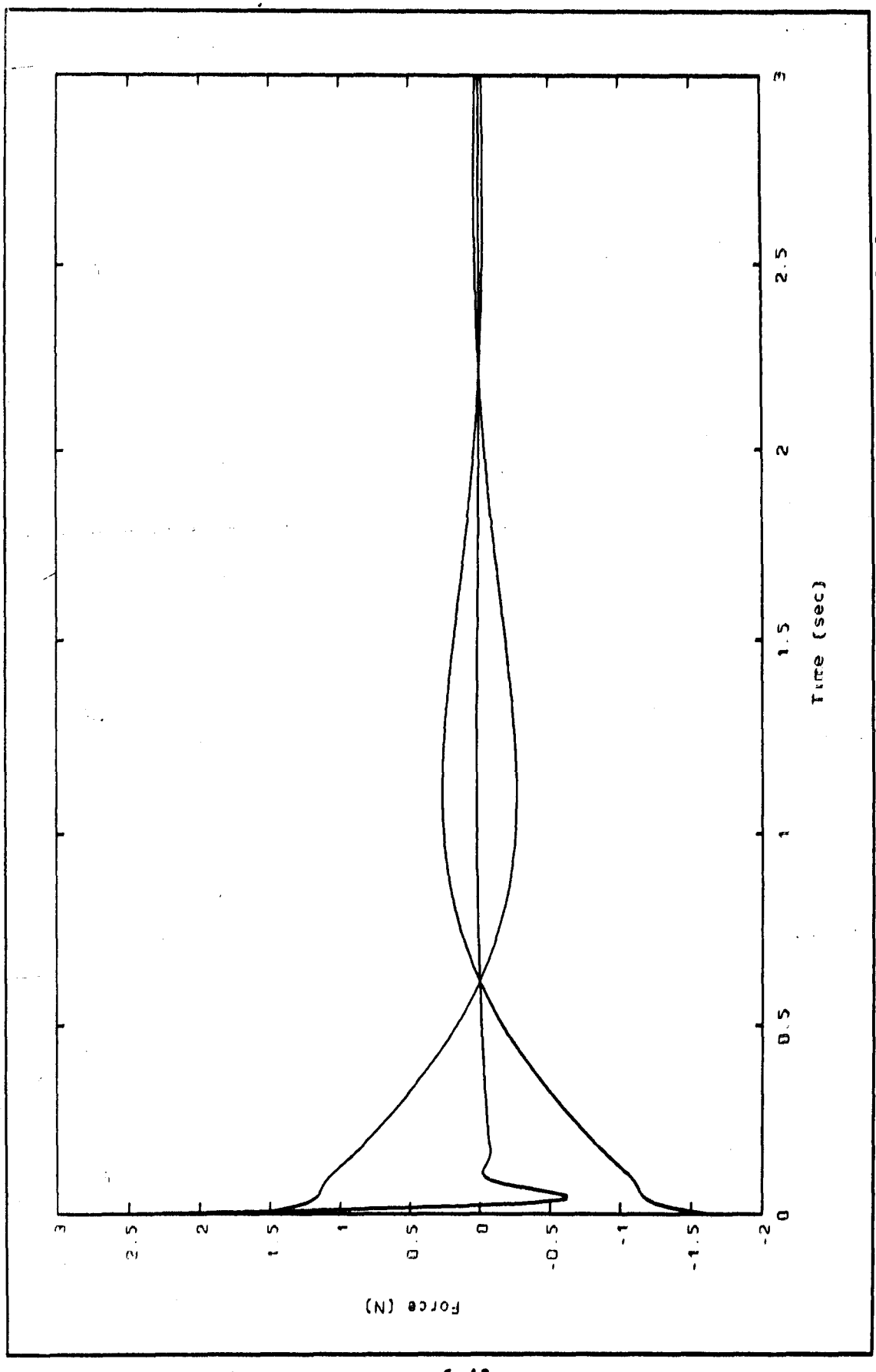

Figure 6.33 Beam #1 Actuator Responses - Q/R Vary (Undamped Structure, $\theta_Q=\theta_R=1$)

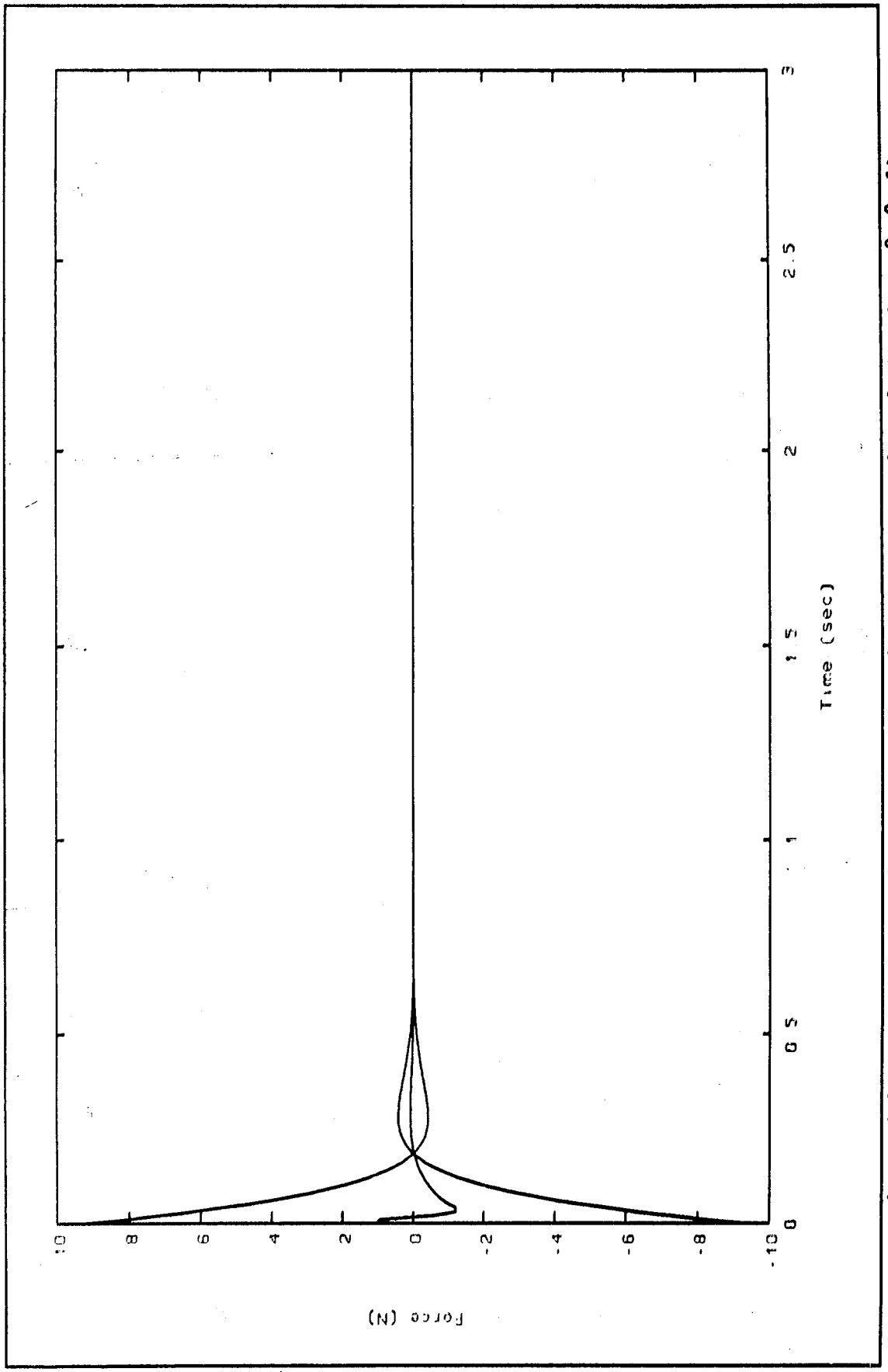

Figure 6.34 Beam #1 Actuator Responses - Q/R Constant (Undamped Structure $\theta_Q=\theta_R=1$)

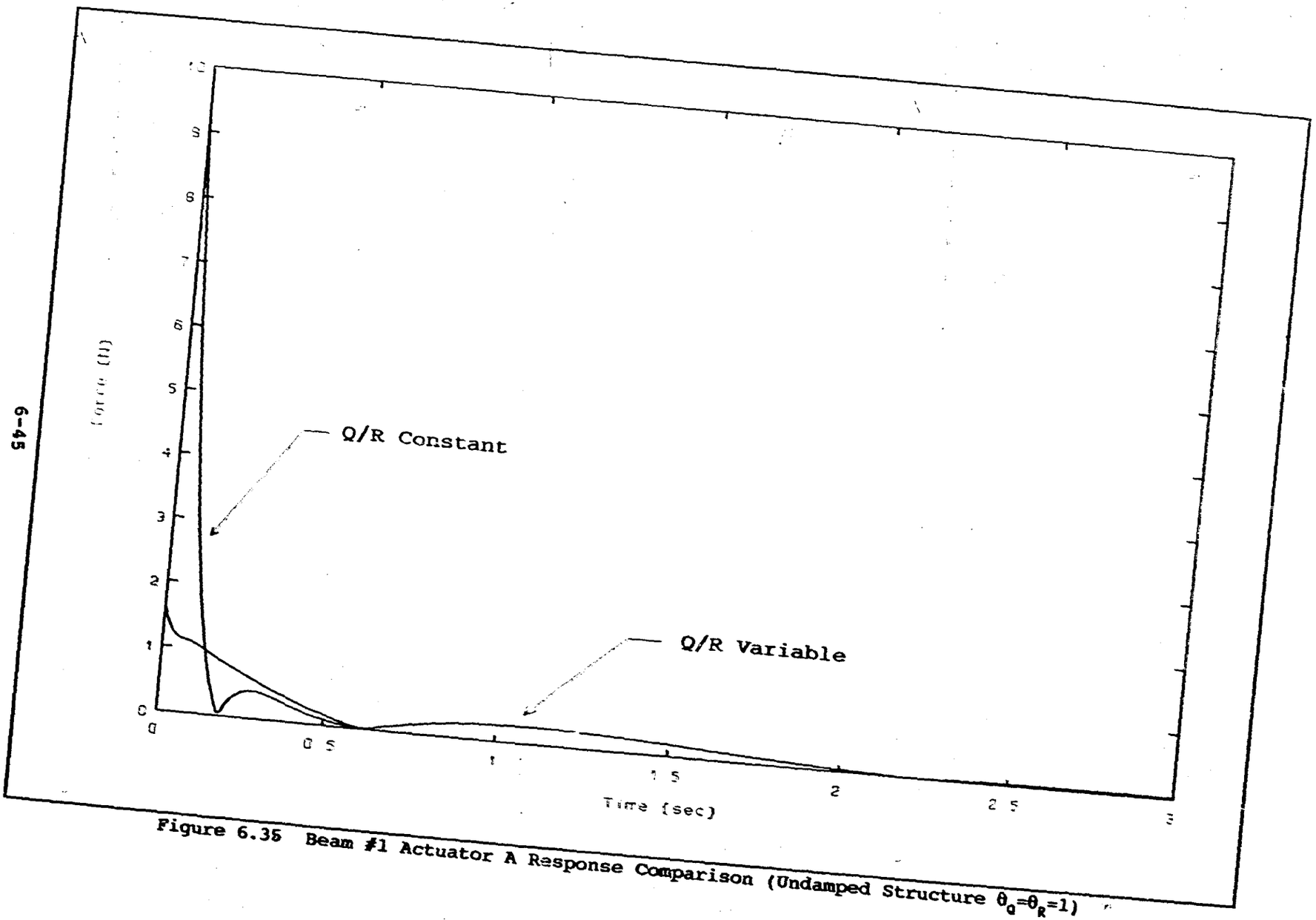

Figure 6.35 Beam #1 Actuator A Response Comparison (Undamped Structure $\theta_Q=\theta_R=1$)

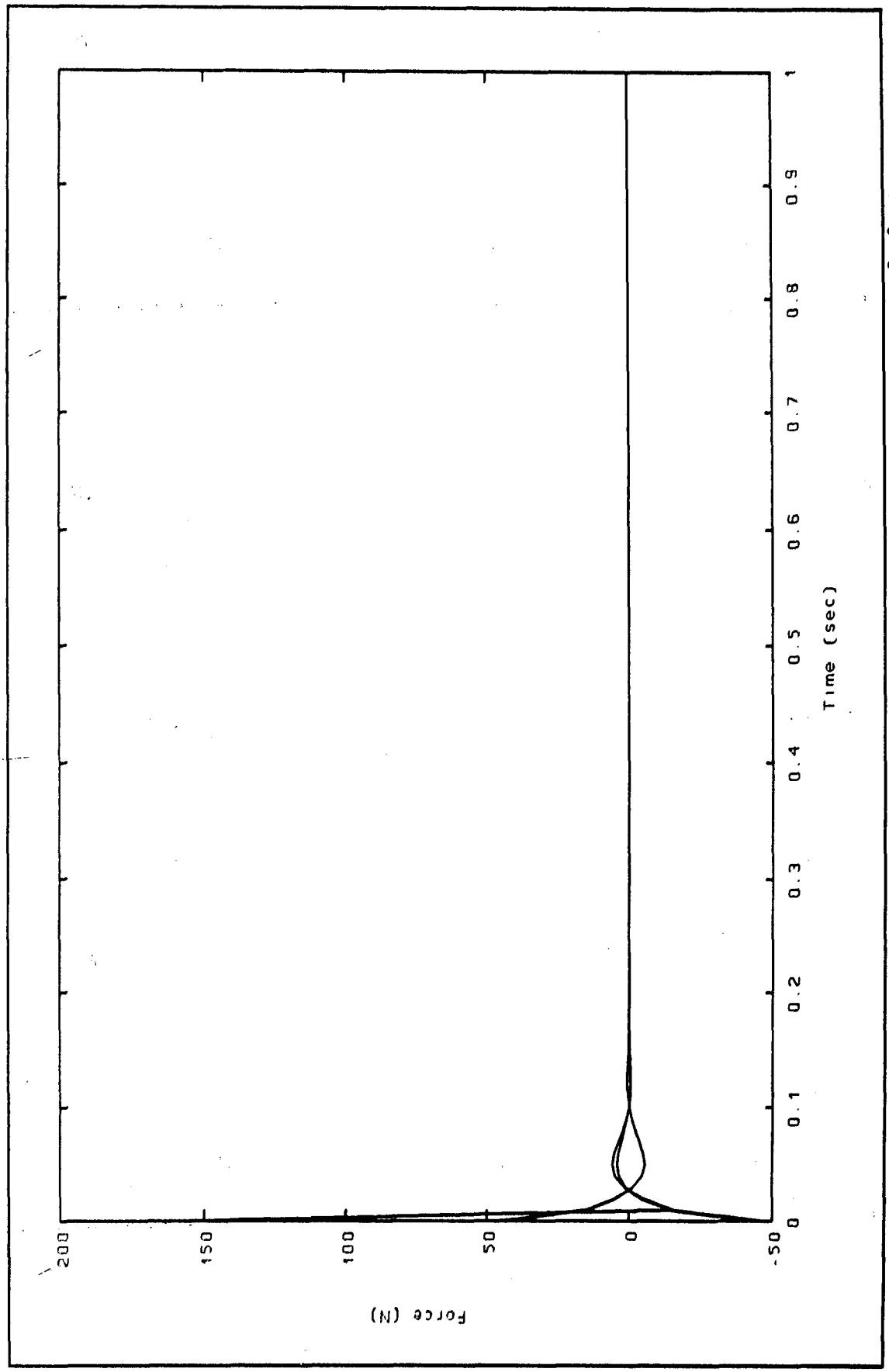

Figure 6.36 Beam #17 Actuator Responses - Q/R Vary (Undamped Structure $\theta_Q=\theta_R=1$)

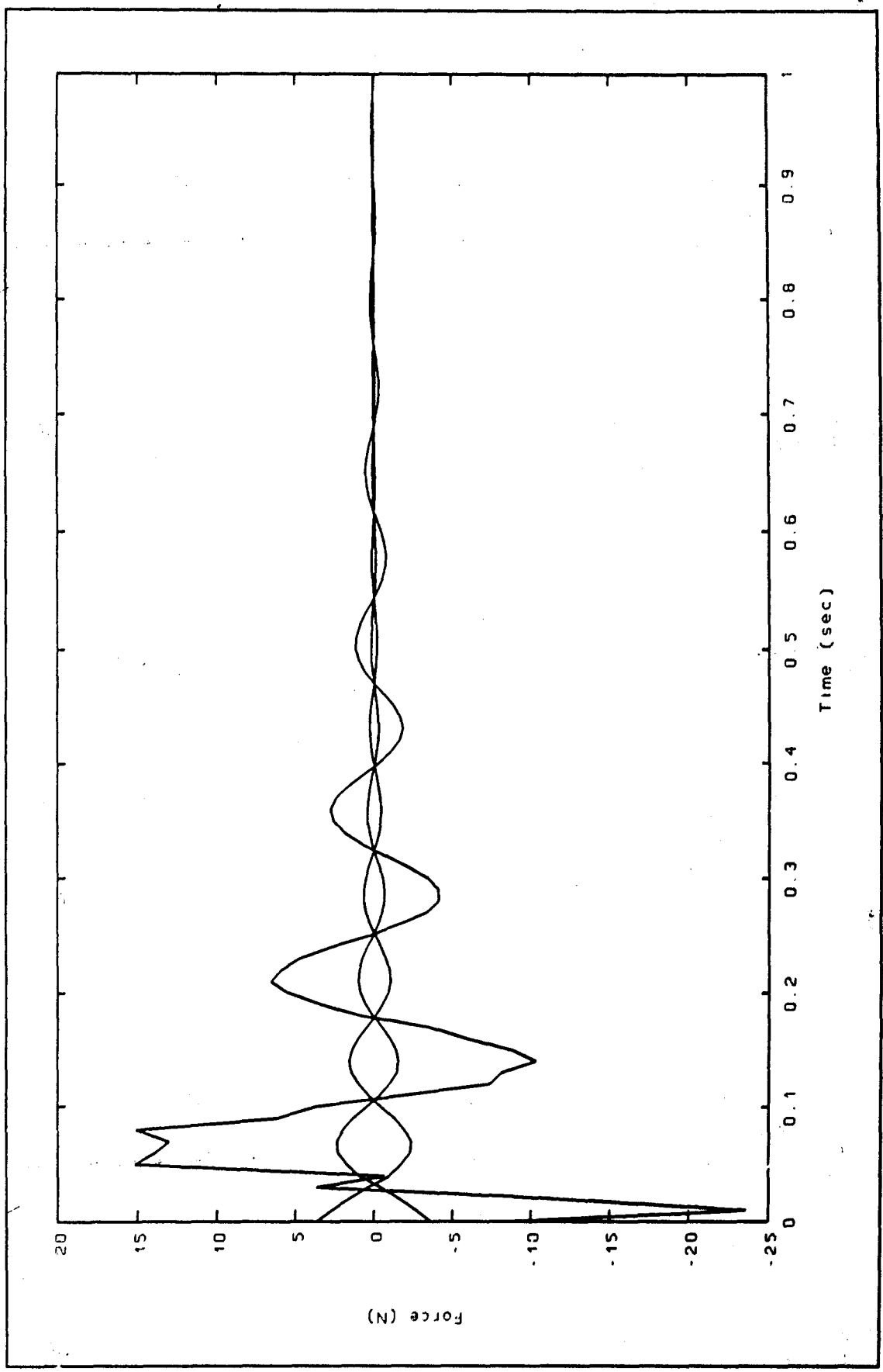

Figure 6.37 Beam #17 Actuator Responses - Q/R Constant (Undamped Structure $\theta_Q=\theta_R=1$)

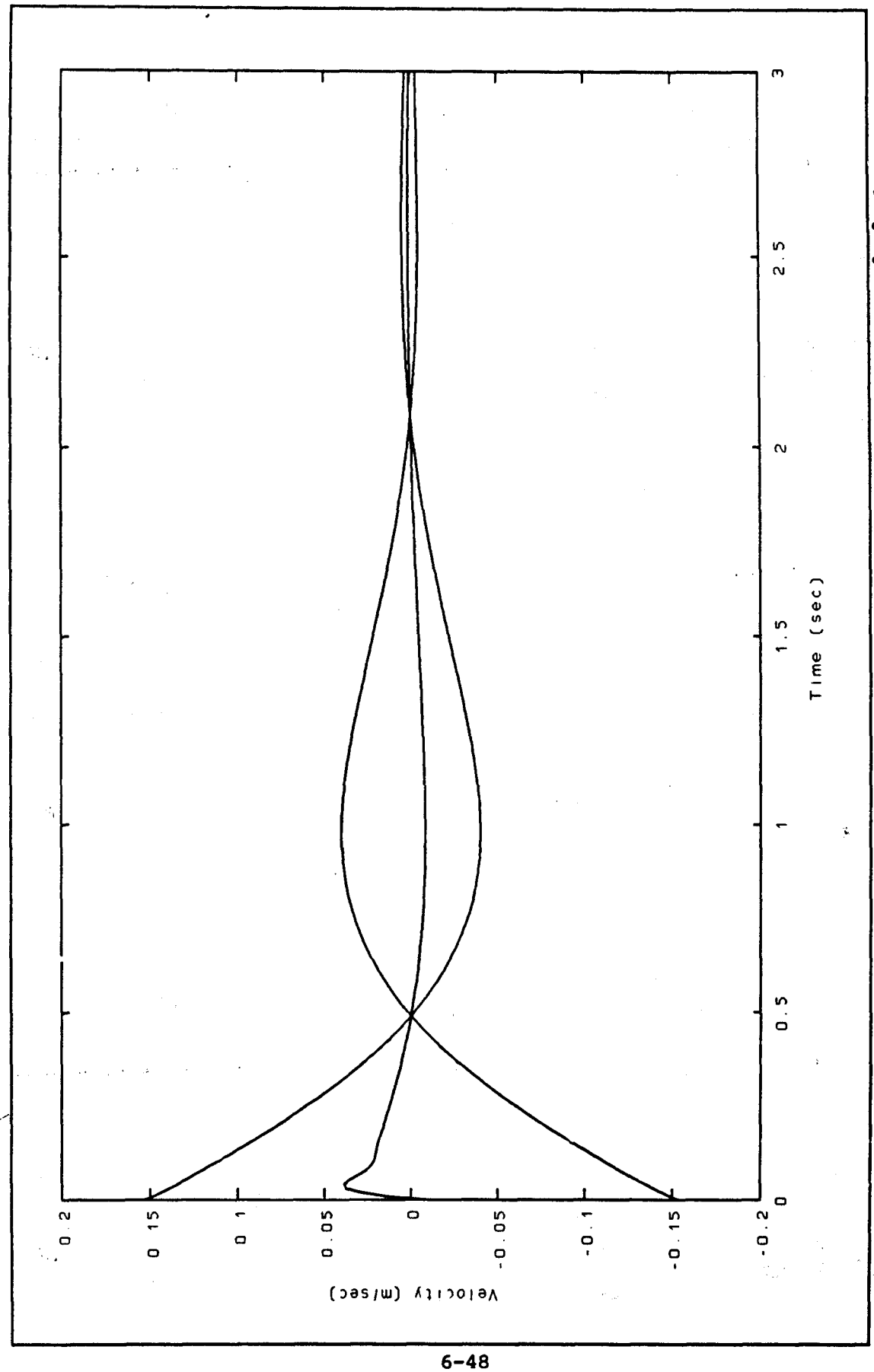

Figure 6.38 Beam #1 Structural Response - Q/R Vary (Undamped Structure $\theta_Q=\theta_R=1$)

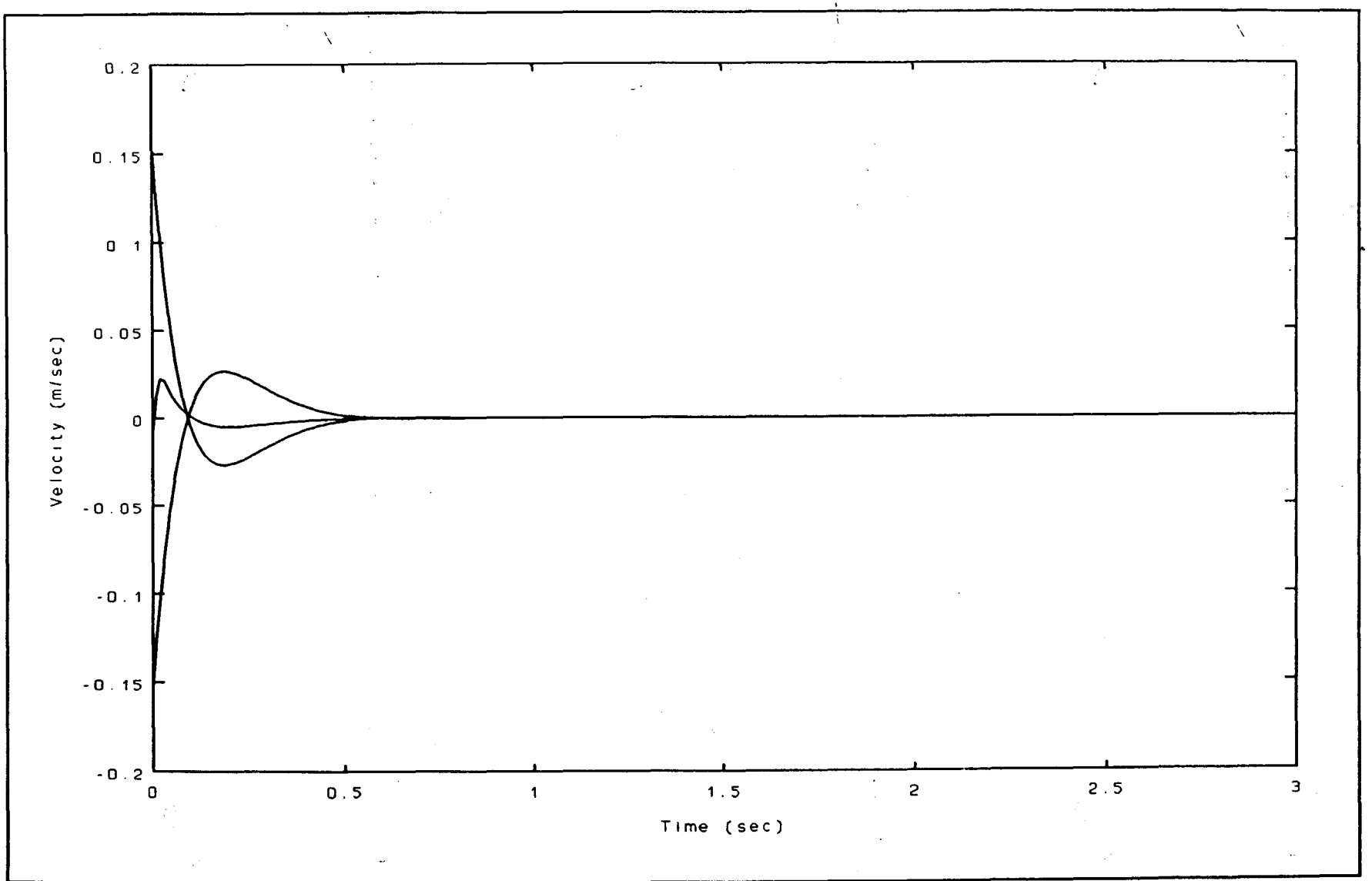

Figure 6.39 Beam #1 Structural Response - Q/R Constant (Undamped Structure $\theta_Q=\theta_R=1$)

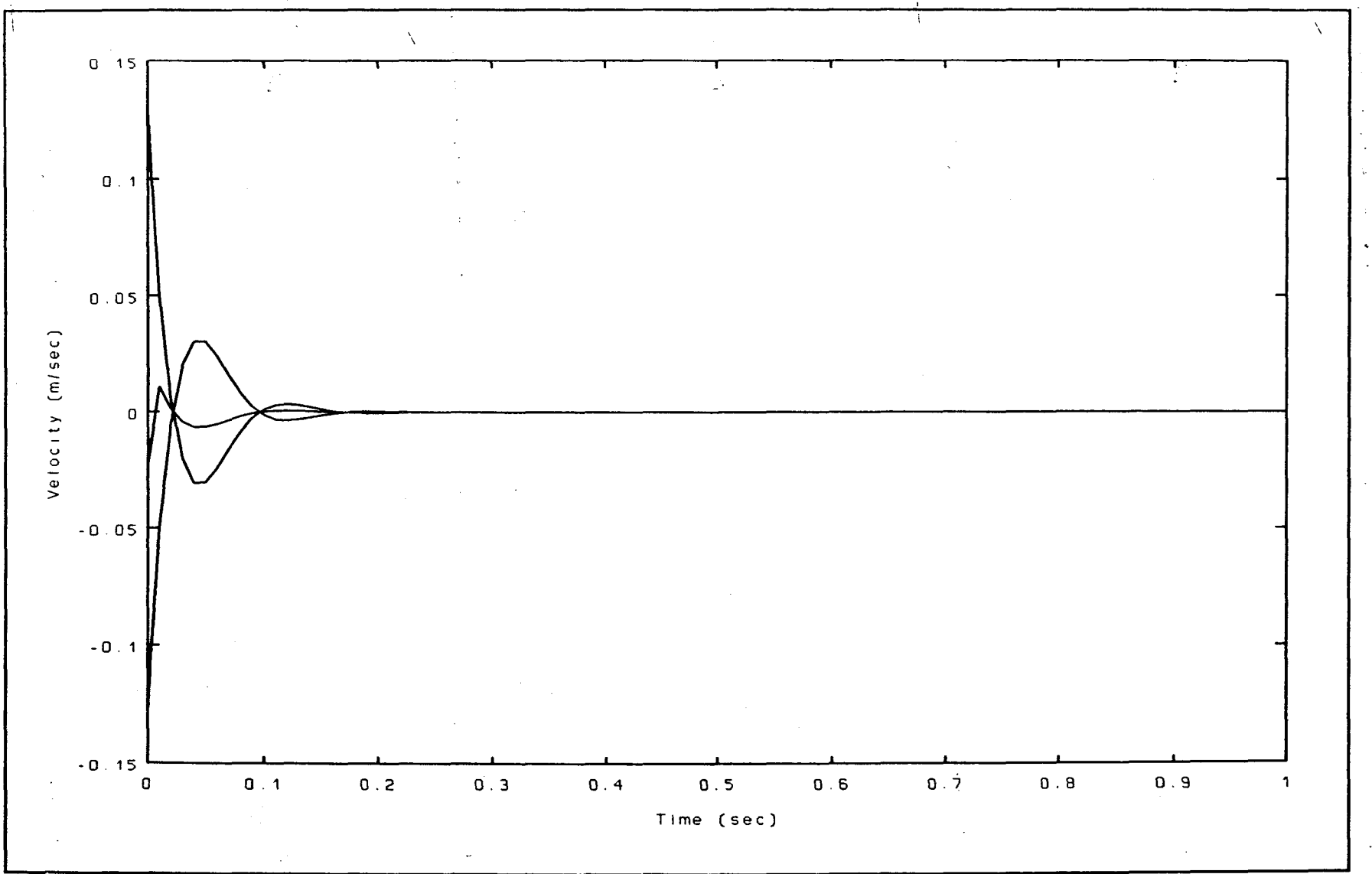

Figure 6.40 Beam #17 Structural Response - Q/R Vary (Undamped Structure $\theta_Q=\theta_R=1$)

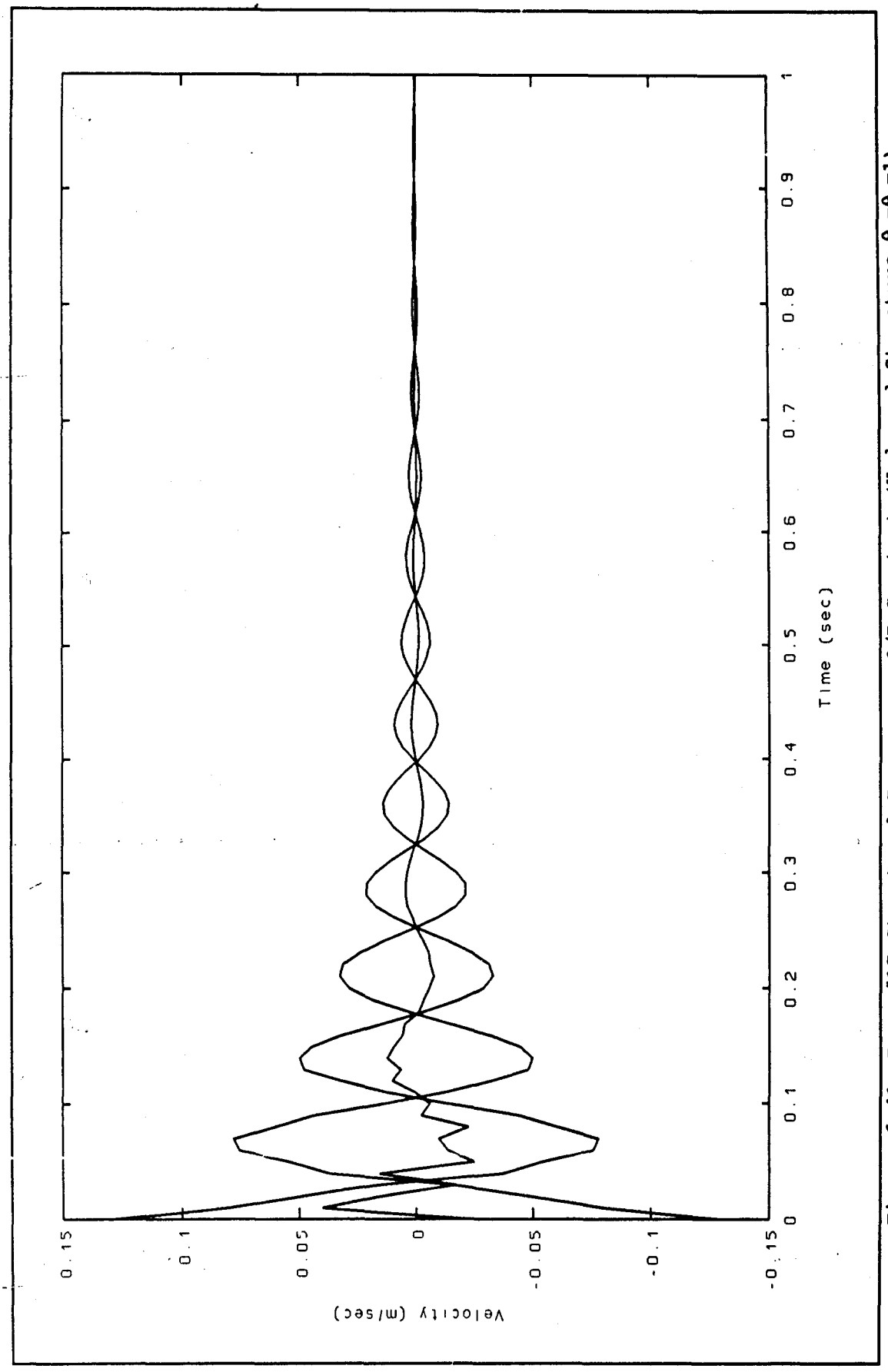

Figure 6.41 Beam #17 Structural Response - Q/R Constant (Undamped Structure $\theta_Q=\theta_R=1$)

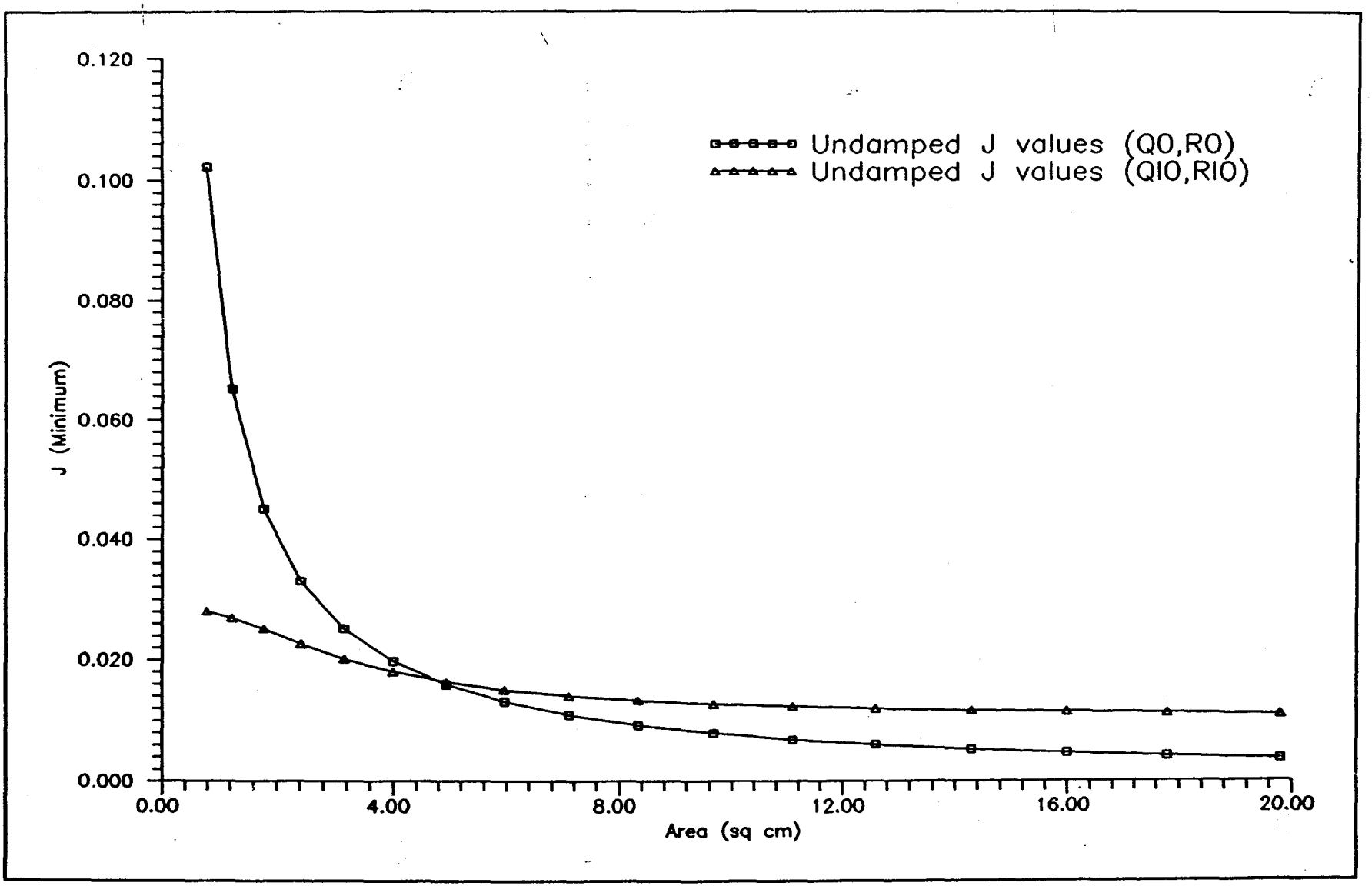

Figure 6.42 J Value Comparison

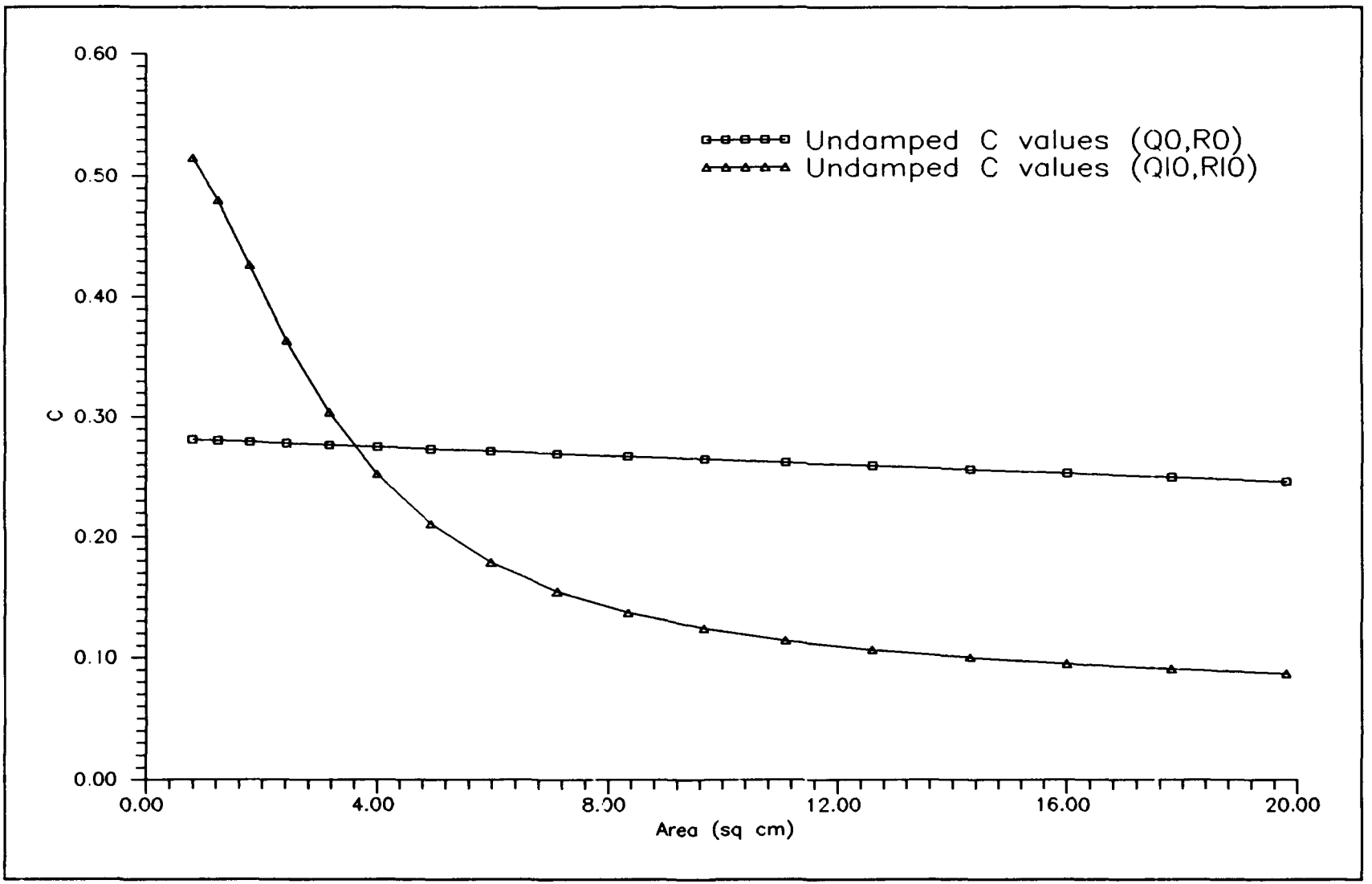

Figure 6.43 C Value Comparison

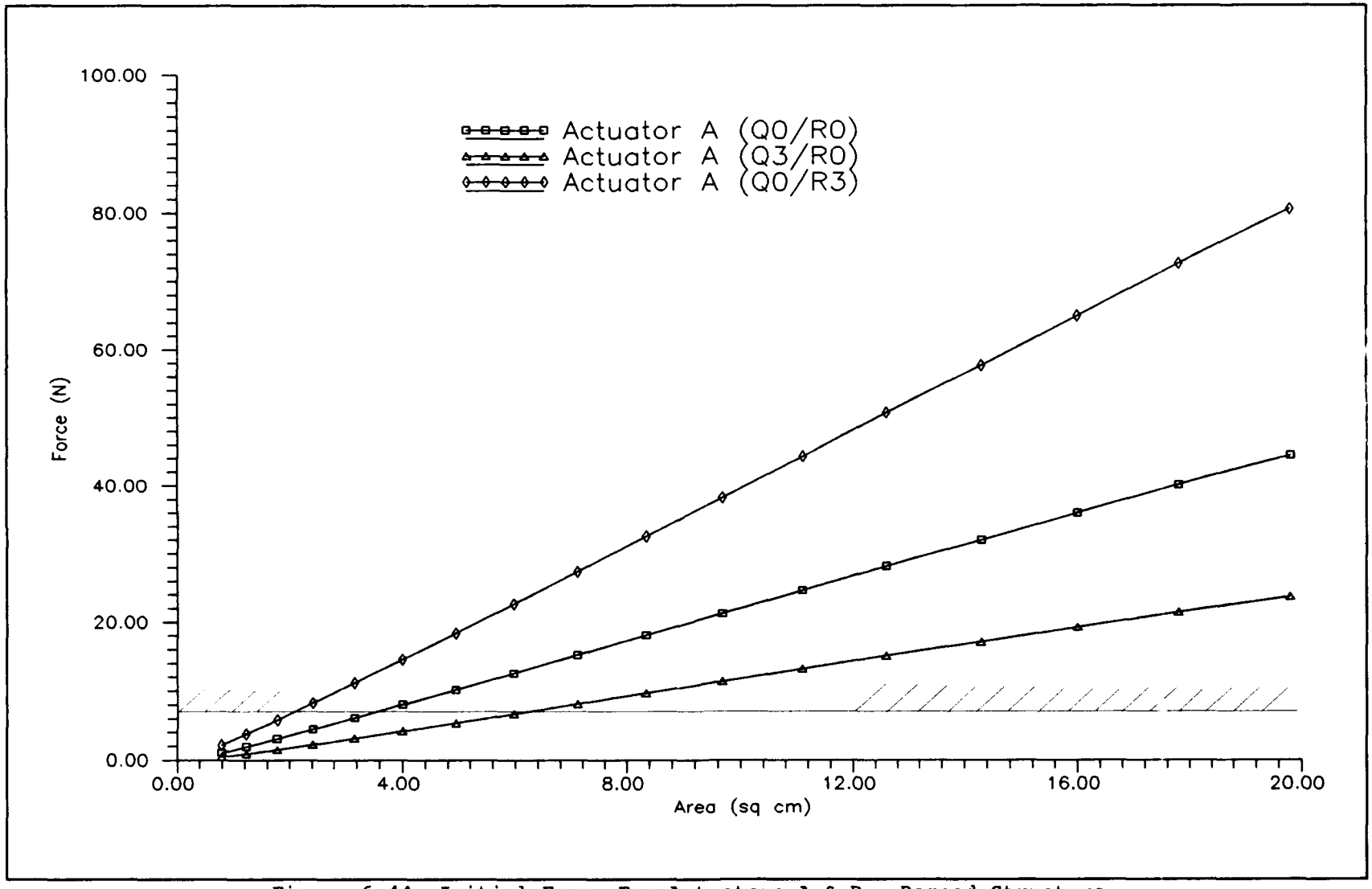

Figure 6.44 Initial Force For Actuators A & B - Damped Structure

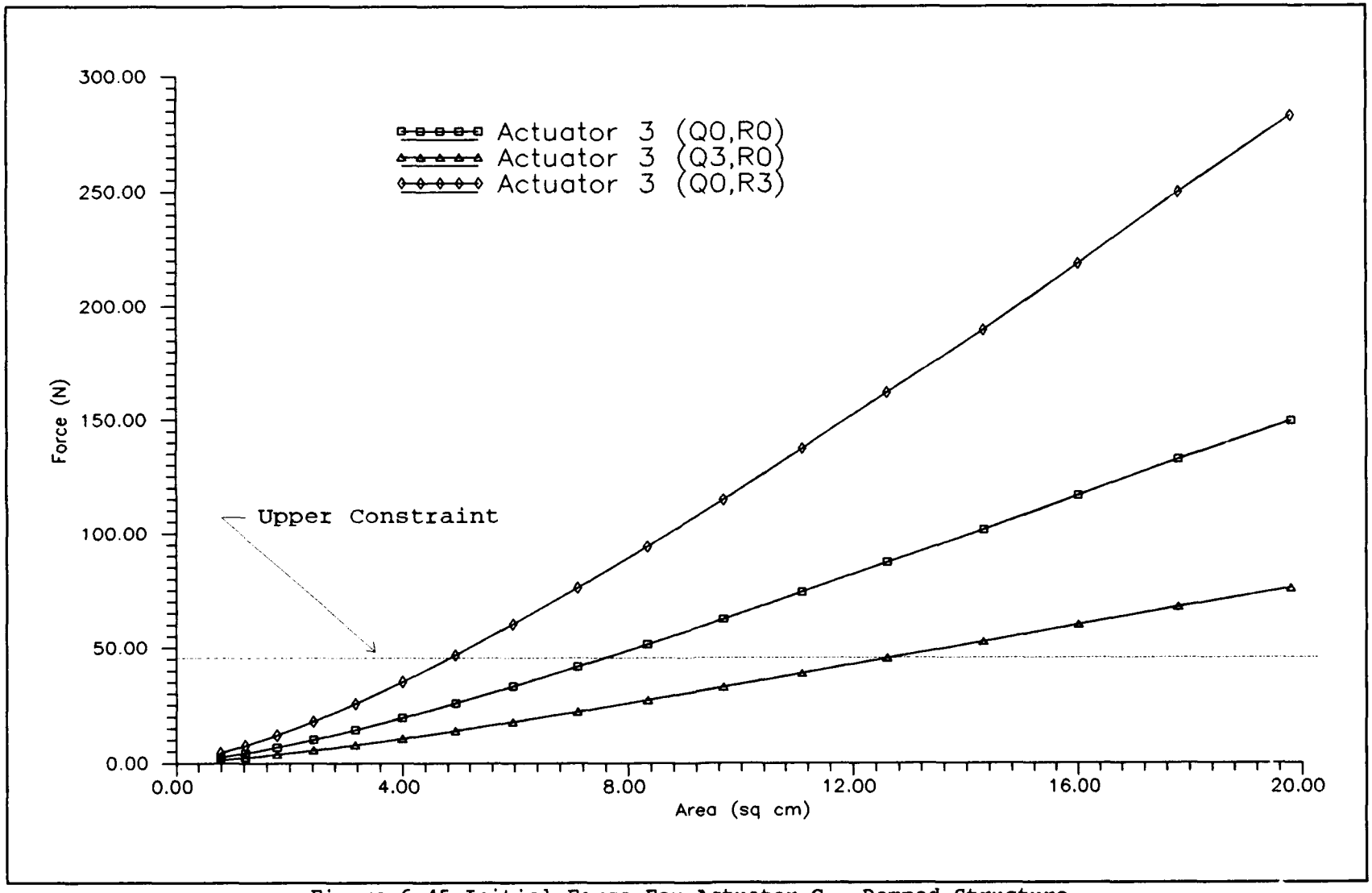

Figure 6.45 Initial Force For Actuator C - Damped Structure

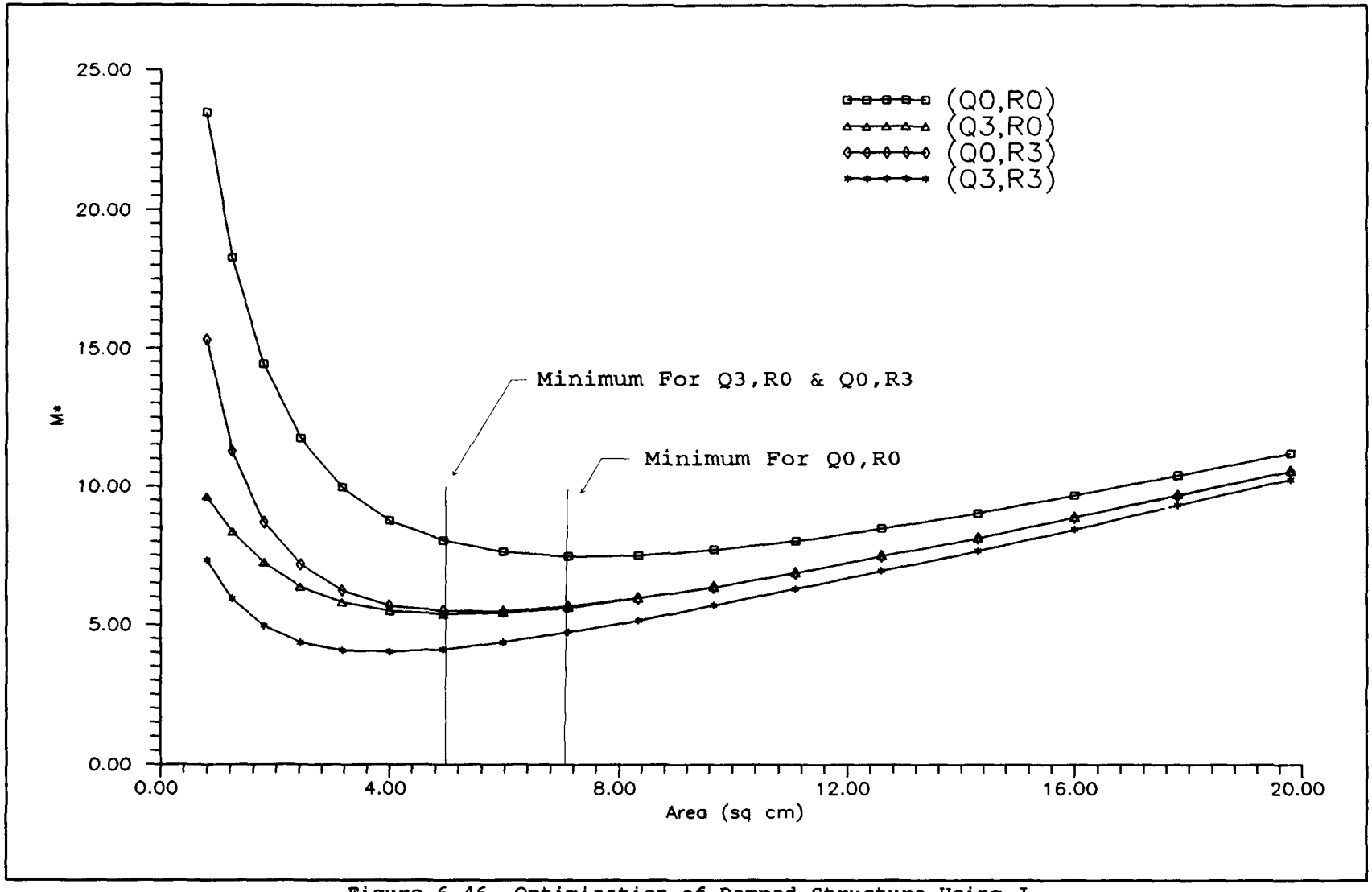

Figure 6.46 Optimization of Damped Structure Using J

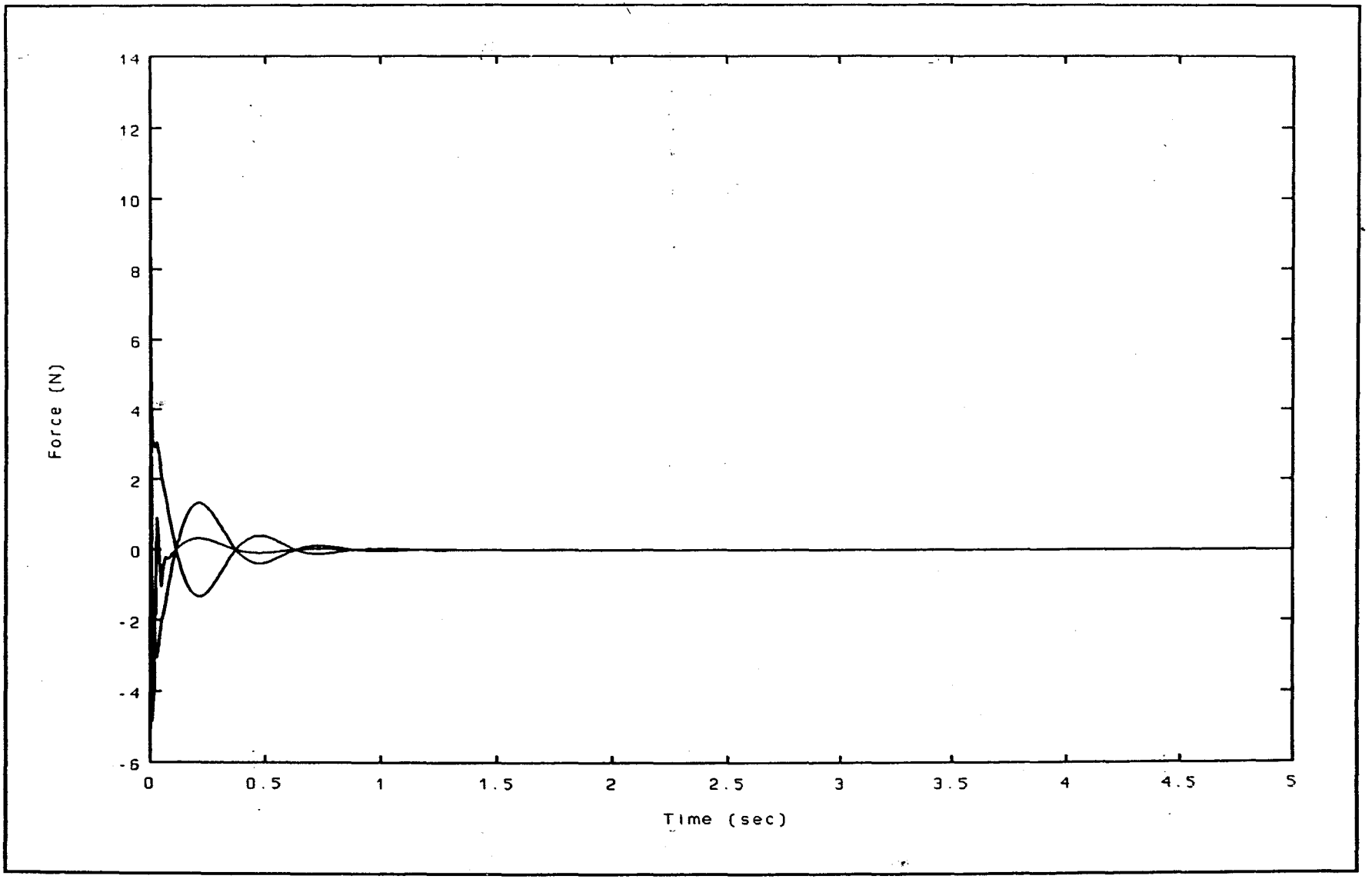

Figure 6.47 Optimized Control Response

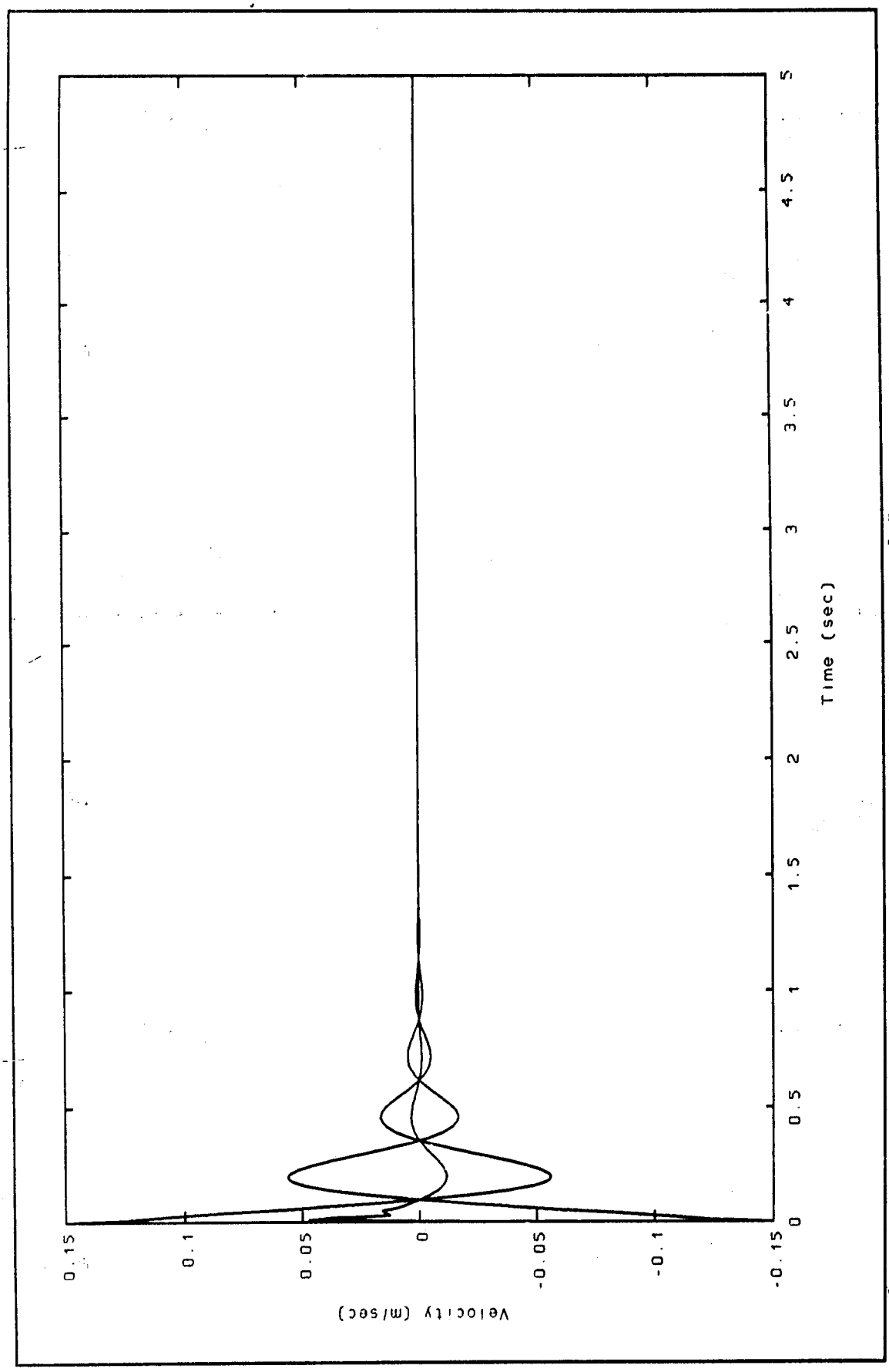

Figure 6.48 Optimized Structural Response

VII. Conclusions and Recommendations

Conclusions

Our goal is to place large structures in space. Both NASA and DOD are working on systems to be launched by the year 2000. If we are to realize this goal, we must explore every avenue to limit the economic costs. The cost of launching large structures into space will dominate the overall system cost. Since launch costs are driven by weight, reducing the weight of our structures will help keep them within our economic limits.

The purpose of this work was to model an existing structure and then to examine the structure/control optimization process. Since weight reduction was desired, two optimization processes were selected which minimize mass. The first method optimized the combined mass of the structure and the total system energy of the structure and the control system. The second method related the mass of the control system to the required control energy, then optimized the mass of the control system and the mass of the structure. Both methods proved successful, but each method resulted in different optimized structures.

The reason for the difference can be linked to the selection of Q and R. When Q and R are allowed to vary, the effect on control theory is to maintain a constant percent overshoot. For the lighter structures, a smaller control system can prevent the system from exceeding the overshoot specification. However, the smaller control system will not dampen the vibration as quickly. Since the first method uses the total system energy, a higher J value will result for the smaller structures. The goal is to then lower this system energy by increasing the structural mass and the control system inputs to a point where system mass and system energy are optimized. Onada's formulation has the opposite effect. Since the control effort required is lower

when constant overshoot requirements are needed, the optimization implies that the smallest structure which meets the load specifications is the optimized structure. When settling time requirements drive the control design, more control energy is needed to quickly dampen out the lighter structures. This results in a higher C value for Onada's formulation but since the vibrations have been quickly attenuated, the overall J value is small. Onada's optimization results in very heavy control systems then for the smaller structures.

Contributions

Which optimization method do you use then and how do you select Q and R with their appropriate weighing parameters? The answer to this question is highly dependent on the design goals you are trying to achieve. Trends were shown which should help other researchers select Q/R and an appropriate optimization procedure for various control specifications. For the ABE, this work has provided a baseline for additional research on the structure/control optimization problem.

Recommendations For Future Work

1. Additional work is needed to characterize the actuator dynamics. The finite element model created for this work included the viscous damping of the actuators. The viscous damping assumption was verified (7:19) by modal testing. Stiffness effects from the electronic centering spring, however, were not modeled and this contributed to the high error rate in Table 4.6.

2. One of the biggest challenges (4:472) facing LSS control engineers is the development of inertial actuators. The ABE provides an excellent test bed on which to design new actuators and to compare the performance of different actuators. Cristler (5) goes to some length in documenting the problems associated with developing the existing proof mass actuators. Theoretical work charting the stability regions of the

structure/control system would help future engineers design new actuators. This work should include the effects of damping, stiffness, and control gain.

3. To examine the control/structure optimization process, this work assumed that all modes were observable. Clearly this is not the case. The initial conditions suggest that higher order modes are being excited to a greater degree in the smaller structures than in the larger structures. A comparison between the results of this work and one which includes a state estimator would be interesting to determine the effect higher order modes have on the selection of the optimal structure-control system.

4. A "true" optimum was not determined in this work. An opportunity exists to program the methods presented in Chapter VI subject to the constraints on the ABE control system. In addition, the selection of q_1 and q_2 can be nested in the optimization process. If physical meaning can be given to q_1 and q_2, their inclusion in the optimization loop will be necessary to achieve a true optimum design.

5. Damping inherent in the both the structure and the control system was modeled by proportional damping. For the lighter structures, inertia played a greater role in the damping factor. Stiffness, on the other hand, was predominate for the larger structures. As a parallel, different parameters were used to weight Q and R for comparison. When Q and R were selected by equations 5.25 and 5.26, it was assumed that $\theta_m = \theta_k$. What effect does varying these parameters have on the structure-control optimization?

6. Finally, Jacques pointed out in his conclusion (7:87-88) that the ABE was an excellent test bed for further controls experiments and research. Additional work can be done to compare the various control laws and estimator designs. Other optimization schemes can be tested on the ABE before their use on more complicated structures. In short, new ideas should be tested in a known environment so their true merits can

be determined. With the base line experimental and theoretical research accomplished, the ABE is a known environment.

Appendix A: Calculation of ABE Physical Properties

Beam Physical Properties

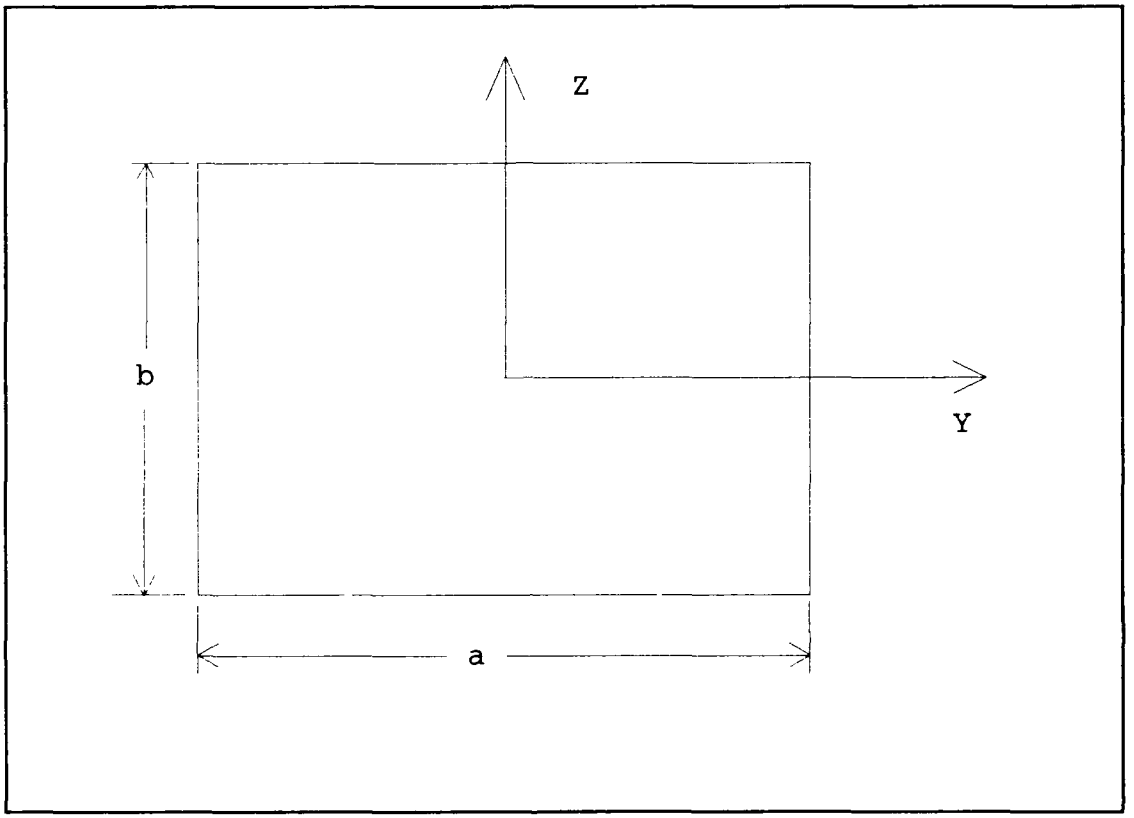

Figure A.1 Beam Cross Section

$$I_y = \frac{ab^3}{12} \qquad \text{(A.1)}$$

$$I_z = \frac{a^3 b}{12} \qquad \text{(A.2)}$$

$$I_p = I_y + I_z \qquad \text{(A.3)}$$

In general, if the cross-section is not circular, there will be some warping of the cross-sectional plane. For circular cross sections (9:200),

$$J = I_p \tag{A.4}$$

For noncircular cross sections, however,

$$J \neq I_p \tag{A.5}$$

J can be obtained from texts on advanced strength of materials. From (24:290), the value of J for a rectangular beam is

$$J = \frac{ab^3}{16}\left[\frac{16}{3} - 3.36\left(\frac{b}{a}\right)\left(1 - \frac{b^4}{12a^4}\right)\right] \tag{A.6}$$

Disk Physical Properties

$$I_{dxx} = m_d\left[\frac{r^2}{2}\right] \tag{A.7}$$

$$I_{dyy} = m_d\left[\frac{3r^2+t^2}{12}\right] \tag{A.8}$$

$$I_{dzz} = m_d\left[\frac{3r^2+t^2}{12}\right] \tag{A.9}$$

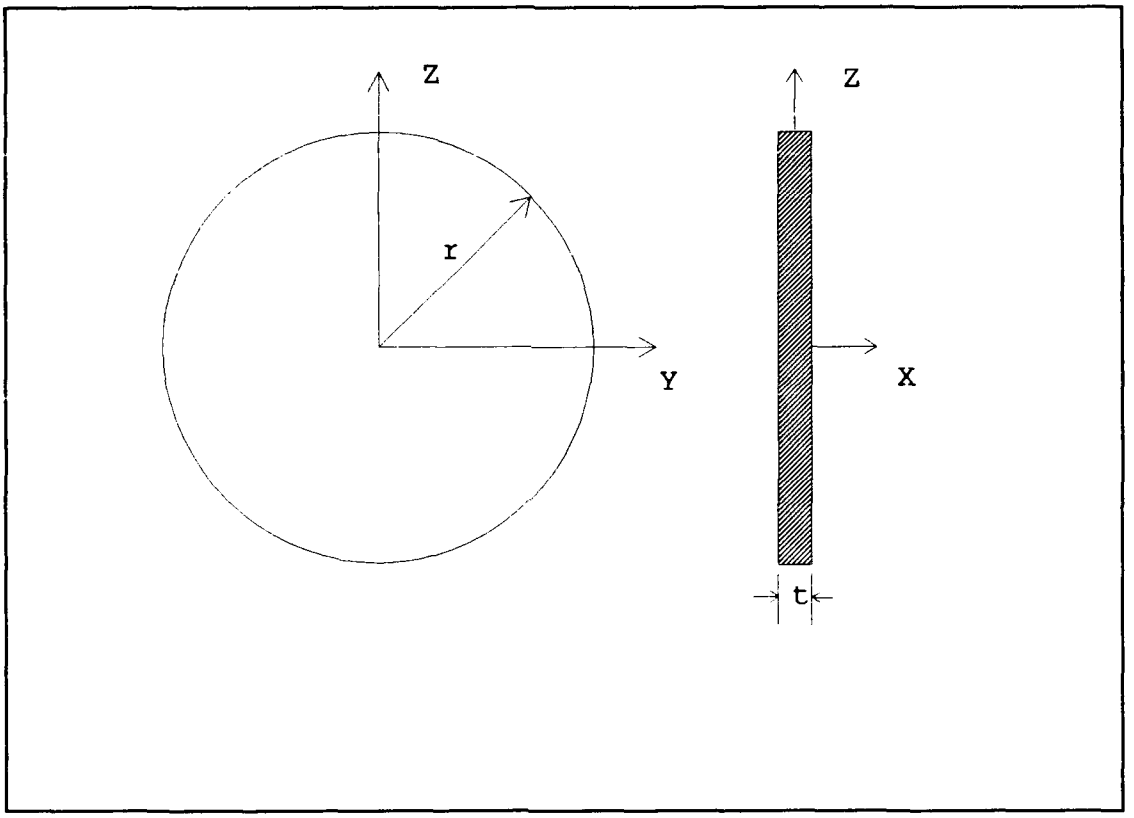

Figure A.2 Disk Dimensions

LINEAR MOTORS

KAISER ELECTROPRECISION

DEFINITIONS (Continued)

CONTINUOUS RMS CURRENT – Using maximum power dissipation and 60Hz impedance (since it is essentially resistive) a maximum current rating can be calculated from $P = I^2R$. However, the resistance used in this calculation is at maximum temperature, not the room temperature value given on the data sheet.

The resistances of both the coil and the secondary increase at 0.4% per degree Celsius, and the typical temperature rise of the secondary is about 2/3 that of the coil. RMS current rating is calculated from this information or measured experimentally.

RMS current rating multiplied by force constant gives RMS force rating. This is a useful number of comparing capabilities of motors, and is similar to rated torque of a rotary motor.

PULSE CURRENT – Three factors limit the maximum current pulse that may be applied to the motor.

- Demagnetization
- Heating damage to the coil connectors
- Physical strength of the armature assembly

Armatures are normally tested for strength at high temperature so that this failure mode should not be the limiting one. The other two processes depend on current pulse width as well as amplitude. Demagnetization only becomes a problem after secondary current, whose flux opposes armature flux, decays. Damage to connections only occurs if the current pulse is long enough to heat them excessively. The value given on the data sheet is a conservative one based on tests and experience.

MODEL 512 LINEAR MOTOR

The Model 512 is for use in disc recording systems, and other applications requiring servo-controlled linear motion. Constant force range is 0.9 inches. Total stroke is 1 inch.

Special units can be built with force constant up to 2.5 lb/amp.

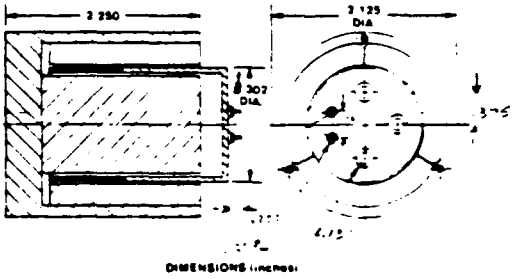

DIMENSIONS (inches)

MOTOR CHARACTERISTICS AT 25 C

Force Constant	= 1.0 lb/amp
Coil DC Resistance	= 6 ohms
Coil Inductance (1 kHz)	= 1.52 mH @ 1 kHz
Coil Mass	= 22.5 gm
Total Motor Weight	= 795 gm (1.75 lb)

MAXIMUM RATINGS AT 25°C AMBIENT

Coil Temperature	= 130°C
Power Dissipation	= 34 watts
Continuous RMS Current (dissipation limited)	= 2 amps
Pulse Current	= 10 amps, 10 msec

MODEL 517 LINEAR MOTOR

The Model 517 is a permanent-magnet moving-coil DC linear motor designed for positioning heads on floppy disc drives and for other applications requiring a compact linear driver. The constant force stroke length of the standard unit is 1.6 inches. Special motors of the same diameter but greater length can be designed for stroke requirements up to 3 inches without loss of efficiency. Customer-specified coil resistances and mounting interfaces can be provided. Single and bifilar-wound coils are available.

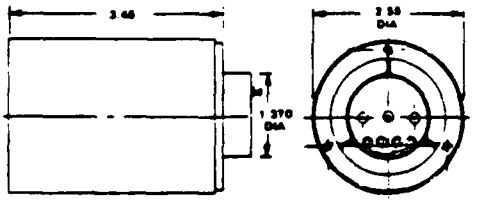

DIMENSIONS (inches)

MOTOR CHARACTERISTICS AT 25 C
Bifilar Winding – electrical characteristics for one half of winding

Force Constant	1.0 lb/amp
Coil DC Resistance	1.5 ohms
Coil Inductance (unretracted	2.0 mH at 1 kHz
.6 extended	3.4 mH at 1 kHz
Thermal Resistance (coil to	7°C/watt
Coil Mass	.36 oz
Total Motor Weight	3.1 lb

MAXIMUM RATINGS AT 25°C AMBIENT

Coil Temperature	130°C
Power Dissipation	15 watts
Continuous RMS Current (dissipation limited)	2 amps
Pulse Current	10 amps, 10 msec

Figure B.1 Linear Motor Specifications

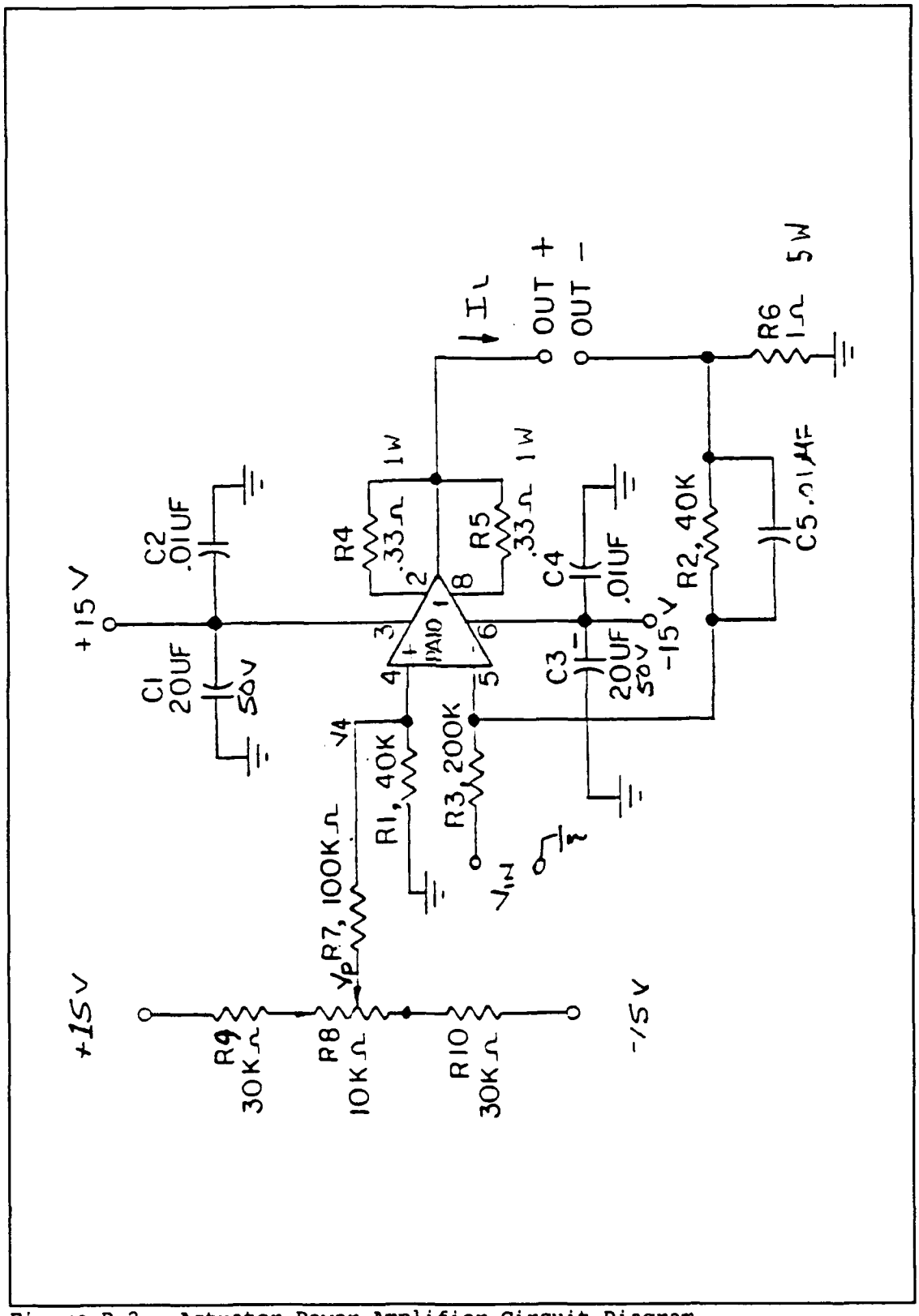

Figure B.2 Actuator Power Amplifier Circuit Diagram

HPD SERIES—HERMETICALLY SEALED (PIN TERMINATION)

- HERMETICALLY SEALED BY TIG AND EB WELDING
- IMPERVIOUS TO HOSTILE ENVIRONMENTS
- THROUGH-BORE CONSTRUCTION

HPD Series units are similar to the DC-D and HCD Series. Tungsten inert gas (TIG) and electron beam (EB) welding provide hermetic sealing that is free from oxidation-producing faults that may cause leakage. For this reason, HPD Series LVDT's are impervious to dirt, water, steam spray, and most corrosives. They have been qualified at pressures up to 1000 psig (70 bars) and are suitable for numerous high-pressure applications. HPD units employ a glass-sealed, pin-terminal header that allows the core and core rod to pass through the unit. HPD units have double magnetic shielding that makes them insensitive to external magnetic influences.

GENERAL SPECIFICATIONS

Input . . . . . ±15 V DC (nominal), ±20 mA
Operating Temperature Range . . . . . 0°F to +160°F (-18°C to +70°C)
Survival Temperature Range . . . . . -65°F to +200°F (-55°C to +95°C)
Null Voltage . . . . . 0 V DC
Ripple . . . . . Less than 25 mV rms
Linearity . . . . . ±0.25% full range
Stability . . . . . 0.125% full scale

Temperature Coefficient of Scale Factor . . . . 0.04%/°F (0.08%/°C)
Shock Survival . . . . . 250 *g* for 11 milliseconds
Vibration Tolerance . 10 *g* up to 2 kHz
Coil Form Material . . High density, glass-filled polymer
Housing Material . . . AISI 400 series stainless steel
Electrical Termination . . . . 6-pin terminal header
Output Impedance . . Less than 1 Ohm

PERFORMANCE SPECIFICATIONS AND DIMENSIONS

LVDT MODEL NUMBER	NOMINAL LINEAR RANGE	SCALE FACTOR	RESPONSE -3dB	WEIGHT Grams		DIMENSIONS A (Body)	DIMENSIONS B (Core)	DIMENSIONS P
	Inches	V/Inch	Hz	Body	Core	Inches	Inches	Inches
050 HPD	±0.050	200	500	36	2	2.40	0.59	0.55
125 HPD	±0.125	80	500	45	3	3.23	1.10	0.96
250 HPD	±0.250	40	500	57	5	4.10	1.80	1.38
* 500 HPD	±0.500	20	200	77	8	5.78	3.00	2.23
1000 HPD	±1.000	10	200	115	10	8.05	3.80	3.32
2000 HPD	±2.000	5.0	200	169	13	11.42	5.00	5.05
3000 HPD	±3.000	3.3	200	231	14	16.62	6.20	7.58
5000 HPD	±5.000	2.0	200	288	17	20.45	6.20	9.86
10000 HPD	±10.00	1.0	200	520	24	34.57	12.80	16.61

ORDERING INFORMATION

(Fold out page 32 for instructions on how to use this chart.)

OPTION NO	006 METRIC THREAD CORE (NOTE 1)	010 TEFLON BORELINER	020 SMALL DIAMETER CORE (NOTE 2)	040 10 FOOT (3m) LEADS	080 MILDLY RADIATION RESISTANT
MODEL NO					
050 HPD	N	B	B	–	X
125 HPD	N	B	B	–	X
250 HPD	N	B	B	–	X
500 HPD	N	B	B	–	X
1000 HPD	N	C	X	–	X
2000 HPD	N	C	X	–	X
3000 HPD	N	C	X	–	X
5000 HPD	N	C	X	–	X
10000 HPD	N	C	X	–	X

Note 1 See outline drawing for metric thread size
Note 2 Consult factory for max. dimensions and thread size

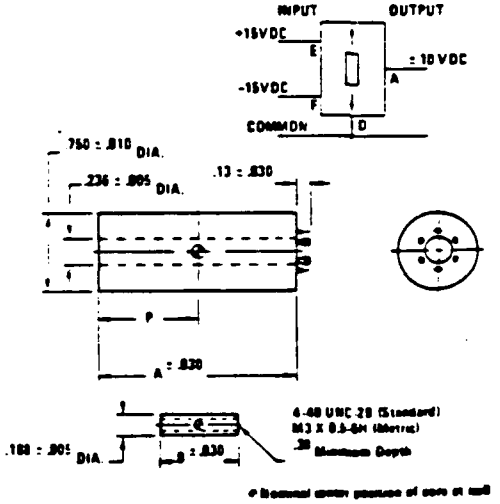

Figure B.3 LVDT Specifications

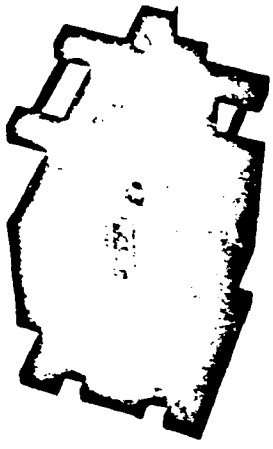

APS 113 with
0112 Reaction Mass

APS 113 Air Bearing Shaker

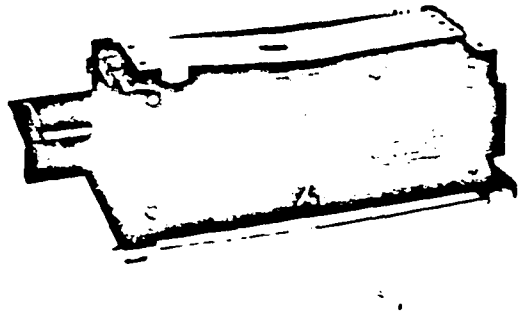

OPTIONAL CONFIGURATIONS

APS 113-AB Air Bearing Model Air lubricated bushings replace the linear ball bushings used in the basic **ELECTRO-SEIS** armature guidance system. In addition an air distribution system, tie down and leveling base are provided.

The near zero friction of the air bushings is an essential feature for measuring resonance decay rates in very lightly damped structures.

The Air Bearing configuration extends the application of the basic APS 113 to include the calibration and evaluation of accelerometers and other motion transducers in the seismic frequency range.

APS 113-LZ Low Impedance Coil
All features of the basic **ELECTRO-SEIS** Shaker are retained. The drive coil is wound in a manner which allow series or parallel connection, offering the user the choice of standard or low impedance. This option is required if the shaker is to be used with the APS 124 DUAL-MODE Power Amplifier for extended frequency range or random noise excitation.

APS 113-HF High Force Coil
All features of the basic **ELECTRO-SEIS** Shaker are retained as in the APS 113-LZ. The drive coil is provided to match the APS 124 DUAL-MODE Power Amplifier for 40% increase in force with a 50% duty cycle (1/2 hr cycle).

APS 113-LA Lightweight Armature
The body of the **ELECTRO-SEIS** Shaker is retained but the armature and guidance system are replaced with elements offering substantial weight reduction. The drive coil is lightened — with corresponding reduction in maximum force — and the armature guidance system elements are reduced in size and weight. This results in a corresponding reduction in cross axis stiffness and load carrying ability. The long stroke capability is retained and the frequency range for maximum force output is extended to 1000 Hz.

The Lightweight Armature is a desirable feature when using the shaker for exciting structures having low modal mass.

SPECIFICATIONS	Model 113	Model 113-AB	Model 113-LA	Model 113-LZ	Model 113-HF
Maximum Force Vector	30 lb 133 N	30 lb 133 N	10 lb 45 N	30 lb 133 N	42 lb 186 N*
Maximum Velocity Vector	30 in/s 76 cm/s	30 in/s 76 cm/s	30 in/s 76 cm/s	30 in/s 76 cm/s	30 in/s 76 cm/s
Maximum Stroke p-p	6.25 in 158 mm	6.25 in 158 mm	6.25 in 158 mm	6.25 in 158 mm	6.25 in 158 mm
Armature Weight	4.9 lb 2.2 kg	5.1 lb 2.3 kg	67 lb 300 g	5.0 lb 2.27 kg	4.9 lb 2.20 kg
Maximum Overhung Load at Armature Attachment Point	20 lb 9 kg	2 lb 9 kg	2 lb 9 kg	20 lb 9 kg	20 lb 9 kg
Air Pressure Required	N/A	30 psig, 2 kg/cm²	N/A	N/A	N/A
Armature Coil Impedance	8 Ohm	8 Ohm	4 Ohm	8 Ohm 2 Ohm	4 Ohm
Total Shaker Weight	80 lb 36 kg	80 lb 36 kg	75 lb 34 kg	80 lb 36 kg	80 lb 36 kg
Shipping Weight	100 lb 45 kg	100 lb 45 kg	95 lb 43 kg	100 lb 45 kg	100 lb 45 kg
Overall Dimensions					
Length	20.7 in 526 mm	20.7 in 526 mm	20.7 in 526 mm	20.7 in 526 mm	20.7 in 526 mm
Width	8.4 in 213 mm	8.4 in 213 mm	8.4 in 213 mm	8.4 in 213 mm	8.4 in 213 mm
Height	6.6 in 168 mm	6.6 in 168 mm	6.6 in 168 mm	6.6 in 168 mm	6.6 in 168 mm
Matching Power Amplifier					
Sinewave	APS 114	APS 114	APS 114	APS 124	APS 124
Random				APS 124-EP	APS 124-EP

*40% Duty Cycle

Figure B.4 Acoustic Power Systems Model 113-LA Structural Dynamics Shaker Specifications

ACOUSTIC POWER SYSTEMS, INC.
Systems for Generating Controlled Vibration

SPECIFICATIONS	Model 114	Model 124	Model 124-EP
Average Output, into shaker reactive load	125 V-A rms	250 V-A rms	250 V-A rms
Peak Output, into shaker reactive load	250 V-A rms	500 V-A rms	750 V-A peak
Current Output, peak (random noise)	6.0 A peak	12.0 A peak	18.0 A peak
Current Output, continuous	4.0 A rms	8.0 A rms	8.0 A rms
Frequency Range	0-2000 Hz	0-2000 Hz	0-2000 Hz
Input Signal Voltage	2 V peak	2 V peak	2 V peak
Input Impedance	100 K ohm	100 K ohm	100 K ohm
Noise — referred to max. output	-90 dB	-90 dB	-90 dB
Current Monitor output	250 mV/A	125 mV/A	125 mV/A
Input Power	120 V, 50/60 Hz, 300 W 220/240 V optional	120 V, 50/60 Hz, 600 W 220/240 V optional	120 V, 50/60 Hz, 600 W 240 V optional
Rear Panel Connectors			
Power Output	WK3-31S (Cannon)	WK3-31S (Cannon)	WK3-31S (Cannon)
Input, Current Monitor	BNC Type, 3 ea	BNC Type, 3 ea	BNC Type, 3 ea
AC Power	Std 3-Pin Receptacle	Std 3-Pin Receptacle	Std 3-Pin Receptacle
Weight	25 lb (11.3 kg)	45 lb (20 kg)	45 lb (20 kg)
Size HxWxD	5.22 x 17 x 9.25 inches 133 x 432 x 235 mm	5.22 x 17 x 13.25 inches 133 x 432 x 337 mm	5.22 x 17 x 13.25 inches 133 x 432 x 337 mm

SPECIFICATIONS	Model 115
Input Signal Level	1 V peak
Input Impedance	100 K ohm
Output Signal Level	0 to 10 V peak
Output Source Impedance	50 ohm
Frequency Range	0-5000 Hz
Noise — referred to max. output	-90 dB
Weight	10 lb (4.5 kg)
Size HxWxD	5.22 x 17 x 6.25 inches 133 x 432 x 159 mm

Note: Rack adapters are included with amplifiers & control panels for standard 19-in rack mounting

SYSTEM CABLES Shaker to Power Amplifier

System Interconnect Cable 0081-20A/2C Standard length 20 feet section A, 2 ft. section C

Models 113, 113-AB and 113-LZ to Models 114, 123 & 124

System Interconnect Cable 0081-20A Standard length 20 feet

Models 113-LA, 120S, 129, and 220, to Models 114, 123, 124 and Extension

5731 PALMER WAY, SUITE A, CARLSBAD, CA 92008 U.S.A. • (619) 438-4848 • FAX (619) 438-8845 • TELEX 4995113 (SHAKE)

Figure B.5 Acoustic Power Systems Model 114 Power Amplifier Specifications

Appendix C: MSC/NASTRAN Input Decks

Input Deck 1: Orginal ABE with impact load; no damping.

```
ASSIGN OUTPUT2=RUN2.OP2,STATUS=NEW,UNIT=12,FORMAT=UNFORMATTED
TIME 30
DIAG 64
SOL 112                          $MODAL TRANSIENT RESPONSE
CEND
TITLE = ABE FEM  -- UNITS = SI
METHOD = 97
DLOAD = 40
SET 1 = 5 11
TSTEP = 98
SVECTOR = ALL
VELOCITY = 1
DISPLACEMENT = 1
     SPC =          1
SUBCASE          1
SUBTITLE =   CASE SET 1
BEGIN BULK
GRID            1       0      0.      0.      0.       0

GRID            2       01.78E-01      0.      0.       0

GRID            3       03.56E-01      0.      0.       0

GRID            4       05.34E-01      0.      0.       0

GRID            5       07.12E-01      0.      0.       0

GRID            6       0    .889      0.      0.       0

GRID            7       0   1.067      0.      0.       0

GRID            8       0   1.245      0.      0.       0

GRID            9       0   1.422      0.      0.       0

GRID           10       0     1.6      0.      0.       0

GRID           11       0   1.797      0.      0.       0

CBAR            1       1       1       2       1.      1.
+EA    1
+EA    1       0

CBAR            2       1       2       3       1.      1.
+EA    2
+EA    2       0

CBAR            3       1       3       4       1.      1.
+EA    3
+EA    3       0

CBAR            4       1       4       5       1.      1.
+EA    4
```

```
+EA     4        0

CBAR             5        1        5        6       1.       1.
+EA     5
+EA     5        0

CBAR             6        1        6        7       1.       1.
+EA     6
+EA     6        0

CBAR             7        1        7        8       1.       1.
+EA     7
+EA     7        0

CBAR             8        1        8        9       1.       1.
+EA     8
+EA     8        0

CBAR             9        1        9       10       1.       1.
+EA     9
+EA     9        0

CBAR            10        1       10       11       1.       1.
+EA    10
+EA    10        0

CONM2,11,11,0,4.986,0.,0.,0.,,+EA11
+EA11,5.79E-02,0.,2.895E-2,0.,0.,2.895E-2
CONM2,12,11,-1,2.49E-02,1.7755,-.0572,-.1016,,+EA12
+EA12,.17E-05,0.,.55E-05,0.,0.,.40E-05
CONM2,13,11,-1,3.49E-02,1.7678,0.,-.1016,,+EA13
+EA13,3.81E-05,0.,.018E-05,0.,0.,3.81E-05
CONM2,14,11,-1,8.48E-02,1.7755,.0572,-.1016,,+EA14
+EA14,.59E-05,0.,1.87E-05,0.,0.,1.36E-05
CONM2,15,11,-1,3.49E-02,1.727,0.0572,-.1016,,+EA15
+EA15,.24E-05,0.,1.07E-05,0.,0.,.86E-05
CONM2,16,11,-1,9.47E-02,1.7132,.062,-.1016,,+EA16
+EA16,15.62E-5,0.,.43E-05,0.,0.,15.62E-5
CONM2,17,11,-1,2.49E-02,1.7755,.0572,.1016,,+EA17
+EA17,.17E-05,0.,.55E-05,0.,0.,.40E-05
CONM2,18,11,-1,3.49E-02,1.7678,0.,.1016,,+EA18
+EA18,3.81E-05,0.,.18E-06,0.,0.,3.81E-05
CONM2,19,11,-1,8.48E-02,1.7755,-.0572,.1016,,+EA19
+EA19,.59E-05,0.,1.87E-05,0.,0.,1.36E-05
CONM2,20,11,-1,3.49E-02,1.727,-.0572,.1016,,+EA20
+EA20,.24E-05,0.,1.07E-05,0.,0.,.86E-05
CONM2,21,11,-1,9.47E-02,1.7132,-.062,.1016,,+EA21
+EA21,15.62E-5,0.,.43E-05,0.,0.,15.62E-5
CONM2,22,11,-1,51.36E-2,1.7678,0.,-.1016,,+EA22
+EA22,40.99E-5,0.,33.13E-5,0.,0.,40.99E-5
CONM2,23,11,-1,51.36E-2,1.7678,0.,.1016,,+EA23
+EA23,40.99E-5,0.,33.13E-5,0.,0.,40.99E-5
MAT1             17.45E+102.83E+10     .317   2766.3.61E-06
+MA     1
+MA     1 1.5E+09 1.5E+09 6.8E+07

PBAR             1        14.94E-042.71E-081.53E-083.30E-08       0.
+PA     1
+PA     1       0.       0.       0.       0.       0.       0.       0.
0.+PB    1
+PB     16.68E-011.19E+00      0.
```

```
SPC             1       1  123456      0.
SPC             1       2     135      0.
SPC             1       3     135      0.
SPC             1       4     135      0.
SPC             1       5     135      0.
SPC             1       6     135      0.
SPC             1       7     135      0.
SPC             1       8     135      0.
SPC             1       9     135      0.
SPC             1      10     135      0.
SPC             1      11     135      0.
TLOAD1,40,41,,0,42
DAREA,41,11,2,1000.
TABLED1,42,,,,,,,,+E42
+E42,0.,0.,0.001,0.,.002,1.,.003,0.,+E43
+E43,.004,0.,ENDT
PARAM   AUTOSPC YES
EIGR,97,MGIV,0.,150.,3,3,,,ABC
+BC,MASS
TSTEP,98,10,.001,1,,,,,+E98
+E98,,100,.01,1
PARAM,POST,-2
ENDDATA
```

Input Deck 2: Orginal ABE with impact load; damping included.

```
ASSIGN OUTPUT2=RUN2.OP2,STATUS=NEW,UNIT=12,FORMAT=UNFORMATTED
TIME 30
DIAG 64
SOL 112                         $MODAL TRANSIENT RESPONSE
CEND
TITLE = ABE FEM  -- UNITS = SI
METHOD = 97
SDAMPING = 99
DLOAD = 40
SET 1 = 5 11
TSTEP = 98
SVECTOR = ALL
VELOCITY = 1
DISPLACEMENT = 1
     SPC =          1
SUBCASE          1
SUBTITLE =   CASE SET 1
BEGIN BULK
GRID            1       0      0.      0.      0.       0
```

```
GRID            2       01.78E-01       0.      0.      0
GRID            3       03.56E-01       0.      0.      0
GRID            4       05.34E-01       0.      0.      0
GRID            5       07.12E-01       0.      0.      0
GRID            6       0     .889      0.      0.      0
GRID            7       0    1.067      0.      0.      0
GRID            8       0    1.245      0.      0.      0
GRID            9       0    1.422      0.      0.      0
GRID           10       0      1.6      0.      0.      0
GRID           11       0    1.797      0.      0.      0
CBAR            1       1       1       2       1.      1.
+EA     1
+EA     1       0
CBAR            2       1       2       3       1.      1.
+EA     2
+EA     2       0
CBAR            3       1       3       4       1.      1.
+EA     3
+EA     3       0
CBAR            4       1       4       5       1.      1.
+EA     4
+EA     4       0
CBAR            5       1       5       6       1.      1.
+EA     5
+EA     5       0
CBAR            6       1       6       7       1.      1.
+EA     6
+EA     6       0
CBAR            7       1       7       8       1.      1.
+EA     7
+EA     7       0
CBAR            8       1       8       9       1.      1.
+EA     8
+EA     8       0
CBAR            9       1       9      10       1.      1.
+EA     9
+EA     9       0
CBAR           10       1      10      11       1.      1.
+EA    10
+EA    10       0
CONM2,11,11,0,4.986,0.,0.,0.,,+EA11
```

```
+EA11,5.79E-02,0.,2.895E-2,0.,0.,2.895E-2
CONM2,12,11,-1,2.49E-02,1.7755,-.0572,-.1016,,+EA12
+EA12,.17E-05,0.,.55E-05,0.,0.,.40E-05
CONM2,13,11,-1,3.49E-02,1.7678,0.,-.1016,,+EA13
+EA13,3.81E-05,0.,.018E-05,0.,0.,3.81E-05
CONM2,14,11,-1,8.48E-02,1.7755,.0572,-.1016,,+EA14
+EA14,.59E-05,0.,1.87E-05,0.,0.,1.36E-05
CONM2,15,11,-1,3.49E-02,1.727,0.0572,-.1016,,+EA15
+EA15,.24E-05,0.,1.07E-05,0.,0.,.86E-05
CONM2,16,11,-1,9.47E-02,1.7132,.062,-.1016,,+EA16
+EA16,15.62E-5,0.,.43E-05,0.,0.,15.62E-5
CONM2,17,11,-1,2.49E-02,1.7755,.0572,.1016,,+EA17
+EA17,.17E-05,0.,.55E-05,0.,0.,.40E-05
CONM2,18,11,-1,3.49E-02,1.7678,0.,.1016,,+EA18
+EA18,3.81E-05,0.,.18E-06,0.,0.,3.81E-05
CONM2,19,11,-1,8.48E-02,1.7755,-.0572,.1016,,+EA19
+EA19,.59E-05,0.,1.87E-05,0.,0.,1.36E-05
CONM2,20,11,-1,3.49E-02,1.727,-.0572,.1016,,+EA20
+EA20,.24E-05,0.,1.07E-05,0.,0.,.86E-05
CONM2,21,11,-1,9.47E-02,1.7132,-.062,.1016,,+EA21
+EA21,15.62E-5,0.,.43E-05,0.,0.,15.62E-5
CONM2,22,11,-1,51.36E-2,1.7678,0.,-.1016,,+EA22
+EA22,40.99E-5,0.,33.13E-5,0.,0.,40.99E-5
CONM2,23,11,-1,51.36E-2,1.7678,0.,.1016,,+EA23
+EA23,40.99E-5,0.,33.13E-5,0.,0.,40.99E-5
MAT1            17.43E+102.83E+10     .317    2766.3.61E-06
+MA     1
+MA     1 1.5E+09 1.5E+09 6.8E+07

PBAR            1        14.94E-042.71E-081.53E-083.30E-08       0.
+PA     1
+PA     1       0.       0.       0.       0.       0.       0.       0.
0.+PB    1
+PB     16.68E-011.19E+00       0.

SPC             1       1  123456       0.
SPC             1       2     135       0.
SPC             1       3     135       0.
SPC             1       4     135       0.
SPC             1       5     135       0.
SPC             1       6     135       0.
SPC             1       7     135       0.
SPC             1       8     135       0.
SPC             1       9     135       0.
SPC             1      10     135       0.
SPC             1      11     135       0.

TLOAD1,40,41,,0,42
DAREA,41,11,2,1000.
TABLED1,42,,,,,,,,+E42
+E42,0.,0.,0.001,0.,.002,1.,.003,0.,+E43
+E43,.004,0.,ENDT
TABDMP1,99,CRIT,,,,,,,+EA99
+EA99,.1,.065,30.,.023,100.,.01,ENDT
PARAM   AUTOSPC YES
EIGR,97,MGIV,0.,150.,3,3,,,ABC
+BC,MASS
TSTEP,98,10,.001,1,,,,,+E98
+E98,,100,.01,1
PARAM,POST,-2
ENDDATA
```

Appendix D: MATLAB .M File

This MATLAB .M file was written to perform the control optimization calculations in Chapter V.

MATLAB .M File

```
%This program uses the MATLAB subroutine LQR to solve
%for the gain K where u = -Kx. In addition, the Riccati
%matrix is given.  With the K & S matrices, the cost functions
%J and C are found. This ".m" file supports three mode shapes.
%
%The state-space equations are:
%
%                          x'= Ax + Bu
%                          y = Cx + Du
%
%The closed loop A matrix becomes:
%
%                          ACL = (A - B*K)
%
%Initial conditions can be obtained from a finite element
%program.  w1, w2, w3, s1, s2, s3, q01, q02, P, and k must be
%defined prior to running this .m file.   w# are the natural
%frequencies in rad/sec; s# are the damping factors; q01 is the 3x1
%matrix of initial displacements; q02 is the 3x1 matrix of
%initial velocities; P is the 3x3 matrix of eigenvectors; and k is
%the modal stiffness matrix such that PI*K*P=k for PI*M*P=m=I.
%
diary on
%
%Equation parameters are:
w1
w2
w3
s1
s2
s3
P
k
%
%Calculate the inverse of P and k.
PI=inv(P)
ki=inv(k)
%
%Initial conditions given are.
q01
q02
%Transformation of initial conditions to modal coordinates.
n01=PI*q01
n02=PI*q02
x0=[n01;n02]
%
%Define undamped A and damped AD matrix.
```

```
A=[0 0 0 1 0 0
   0 0 0 0 1 0
   0 0 0 0 0 1
   -w1^2 0 0 0 0 0
   0 -w2^2 0 0 0 0
   0 0 -w3^2 0 0 0]
%
%
AD=[0 0 0 1 0 0
    0 0 0 0 1 0
    0 0 0 0 0 1
    -w1^2 0 0 -2*w1*s1 0 0
    0 -w2^2 0 0 -2*w2*s2 0
    0 0 -w3^2 0 0 -2*w3*s3]
%
%Define the B matrix.
b=[-1 1 0;1 1 0;0 0 1]
bb=P'*b
B=[0 0 0;0 0 0;0 0 0;bb]
%
%Define the C matrix.
CP=[0 0 0;0 0 0;0 0 0]
CV=[-1 1 0;1 1 0;0 0 1]
CPP=CP*P
CVP=CV*P
C=[CPP(1,:) CVP(1,:);CPP(2,:) CVP(2,:);CPP(3,:) CVP(3,:)]
%
%Define the D matrix.
D=[0 0 0;0 0 0;0 0 0]
%
%The gain matrix is found from the Ricatti equation by
%minimizing the cost function
%
%                        J = int(x'*Q*x + u'*R*u)dt
%
%The control theory weighing matrices are defined by:
%
Q0=[w1^2 0 0 0 0 0
    0 w2^2 0 0 0 0
    0 0 w3^2 0 0 0
    0 0 0    1 0 0
    0 0 0    0 1 0
    0 0 0    0 0 1]
%
Q3=0.3*Q0
%
R0=b'*P*ki*P'*b
R3=0.3*R0
%
QI0=[150 0    0     0 0 0
     0   6750 0     0 0 0
     0   0    30375 0 0 0
     0   0    0     1 0 0
     0   0    0     0 1 0
     0   0    0     0 0 1]
%
QI3=0.3*QI0
%
RI0=[0.003 0 0;0 0.003 0;0 0 0.0001]
RI3=0.3*RI0
%
%
```

```
%Use MATLAB subroutine "lqr" to solve the Riccati equation
%for the Riccati matrix S and the gain matrix K.
%
[K00,S00]=lqr(A,B,Q0,R0)
[K30,S30]=lqr(A,B,Q3,R0)
[K03,S03]=lqr(A,B,Q0,R3)
[K33,S33]=lqr(A,B,Q3,R3)
[KD00,SD00]=lqr(AD,B,Q0,R0)
[KD30,SD30]=lqr(AD,B,Q3,R0)
[KD03,SD03]=lqr(AD,B,Q0,R3)
[KD33,SD33]=lqr(AD,B,Q3,R3)
[KI00,SI00]=lqr(A,B,QI0,RI0)
[KI30,SI30]=lqr(A,B,QI3,RI0)
[KI03,SI03]=lqr(A,B,QI0,RI3)
[KI33,SI33]=lqr(A,B,QI3,RI3)
[KID00,SID00]=lqr(AD,B,QI0,RI0)
[KID30,SID30]=lqr(AD,B,QI3,RI0)
[KID03,SID03]=lqr(AD,B,QI0,RI3)
[KID33,SID33]=lqr(AD,B,QI3,RI3)
%
%Initial conditions are used to determine the minimum J
%values of the control cost function.
%
J00=x0'*S00*x0
J30=x0'*S30*x0
J03=x0'*S03*x0
J33=x0'*S33*x0
JD00=x0'*SD00*x0
JD30=x0'*SD30*x0
JD03=x0'*SD03*x0
JD33=x0'*SD33*x0
JI00=x0'*SI00*x0
JI30=x0'*SI30*x0
JI03=x0'*SI03*x0
JI33=x0'*SI33*x0
JID00=x0'*SID00*x0
JID30=x0'*SID30*x0
JID03=x0'*SID03*x0
JID33=x0'*SID33*x0
%
%Initial control inputs are determined from the control law.
%
F00=-1*K00*x0
F30=-1*K30*x0
F03=-1*K03*x0
F33=-1*K33*x0
FD00=-1*KD00*x0
FD30=-1*KD30*x0
FD03=-1*KD03*x0
FD33=-1*KD33*x0
FI00=-1*KI00*x0
FI30=-1*KI30*x0
FI03=-1*KI03*x0
FI33=-1*KI33*x0
FID00=-1*KID00*x0
FID30=-1*KID30*x0
FID03=-1*KID03*x0
FID33=-1*KID33*x0
%
```

```
%Expected values of the control cost function C = u'*R*u
%are determined.
%
C00=F00'*R0*F00
C30=F30'*R0*F30
C03=F03'*R3*F03
C33=F33'*R3*F33
CD00=FD00'*R0*FD00
CD30=FD30'*R0*FD30
CD03=FD03'*R3*FD03
CD33=FD33'*R3*FD33
CI00=FI00'*RI0*FI00
CI30=FI30'*RI0*FI30
CI03=FI03'*RI3*FI03
CI33=FI33'*RI3*FI33
CID00=FID00'*RI0*FID00
CID30=FID30'*RI0*FID30
CID03=FID03'*RI3*FID03
CID33=FID33'*RI3*FID33
%
%Open loop frequencies and damping factors are calculated.
%
[WA,ZA]=damp(A)
[WAD,ZAD]=damp(AD)
%
%Closed loop frequencies and damping factors are calculated.
%
[W00,Z00]=damp(A-B*K00)
[W30,Z30]=damp(A-B*K30)
[W03,Z03]=damp(A-B*K03)
[W33,Z33]=damp(A-B*K33)
[WD00,ZD00]=damp(AD-B*KD00)
[WD30,ZD30]=damp(AD-B*KD30)
[WD03,ZD03]=damp(AD-B*KD03)
[WD33,ZD33]=damp(AD-B*KD33)
[WI00,ZI00]=damp(A-B*KI00)
[WI30,ZI30]=damp(A-B*KI30)
[WI03,ZI03]=damp(A-B*KI03)
[WI33,ZI33]=damp(A-B*KI33)
[WID00,ZID00]=damp(AD-B*KID00)
[WID30,ZID30]=damp(AD-B*KID30)
[WID03,ZID03]=damp(AD-B*KID03)
[WID33,ZID33]=damp(AD-B*KID33)
%
diary off
```

Appendix E: Q and R Weights

Table E.1 Q and R Nomenclature

Weigh Factor	θ_m	θ_k	θ_R
Q00	1.0	1.0	1.0
Q30	0.3	0.3	1.0
Q03	1.0	1.0	0.3
Q33	0.3	0.3	0.3
R00	1.0	1.0	1.0
R30	0.3	0.3	1.0
R03	1.0	1.0	0.3
R33	0.3	0.3	0.3
QI00	1.0	1.0	1.0
QI30	0.3	0.3	1.0
QI03	1.0	1.0	0.3
QI33	0.3	0.3	0.3
RI00	1.0	1.0	1.0
RI30	0.3	0.3	1.0
RI03	1.0	1.0	0.3
RI33	0.3	0.3	0.3

$$QI = \begin{bmatrix} 150 & 0 & 0 & 0 & 0 & 0 \\ 0 & 6750 & 0 & 0 & 0 & 0 \\ 0 & 0 & 30375 & 0 & 0 & 0 \\ 0 & 0 & 0 & 1 & 0 & 0 \\ 0 & 0 & 0 & 0 & 1 & 0 \\ 0 & 0 & 0 & 0 & 0 & 1 \end{bmatrix} \qquad \text{(E.1)}$$

$$RI = \begin{bmatrix} 0.003 & 0 & 0 \\ 0 & 0.003 & 0 \\ 0 & 0 & 0.0001 \end{bmatrix} \qquad \text{(E.2)}$$

Appendix F: Optimized ABE Control Law

```
w1 =

   12.1440

w2 =

   82.1190

w3 =

  174.2800

s1 =

    0.0640

s2 =

    0.0084

s3 =

    0.0236

P =

    0.3759         0    0.0823
         0   -3.6022         0
    0.0775         0   -0.6853

k =

  1.0e+004 *

    0.0147         0         0
         0    0.6744         0
         0         0    3.0374


q01 =

  1.0e-003 *

    0.1480
         0
   -0.0268
```

```
q02 =

    0.1479
         0
   -0.0263


x0 =

    0.0004
         0
    0.0001
    0.3758
         0
    0.0808


A =

  1.0e+004 *

         0         0         0    0.0001         0         0
         0         0         0         0    0.0001         0
         0         0         0         0         0    0.0001
   -0.0147         0         0         0         0         0
         0   -0.6744         0         0         0         0
         0         0   -3.0374         0         0         0


AD =

  1.0e+004 *

         0         0         0    0.0001         0         0
         0         0         0         0    0.0001         0
         0         0         0         0         0    0.0001
   -0.0147         0         0   -0.0002         0         0
         0   -0.6744         0         0   -0.0001         0
         0         0   -3.0374         0         0   -0.0008


b =

    -1     1     0
     1     1     0
     0     0     1


B =

         0         0         0
         0         0         0
         0         0         0
   -0.3759    0.3759    0.0775
   -3.6022   -3.6022         0
   -0.0823    0.0823   -0.6853
```

CV =

```
    -1     1     0
     1     1     0
     0     0     1
```

C =

```
         0         0         0   -0.3759   -3.6022   -0.0823
         0         0         0    0.3759   -3.6022    0.0823
         0         0         0    0.0775         0   -0.6853
```

D =

```
     0     0     0
     0     0     0
     0     0     0
```

Q3 =

```
  1.0e+003 *

    0.0442         0         0         0         0         0
         0    2.0231         0         0         0         0
         0         0    9.1121         0         0         0
         0         0         0    0.0003         0         0
         0         0         0         0    0.0003         0
         0         0         0         0         0    0.0003
```

R0 =

```
    0.0029    0.0010   -0.0002
    0.0010    0.0029    0.0002
   -0.0002    0.0002    0.0001
```

KD30 =

```
  1.0e+003 *

   -0.0268   -0.1312   -0.6254   -0.0102   -0.0085   -0.0183
    0.0268   -0.1312    0.6254    0.0102   -0.0085    0.0183
    0.0064    0.0000   -6.0627    0.0024    0.0000   -0.1777
```

SD30 =

```
    9.1418   -0.0000   -0.0000    0.1402   -0.0000   -0.0000
    0.0000   69.9676   -0.0000   -0.0000    0.1402    0.0000
   -0.0000   -0.0000  143.4420   -0.0000   -0.0000    0.1402
    0.1402    0.0000    0.0000    0.0531    0.0000    0.0000
    0.0000    0.1402   -0.0000   -0.0000    0.0091    0.0000
    0.0000   -0.0000    0.1402   -0.0000   -0.0000    0.0041
```

```
JD30 =

    0.0076


FD30 =

    5.3613
   -5.3613
   13.9415


CD30 =

    0.0626


WD30 =

   12.9672
   12.9672
  186.0946
  186.0946
   87.6858
   87.6858


ZD30 =

    0.3617
    0.3617
    0.3574
    0.3574
    0.3568
    0.3568
```

Bibliography

1. Nurre, G. S., R. S. Ryan, H. N. Scofield, and J. L. Sims. "Dynamics and Control of Large Space Structures," Journal of Guidance and Control, 7: 514-526 (September-October 1984).

2. Craig, Roy R. "Recent Literature on Structural Modeling, Identification , and Analysis," Mechanics and Control of Large Flexible Structures, Progress in Astronautics and Aeronautics Volume 129, edited by John L. Junkins. Washington DC: American Institute of Aeronautics and Astronautics, 1990.

3. Miller, David F., Vipperla B. Venkayya and Victoria A. Tischler. "Integration of Structures and Controls - Some Computational Issues," Proceedings of 24th Conference on Decision and Control. 924-931. IEEE, 1985.

4. Hallauer, William L. "Recent Literature on Experimental Strutural Dynamics and Control Research," Mechanics and Control of Large Flexible Structures, Progress in Astronautics and Aeronautics Volume 129, edited by John L. Junkins. Washington DC: American Institute of Aeronautics and Astronautics, 1990.

5. Cristler, Capt Thomas A. Active Vibration Control of a Cantilevered Beam with Three Elastic Coordinates. MS Thesis, AFIT/GA/AA/87D-1. School of Engineering, Air Force Institute of Technology (AU), Wright-Patterson AFB OH, December 1987.

6. Breitfeller, Eric F. Modelling and Control of a Cantilevered Beam with End-Mass. MS Thesis. The Ohio State University, Columbus OH, 1988.

7. Jacques, Capt David R. Baseline Experiment for Active Control of Structural Vibrations. MS Thesis, AFIT/GAE/ENY/89D-15. School of Engineering, Air Force Institute of Technology (AU), Wright-Patterson AFB OH, December 1989.

8. Haftka, Raphael T. "Integrated Structure-Control Optimization of Space Structures," Mechanics and Control of Large Flexible Structures, Volume 129, edited by John L. Junkins. Washington DC: American Institute of Aeronautics and Astronautics, 1990.

9. Craig, Roy R. Jr. Structural Dynamics: An Introduction to Computer Methods. New York: John Wiley & Sons, 1981.

10. Cook, Robert D., David S. Malkus, and Michael E. Plesha. Concepts and Applications of Finite Element Analysis (Third Edition). New York: John Wiley & Sons, 1989.

11. Gockel, M. A., ed. MSC/NASTRAN Handbook For Dynamic Analysis, MSC/NASTRAN Version 63. Los Angeles: The MacNeal-Schwendler Corporation, 1983.

12. SDRC I-DEAS. Systan Engineering Analysis - System Dynamics User's Guide, I-DEAS Level 4. Milford OH: Structural Dynamics Research Corporation, 1988.

13. Anderson, William J. Finite Elements In Mechanical And Structural Design. Ann Arbor MI: Automated Analysis Corporation, 1985.

14. Dovel, George. "Modal Analysis: A Dynamic Tool For Design and Troubleshooting," Mechanical Engineering: 82-86 (March 1989).

15. Inman, Daniel. "Control/Structure Interaction: Effects of Actuator Dynamics," Mechanics and Control of Large Flexible Structures, Volume 129, edited by John L. Junkins. Washington DC: American Institute of Aeronautics and Astronautics, 1990.

16. Ridgely, Brett D. and Siva S. Banda. Introduction to Robust Multivariable Control. AFWAL-TR-85-3102, Flight Dynamics Laboratory, Air Force Wright Aeronautical Laboratories, Air Force Systems Command, Wright Patterson AFB OH, 1986.

17. Balas, M. J. "Active Control of Flexible Systems," Journal of Optimization Theory And Applications, 25: 415-436 (July 1978).

18. Calico, Robert A., Jr, and A. M. Janiszewski. "Control of a Flexible Satellite via Elimination of Observation Spillover," Proceedings of the Third VPI&SU/AIAA Symposium on the Dynamics and Controls of Large Flexible Spacecraft. Blackburg, VA, June 1981.

19. PC-MATLAB. Sherborn MA: The MathWorks, Inc., 1987.

20. Venkayya, Vipperla B. and Victoria A. Tischler. "Frequency Control and the Effect on the Dynamic Response of Flexible Structures," Proceedings of the AIAA Structures, Structural Dynamics and Materials Conference. Palm Springs CA: 431-441 (May 1984).

21. Franklin, Gene F., J. David Powell, and Abbas Emami-Naeini. Feedback Control of Dynamic Systems. Reading MA: Addison-Wesley Publishing Company, 1986.

22. Miller, David F. and Jaedong Shim. "Gradient-Based Combined Structural and Control Optimization," Journal of Guidance and Control, 10: 291-298 (May-June 1987).

23. Onoda, Junjiro and Raphael T. Haftka. "An Approach to Structure/Control Simultaneous Optimization for Large Flexible Spacecraft," AIAA Journal, 25: 1133-1138 (August 1987).

24. Roark, R. J. and W. C. Young. Formulas for Stress and Strain (Fifth Edition). New York: McGraw-Hill Book Company, 1975.

Vita

Steven L. Story was born on 13 June 1962 in Okinawa. At an early age, his parents were transferred back to Sewart AFB in Nashville, Tennessee. His father's military career took him to Little Rock, Arkansas and Enid, Oklahoma before settling down in Shalimar, Florida. After graduating from Choctawhatchee High School in May 1980, he attended the Georgia Institute of Technology on an Air Force ROTC 4-year scholarship. He received the degree of Bachelor of Mechanical Engineering in August 1984 and was commissioned as a Second Lieutenant in the Air Force. His first assignment was to the 323rd Civil Engineering Squadron at Mather AFB California, where he served as a mechanical design engineer, Assistant Systems Engineer, and finally Chief of Requirements and Logistics. In July of 1986 he married Joan Jerrett, and in May 1989, he left the 323rd Civil Engineering Squadron and entered the School of Engineering, Air Force Institute of Technology, Wright-Patterson AFB, Ohio.